Title

MATHEMATICAL MODELING OF THE LITHIUM-ALUMINUM, IRON SULFIDE BATTERY

Author

Pollard, Richard

Publication Date

1979-12-01

Lawrence Berkeley Laboratory
UNIVERSITY OF CALIFORNIA

Materials & Molecular Research Division

MATHEMATICAL MODELING OF THE LITHIUM-ALUMINUM, IRON SULFIDE BATTERY

Richard Pollard
(Ph. D. thesis)

December 1979

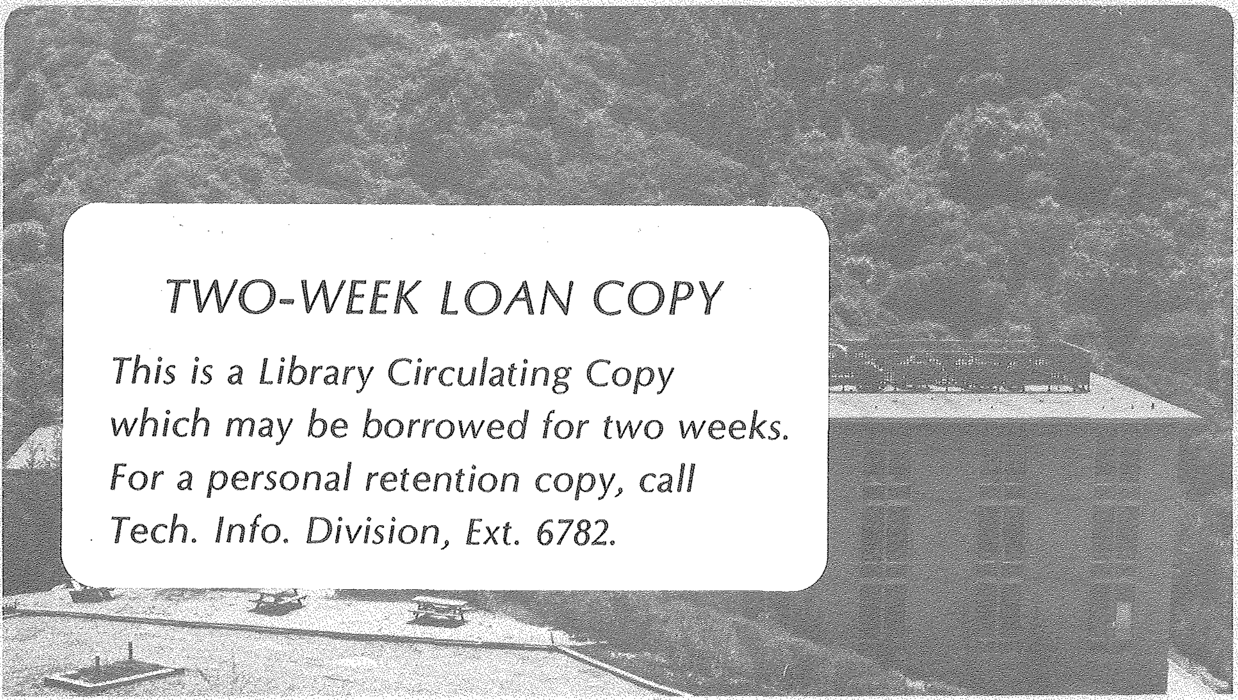

Prepared for the U.S. Department of Energy under Contract W-7405-ENG-48

MATHEMATICAL MODELING OF THE LITHIUM-ALUMINUM, IRON SULFIDE BATTERY

Richard Pollard

Materials and Molecular Research Division,
Lawrence Berkeley Laboratory and
Department of Chemical Engineering,
University of California, Berkeley, California 94720

ABSTRACT

The LiAl/LiCl,KCl/FeS high temperature battery is a candidate for off-peak energy storage and for electric vehicle propulsion. A mathematical model is presented which is able to predict the operational characteristics of the cell and obtain pertinent information for its design and optimization. Material balances and flux equations, based on the macroscopic theory of porous electrodes, are derived for the binary molten salt electrolyte. These equations, together with Ohm's law and relationships for electrode kinetics, are used to describe the time-dependent and position-dependent behavior of the system.

The model considers a whole prismatic cell which consists of negative electrode, separator, electrolyte reservoir,and positive electrode. Physical phenomena described are ohmic potential drop and diffusion potential in the electrolyte, changes in porosity and electrolyte composition due to electrochemical reactions, local reaction rates, and diffusion, convection, and migration of electrolyte. In addition, the analysis includes finite matrix conductivities, variable physical properties, and the possibility of specific simultaneous reactions in the positive electrode.

The theoretical results show many of the trends in behavior observed experimentally. The effects of state of charge, initial electrolyte composition, cell temperature, and current density are presented, and factors that can limit cell performance are identified. The influence of a period of relaxation between the end of discharge and the subsequent charge is also investigated. Furthermore, a separate, analytic treatment of porous electrodes is developed in order to clarify the nature of the highly nonuniform initial reaction distributions that are obtained with high exchange current densities.

ACKNOWLEDGEMENTS

I am extremely grateful to Professor John Newman for his continuous guidance and encouragement throughout this project. I would also like to thank the members of the Chemical Engineering Division at the Argonne National Laboratory for many valuable discussions and suggestions.

This work was supported by the Division of Solar, Geothermal, Electric and Storage Systems, Office of the Assistant Secretary of Energy Technology, U. S. Department of Energy under Contract No. W-7405-ENG-48.

MATHEMATICAL MODELING OF THE LITHIUM-ALUMINUM, IRON SULFIDE BATTERY

Contents

1. INTRODUCTION

The current awareness of the developing shortage of inexpensive energy sources has given new impetus to the development of more efficient methods of energy conversion and storage. Flexible stationary energy storage systems are needed to store off-peak electrical energy, or energy from intermittent sources, for later use during peak demand periods. In addition, alternative techniques for vehicle propulsion are being sought to reduce the dependence on the availability of petroleum feedstocks.

Several rechargeable batteries show promise in being able to meet the performance, lifetime, and cost requirements for economical energy storage and electric vehicle propulsion. At present, only the lead acid battery is available as a commercial system for the electric vehicle. However, there are a number of alternatives that could, with developments and improvements, become competitive. For near-term applications, the nickel/zinc and nickel/iron couples are being considered, whereas, in the longer term, the lithium/iron sulfide and sodium/sulfur high temperature batteries may be able to combine even better performance with lower costs.[1,2]

The lithium/iron sulfide battery offers several potential advantages for electric vehicle applications, such as the apparent safety of the system, the absence of noxious exhaust gases, and a high theoretical specific energy. However, long lifetime and high performance have not yet been achieved in the same cell and therefore it is necessary to analyze the system closely in an effort to reduce the number of design uncertainties and to identify parameters that could have a significant impact on cell performance.

The battery cells that are currently under development[3] consist of LiAl or Li_xSi negative electrodes, FeS or FeS_2 positive electrodes, a porous, ceramic separator to provide electrical isolation of the electrodes, and molten LiCl-KCl electrolyte. The melting point of the electrolyte at the eutectic composition is 352°C and cells are usually operated at temperatures between 400 and 500°C. The present system, and the prismatic cell design, evolved from earlier work on lithium/sulfur cells,[4] which had several engineering problems, including capacity decline due to loss of sulfur from the positive electrode and reaction of lithium with the electrolyte in the negative. The substitution of lithium alloys and iron sulfides for the original reactants has considerable improved the cell stability at the the expense of reducing the cell voltage and maximum specific energy.

The major requirements for an electric vehicle battery to be economically acceptable are high specific energy and energy density, long lifetime, and low cost. In addition, a peak power goal may be stipulated to ensure adequate acceleration. For energy storage applications, there is less emphasis on energy and power capabilities, but the cost and lifetime requirements are more stringent. In general, it is desirable to achieve the highest possible coulombic and energy efficiencies and to maximize the utilization of reactants. Additional considerations are reliability, reproduceability, safety, shelf life, and availability of materials.

In the development of a battery for a specified application, it is necessary to identify the failure mechanisms that have hampered commercialization of the system, and to establish whether the problems are inherent or can be avoided with suitable design modifications. This procedure may necessitate a large experimental program, and a long lead time may be required to obtain an acceptable design. For this reason, it may be advantageous to develop models that can predict results that are costly, time-consuming, or difficult to obtain experimentally. In this way, it should be possible to reduce the time required to bring the system to a point where its economic viability can be realistically assessed.

In this dissertation, a one-dimensional mathematical model is developed that can predict the time-dependent and position-dependent behavior of the lithium-aluminum/iron sulfide cell. The model can be combined with experimental data, and with current collector design studies,[5] to determine the fundamental electrochemical characteristics of the system, and to provide a rational basis for design modifications.

In chapter 2, concentrated solution theory is generalized to provide a framework for the description of isothermal transport processes in binary molten salt mixtures. Electrochemical flux equations are derived for several, commonly-used reference velocities and non-steady state material balances are also presented. The transport theory can be combined with relationships for the ohmic drop in the matrix and solution phases, and with information on electrode kinetics, to predict the behavior of the LiAl/FeS_x system.

Chapter 3 contains an analytic treatment of transient porous electrode behavior at short discharge times, for reactions with high exchange current densities. The simplified model is able to clarify the details of the highly nonuniform reaction distributions that are observed with the more sophisticated approach described in chapters 4 and 5. Chapter 4 focuses attention on the constant current discharge behavior of the LiAl/FeS cell, whereas chapter 5 is concerned with the changes that take place during current interruption and charging.

2. TRANSPORT EQUATIONS FOR A MIXTURE OF TWO BINARY MOLTEN SALTS IN A POROUS ELECTRODE

Introduction

Mass transfer in electrolytic solutions requires a description of the movement of mobile ionic species, together with material balances and equations for current flow and fluid mechanics. A consistent set of transport equations has been established for dilute solutions of electrolytes.[6] This theory can be extended, with the use of the multicomponent diffusion equation, to treat the effects of convection, diffusion, and migration in concentrated solutions with two or more electroactive constituents.[7,8] A parallel analysis, that employs the principles of irreversible thermodynamics, has considered transport phenomena in mixtures of two binary electrolytes with a common ion in a neutral solvent.[9]

For porous media, a macroscopic model has been developed which can describe the essential features of porous materials in terms of readily accessible system parameters. This model can be used in conjunction with concentrated solution theory to elucidate transport processes in porous electrodes.[10] With this approach, detailed studies have been made of electrodes with sparingly soluble reactants in concentrated binary electrolytes,[11] and of the zinc electrode in a ternary electrolyte.[12]

Recent interest in the development of high performance batteries and fuel cells with molten salt electrolytes has focused attention on the need for a rigorous analysis of transport phenomena in these systems. In particular, high temperature, lithium/iron sulfide batteries that are candidates for storage of off-peak electrical energy and for electric vehicle propulsion can use mixtures of binary molten salts with a common ion, such as the lithium chloride/potassium chloride eutectic.[3] These systems have been analyzed previously, but without due regard for the details of the transport phenomena.[13] In this chapter, a consistent set of transport equations for mixtures of two binary molten salts with a common ion is presented. The equations can be applied to free electrolytic solutions or to electrolytes in porous media.

Development of flux equations

The analysis is based on the macrohomogeneous model for porous electrodes in which the solution and matrix phases are treated as superposed continua without regard for the actual geometric details of the pores.[14] With this approach one can obtain a material balance for species i of the form

$$\frac{\partial(\varepsilon c_i)}{\partial t} = aj_{in} - \nabla \cdot \underline{N}_i \ , \tag{2-1}$$

where $\underline{N}_i$ is the flux of species i in the pore solution averaged over the cross-sectional area of the electrode and where aj_{in} represents the transfer rate of species i from the solid phases to the pore solution per unit electrode volume. In addition, the superficial current density in the pore solution is given by

$$\underline{i}_2 = F \sum_i z_i \underline{N}_i \ , \tag{2-2}$$

and the condition of electrical neutrality for each phase gives

$$\sum_i z_i c_i = 0 \tag{2-3}$$

for the electrolyte solution and specifies that the divergence of the total current density is zero. Explicit relationships for the fluxes in terms of the thermodynamic potential driving forces may be derived by inversion of the multicomponent diffusion equation[7]

$$c_i \nabla \mu_i = \frac{RT}{c_T} \sum_j \frac{c_i c_j}{\mathcal{D}_{ij}} (\underline{v}_j - \underline{v}_i) \tag{2-4}$$

for each species in an isothermal, isobaric system.

For a mixture of n species, a set of (n - 1) independent force balances defines the transport coefficients for binary interactions $\mathcal{D}_{ij}$, which are functions of temperature, pressure, and composition. In porous media, each $\mathcal{D}_{ij}$ is related to the transport coefficient $\mathcal{D}^o_{ij}$ for the bulk electrolyte by $\mathcal{D}_{ij} = \mathcal{D}^o_{ij}/\tau^2$, where τ is a tortuosity factor. This parameter is a characteristic of the microscopic electrode structure and is sometimes associated with the porosity by a relation of the form, $\tau^2 = 1/\sqrt{\varepsilon}$.[10] The number of independent transport properties in Eq. (4) is $\frac{1}{2}$ n(n - 1) because $\mathcal{D}_{ii}$ is not defined and, by Newton's third law of motion, $\mathcal{D}_{ij} = \mathcal{D}_{ji}$. Specific combinations of these properties correspond to transport parameters that can be measured directly. The behavior of an electrolyte with three species can be described with a molecular diffusion coefficient, a transference number, and the bulk electrolyte conductivity, together with a single chemical potential or composition variable.

Consider a binary molten salt electrolyte with a common ion. The stoichiometries for dissociation of the individual salts, A and B, are described by

$$\begin{aligned} M_A &= \nu_1^A M_1^{z_1} + \nu_3^A M_3^{z_3} \\ M_B &= \nu_2^B M_2^{z_2} + \nu_3^B M_3^{z_3} \ , \end{aligned} \tag{2-5}$$

where M_3 is the chemical symbol for the common ion and where the electroneutrality condition dictates that

$$\sum_i z_i \nu_i^k = 0 \tag{2-6}$$

for the particular neutral salt, k. The chemical potential of each salt can then be expressed as a sum of the electrochemical potentials of the constituent charged species:

$$\mu_k = \sum_i \nu_i^k \mu_i \ . \tag{2-7}$$

For this system, Eq. (4) yields two independent equations which may be rearranged, with the introduction of the superficial current density from Eq. (2), to give expressions for the fluxes based on a reference velocity characteristic of the bulk motion of the electrolyte. For example, if the velocity $\underline{v}_3$ of the common ion is chosen as the reference velocity, the superficial fluxes in a porous electrode are given by

$$\underline{N}_1 = c_1\underline{v}_1 = -\frac{\varepsilon\,\nu_1^A\nu_3^B\,\mathcal{D}}{RT}\,c_A\nabla\mu_A + \frac{t_1^c\underline{i}_2}{z_1F} + c_1\underline{v}_3$$

$$\underline{N}_2 = c_2\underline{v}_2 = -\frac{\varepsilon\,\nu_2^B\nu_3^A\,\mathcal{D}}{RT}\,c_B\nabla\mu_B + \frac{t_2^c\underline{i}_2}{z_2F} + c_2\underline{v}_3 \qquad (2\text{-}8)$$

$$\underline{N}_3 = c_3\underline{v}_3\ ,$$

where $c_A = c_1/\nu_1^A$ and $c_B = c_2/\nu_2^B$. The effective diffusion coefficient based on a thermodynamic driving force is defined as

$$\mathcal{D} = \frac{z_3^2 c_T/\nu_1^A\nu_2^B}{\dfrac{z_1^2c_1}{\mathcal{D}_{23}} + \dfrac{z_2^2c_2}{\mathcal{D}_{13}} + \dfrac{z_3^2c_3}{\mathcal{D}_{12}}} \qquad (2\text{-}9)$$

where c_T is the total concentration defined as $c_T = \sum_i c_i$. The transference numbers t_i^c relative to the common ion velocity can also be expressed in terms of the coefficients $\mathcal{D}_{ij}$ as,

$$t_2^c = 1 - t_1^c = \frac{\left(\dfrac{z_2}{\mathcal{D}_{13}} - \dfrac{z_3}{\mathcal{D}_{12}}\right)}{\left(\dfrac{z_2}{\mathcal{D}_{13}} - \dfrac{z_3}{\mathcal{D}_{12}}\right) + \dfrac{z_1c_1}{z_2c_2}\left(\dfrac{z_1}{\mathcal{D}_{23}} - \dfrac{z_3}{\mathcal{D}_{12}}\right)}\ . \qquad (2\text{-}10)$$

Equations (9) and (10) are directly analogous to the definitions of transport properties in concentrated binary electrolytes.[6] In contrast to previous work on molten salt electrolytes,[13] the transport parameters defined by the flux expressions (Eq. (8)) are measurable state properties, independent of the fluxes and driving forces for mass transfer.

In parallel with the transport theory for concentrated binary electrolytes, the molar average velocity,[7] the mass average velocity,[8] or the volume average velocity[15] can be used as alternative reference frames for the diffusion fluxes. With the molar average velocity, $\underline{v}^* = \sum_i \underline{N}_i/c_T$, mole fractions of the salts, defined by $x_A = c_A/(c_A + c_B)$ and $x_A + x_B = 1$, become a convenient way to express concentrations. The chemical potentials can be related to the composition variable by suitable definitions for activity coefficients of the salts, that are in turn linked through the Gibbs-Duhem equation. For example, if dissociation of the electrolyte is disregarded,[16] one can obtain

$$\begin{aligned} \mu_A &= RT \ln \left(x_A^{\nu_1^A} \gamma_A \lambda_A^o \right) \\ \mu_B &= RT \ln \left(x_B^{\nu_2^B} \gamma_B \lambda_B^o \right) \end{aligned} \tag{2-11}$$

where the activity coefficients γ_k of the salts are based on the mole fraction of the molten salt mixture. The effective diffusion coefficient based on a gradient of mole fraction is then related to the thermodynamic diffusion coefficient by

$$D = \mathcal{D}\left(\frac{c_3}{c_A + c_B}\right)\left(\nu_1^A + \frac{d \ln \gamma_A}{d \ln x_A}\right) . \tag{2-12}$$

Consequently, for the molar average reference velocity, we have

$$\underline{N}_1 = -\frac{\varepsilon(c_A + c_B)^2 D\, \nu_1^A \nu^B}{c_T} \nabla x_A + \frac{t_1^{\star} \underline{i}_2}{z_1 F} + c_1 \underline{v}^{\star}$$

$$\underline{N}_2 = -\frac{\varepsilon(c_A + c_B)^2 D\, \nu_2^B \nu^A}{c_T} \nabla x_B + \frac{t_2^{\star} \underline{i}_2}{z_2 F} + c_2 \underline{v}^{\star} \tag{2-13}$$

$$\underline{N}_3 = -\frac{\varepsilon(c_A + c_B)^2 D \left(\nu_3^A \nu^B - \nu_3^B \nu^A\right)}{c_T} \nabla x_A + \frac{t_3^{\star} \underline{i}_2}{z_3 F} + c_3 \underline{v}^{\star}$$

where $\nu^A = \nu_1^A + \nu_3^A$, $\nu^B = \nu_2^B + \nu_3^B$, and where the transference numbers are given by

$$t_1^{\star} = \frac{\left(\nu_1^A \nu^B c_3 t_1^c - \nu_3^A \nu_2^B c_1\right)}{\nu_1^A \nu_3^B c_T}$$

$$t_2^{\star} = \frac{\left(\nu_2^B \nu^A c_3 t_2^c - \nu_1^A \nu_3^B c_2\right)}{\nu_2^B \nu_3^A c_T} \tag{2-14}$$

$$t_3^{\star} = 1 - t_1^{\star} - t_2^{\star} .$$

With a mass average reference velocity defined by $\underline{v} = \sum_i \omega_i \underline{v}_i$ it is appropriate to use a mass fraction ω_i as a concentration variable. Equation (8) can then be rearranged to give

$$\underline{N}_1 = -\frac{\varepsilon \rho D \nu_1^A}{M_A} \nabla \omega_A + \frac{t_1 \underline{i}_2}{z_1 F} + c_1 \underline{v}$$

$$\underline{N}_2 = -\frac{\varepsilon \rho D \nu_2^B}{M_B} \nabla \omega_B + \frac{t_2 \underline{i}_2}{z_2 F} + c_2 \underline{v} \tag{2-15}$$

$$\underline{N}_3 = -\varepsilon \rho D \left(\frac{\nu_3^A}{M_A} - \frac{\nu_3^B}{M_B}\right) \nabla \omega_A + \frac{t_3 \underline{i}_2}{z_3 F} + c_3 \underline{v} ,$$

where $\omega_1 = c_1M_1/\rho$, $\omega_A = c_AM_A/\rho$, and $\sum\limits_{\ell=i\,\mathrm{or}\,k} \omega_\ell = 1$. The molecular weight of either salt is defined by $M_k = \sum\limits_i \nu_i^k M_i$, and expressions for the transference numbers based on the mass average velocity, analogous to Eq. (14), are

$$t_1 = \frac{\left(c_3M_Bt_1^c - \nu_2^B\nu_3^Ac_AM_2\right)}{\rho\nu_3^B}$$

$$t_2 = \frac{\left(c_3M_At_2^c - \nu_1^A\nu_3^Bc_BM_1\right)}{\rho\nu_3^A} \tag{2-16}$$

$$t_3 = 1 - t_1 - t_2 \ .$$

Finally, the volume average velocity, $\underline{v}^{\blacksquare} = \sum\limits_i \bar{V}_i\underline{N}_i$, may be used, even though the partial molar volumes of individual ionic species are not accessible to experimental determination. It is required that the quantities $\bar{V}_i$ combine to yield partial molar volumes for the salts according to

$$\bar{V}_k = \sum_i \nu_i^k\bar{V}_i \ , \tag{2-17}$$

where k represents either salt A or salt B. The flux relations are

$$\underline{N}_1 = -\varepsilon\ D\nabla c_1 + \left(\frac{t_1^c}{z_1} - c_1Q\right)\frac{\underline{i}_2}{F} + c_1\underline{v}^{\blacksquare}$$

$$\underline{N}_2 = -\varepsilon\ D\nabla c_2 + \left(\frac{t_2^c}{z_2} - c_2Q\right)\frac{\underline{i}_2}{F} + c_2\underline{v}^{\blacksquare} \tag{2-18}$$

$$\underline{N}_3 = -\varepsilon\ D\nabla c_3 - c_3Q\,\frac{\underline{i}_2}{F} + c_3\underline{v}^{\blacksquare}$$

where Q is taken to be the quantity

$$Q = \sum_i \frac{t_i^c \bar{V}_i}{z_i} \; . \tag{2-19}$$

This quantity cannot be measured independently but, if the transference numbers are arbitrarily chosen to satisfy

$$\frac{t_1^{\blacksquare} \bar{V}_1}{z_1^2 c_1} = \frac{t_2^{\blacksquare} \bar{V}_2}{z_2^2 c_2} = \frac{t_3^{\blacksquare} \bar{V}_3}{z_3^2 c_3} \; , \tag{2-20}$$

it may be shown, by combination and rearrangement of Eqs. (19) and (20), that a consistent definition for Q would be

$$Q = \frac{-t_1^c t_2^c \left(\dfrac{\bar{\bar{V}}_A}{\nu_3^A} - \dfrac{\bar{\bar{V}}_B}{\nu_3^B} \right)}{z_3 \left(t_2^c - c_B \bar{\bar{V}}_B \right)} \; . \tag{2-21}$$

Material balances and conservation equations

The flux relations given by Eqs. (13), (15), and (18) reflect the dependence of the motion of charged species on the driving forces for diffusion, migration, and convection in porous electrodes. Each set of flux expressions, relative to a specific reference velocity can be incorporated into the general material balance, Eq. (1), to give a continuity equation for the electrolyte in the absence of thermal and pressure diffusion. For salt A, these relationships are presented in Table 1 for the mass average, molar average, and volume average reference velocities, and for a reference frame based on the velocity

Table 2-1. Material balance equations for a mixture of two binary molten salts with a common ion.

Mass average reference velocity:

$$\rho\left(\varepsilon \frac{\partial \omega_A}{\partial t} + \underline{v}\cdot\nabla\omega_A\right) = \nabla\cdot(\varepsilon\rho D\nabla\omega_A) + r_{AB} + \frac{\underline{i}_2}{z_3F}\cdot\left(\frac{\omega_B M_A}{\nu_3^A}\nabla t_1 - \frac{\omega_A M_B}{\nu_3^B}\nabla t_2\right) \qquad \text{(2-22A)}$$

Molar average reference velocity:

$$(c_A + c_B)\left(\varepsilon \frac{\partial x_A}{\partial t} + \underline{v}^{\bigstar}\cdot\nabla x_A\right) = \frac{c_T}{c_A + c_B}\nabla\cdot\left(\frac{\varepsilon(c_A + c_B)^2}{c_T} D\nabla x_A\right) + R_{AB} + \frac{\underline{i}_2}{z_3F}\cdot\left(\frac{x_B}{\nu_3^A}\nabla t_1^{\bigstar} - \frac{x_A}{\nu_3^B}\nabla t_2^{\bigstar}\right) \qquad \text{(2-22B)}$$

Volume average reference velocity:

$$\varepsilon \frac{\partial c_A}{\partial t} + \underline{v}^{\blacksquare}\cdot\nabla c_A = \nabla\cdot(\varepsilon D\nabla c_A) + R_A + \frac{\bar{V}_B}{z_3F}\underline{i}_2\cdot\left(\frac{c_B}{\nu_3^A}\nabla t_1^{\blacksquare} - \frac{c_A}{\nu_3^B}\nabla t_2^{\blacksquare}\right) + \frac{c_A\varepsilon D}{c_B\bar{V}_B}\nabla c_A\cdot\nabla\bar{V}_A \qquad \text{(2-22C)}$$

Common ion reference velocity:

$$(c_A + c_B)\left(\varepsilon \frac{\partial x_A}{\partial t} + \underline{v}_3\cdot\nabla x_A\right) = \frac{c_3}{c_A + c_B}\nabla\cdot\left(\frac{\varepsilon(c_A + c_B)^2}{c_3} D\nabla x_A\right) + R_{AB} + \frac{\underline{i}_2}{z_3F}\cdot\left(\frac{x_B}{\nu_3^A}\nabla t_1^{c} - \frac{x_A}{\nu_3^B}\nabla t_2^{c}\right) \qquad \text{(2-22D)}$$

of the common ion. These equations describe the time-dependent behavior of the electrolyte in terms of the composition variable most appropriate for the particular reference velocity used. The factor R_A in Eq. (22-C) represents a combination of production terms of individual species. It is defined as

$$R_A = a\bar{V}_B\left[\frac{j_{1n}}{\nu_1^A}\left(\frac{c_2t_3^r}{\nu_2^B} + \frac{c_3t_2^r}{\nu_3^B}\right) - \frac{j_{2n}}{\nu_2^B}\left(\frac{c_1t_3^r}{\nu_1^A} + \frac{c_3t_1^r}{\nu_3^A}\right) + j_{3n}\left(\frac{c_2}{\nu_2^B\nu_3^A}\,t_1^r - \frac{c_1}{\nu_1^A\nu_3^B}\,t_2^r\right)\right] \tag{2-23}$$

and is found to be independent of the reference frame, r. (Transference numbers with no superscript are relative to the mass average reference velocity.) The corresponding production terms, R_{AB} and r_{AB}, for the alternative reference frames are chosen to simplify the form of the material balance equations. They are directly related to the parameter R_A by:

$$R_A = R_{AB}(c_A + c_B)\bar{V}_B = \frac{r_{AB}\rho\bar{V}_B}{M_AM_B} \tag{2-24}$$

In Eq. (22), it has not been assumed that ε is constant in either position or time. Equations (1), (2), and (3) can also be combined with the flux relationships to give overall conservation or "continuity" equations, which indicate how the reference velocity and porosity change as a result of electrode reactions, migration, and changes in solution composition. For the four reference velocities considered, the corresponding conservation equations are given in Table 2, where

Table 2-2. Continuity equations for a mixture of binary molten salts with a common ion.

Mass average reference velocity:

$$\frac{\partial \varepsilon}{\partial t} + \nabla\cdot\underline{v} = \bar{V}_A S_A + \bar{V}_B S_B + \frac{\underline{i}_2}{z_3 F}\cdot\left(\frac{M_A}{\nu_3^A}\nabla t_1 + \frac{M_B}{\nu_3^B}\nabla t_2\right) \tag{2-25A}$$

Molar average reference velocity:

$$\frac{\partial \varepsilon}{\partial t} + \nabla\cdot\underline{v}^{\star} = \bar{V}_A S_A^{\star} + \bar{V}_B S_B^{\star} + \frac{\underline{i}_2}{z_3 F}\cdot\left(\frac{\bar{V}_A}{\nu_3^A}\nabla t_1^{\star} + \frac{\bar{V}_B}{\nu_3^B}\nabla t_2^{\star}\right) + \left(\bar{V}_A \nu^B - \bar{V}_B \nu^A\right)\nabla\cdot\left(\frac{\varepsilon(c_A + c_B)^2 D}{c_T}\nabla x_A\right) \tag{2-25B}$$

Volume average reference velocity:

$$\frac{\partial \varepsilon}{\partial t} + \nabla\cdot\underline{v}^{\blacksquare} = \bar{V}_A S_A^{\blacksquare} + \bar{V}_B S_B^{\blacksquare} + \frac{\underline{i}_2}{z_3 F}\cdot\left(\frac{\bar{V}_A}{\nu_3^A}\nabla t_1^{\blacksquare} + \frac{\bar{V}_B}{\nu_3^B}\nabla t_2^{\blacksquare}\right) - \frac{\varepsilon D \nabla c_A}{c_B \bar{V}_B}\cdot\nabla\bar{V}_A \tag{2-25C}$$

Common ion reference velocity:

$$\frac{\partial \varepsilon}{\partial t} + \nabla\cdot\underline{v}_3 = \bar{V}_A S_A^{c} + \bar{V}_B S_B^{c} + \frac{\underline{i}_2}{z_3 F}\cdot\left(\frac{\bar{V}_A}{\nu_3^A}\nabla t_1^{c} + \frac{\bar{V}_B}{\nu_3^B}\nabla t_2^{c}\right) + \left(\bar{V}_A \nu_3^B - \bar{V}_B \nu_3^A\right)\nabla\cdot\left(\frac{\varepsilon(c_A + c_B)^2 D}{c_3}\nabla x_A\right) \tag{2-25D}$$

$$S_A^r = \frac{a}{\nu_1^A}\left(j_{1n} - \frac{t_1^r}{z_1}\sum_i z_i j_{in}\right) \tag{2-26}$$

and

$$S_B^r = \frac{a}{\nu_2^B}\left(j_{2n} - \frac{t_2^r}{z_2}\sum_i z_i j_{in}\right) \tag{2-27}$$

for a specified reference frame, r. The parameters S_A^r and S_B^r might be regarded as effective rates of production of the salts per unit volume with due account for the influence of migration. The combination $S_A^r\bar{V}_A + S_B^r\bar{V}_B$ that appears in Eqs. (25-A) to (25-D) is not independent of reference frame, in contrast to the modified production terms R_A, R_{AB}, and r_{AB} in the material balance equations. On the other hand, R_{AB} can be expressed in terms of S_A^r and S_B^r in the form

$$R_{AB} = x_B S_A^r - x_A S_B^r \tag{2-28}$$

which is equivalent to Eq. (23) and which involves a combination of S_A^r and S_B^r that is independent of the choice of reference frame.

The equations in Tables 1 and 2 can be compared with the corresponding relationships for concentrated binary electrolytes[10,11] and with the equations of change for multicomponent, nonelectrolytic systems.[17] The equations presented reduce to simpler forms under various special conditions. For example, for a free electrolytic solution (outside a porous electrode), the conservation equation will only depend on time indirectly, through changes in composition, and transport properties for the bulk electrolyte should be used. If either the current density is zero or the transference numbers are independent of composition then Eqs. (22-A) and (22-C) reduce to forms analogous to the binary diffusion equations for nonelectrolytes. The term R_{AB} in Eq. (28) could be regarded as an effective difference in rates of production of species A and B which takes the influence of migration into account. If Eqs. (22-A) and (22-B) are rewritten for the mole fraction and mass fraction of salt B, it may be shown that $R_{BA} = -R_{AB}$ and that $r_{BA} = -r_{AB}$. By analogy with Eq. (24), it follows that the ratio

$$\frac{R_A}{R_B} = - \frac{\bar{\bar{V}}_B}{\bar{\bar{V}}_A} \tag{2-29}$$

does not depend directly on the stoichiometries for either dissociation of the salts or the electrode reactions.

Several factors can dictate the choice of reference frame for a given application of the material balance equation. The relative complexity of the equations, the form in which data are available for transport properties and activity coefficients, the appropriateness of the composition variable, and the nature of any other equations in the stated problem can all be important criteria. For example, the volume average reference velocity would enable concentration units to be used directly, but there is an ambiguity in the definition of $\underline{v}^{\blacksquare}$ associated with the parameter Q and Eq. (22-C) is in a noncanonical form. Fluid mechanical equations are invariably written in terms of the mass average velocity, but the molar average may be preferred if the velocity is determined from stoichiometry alone or if pertinent data are correlated with the mole fraction. However, with a mole fraction scale one must decide how to treat the dissociated electrolyte. The noncanonical diffusion terms in Eqs. (22-B) and (25-B) result from the divergent definitions for the mole fraction and the molar average velocity. The sum $c_A + c_B$, as distinct from the total concentration c_T, is equal to the inverse of the molar volume of the salt mixture $\tilde{V}$ where $\tilde{V} = \sum_k x_k \bar{V}_k$. Transference numbers are usually measured relative to the solvent velocity and, for binary molten salt mixtures, this gives some support for the use of a common ion reference velocity.

Ohmic potential drop

The potential in the pore electrolyte can be measured with a suitable reference electrode with an electrode reaction defined by

$$\sum_i s_i M_i^{z_i} \rightarrow ne^- \quad . \tag{2-30}$$

This potential can be used as a driving force for the current, and combination of Eqs. (2), (3), and (4) with the thermodynamic relation

$$\sum_i s_i \nabla \mu_i = -nF\nabla\Phi_2 \tag{2-31}$$

yields a modified Ohm's law expression for the superficial current density in the pore solution. This is given by

$$\frac{\underline{i}_2}{\kappa} = -\nabla\Phi_2 - \frac{1}{F}\left[\left(\frac{s_1}{n\nu_1^A} + \frac{t_1^c}{z_1\nu_1^A}\right)\left(1 + \frac{\nu_3^A c_A}{\nu_3^B c_B}\right) - \frac{s_3 c_A}{nc_B\nu_3^B}\right]\nabla\mu_A \ , \tag{2-32}$$

where the second term includes the diffusion potential. Integration of this equation across the electrode shows that the ohmic potential drop in the solution phase is directly related to the distributions of concentration and reaction rate. The effective conductivity within the pores may be written in terms of the binary interaction parameters $\mathcal{D}_{ij}$, as

$$\kappa = \frac{\varepsilon F^2 c_T}{RT} \frac{\left(\frac{z_1^2 c_1}{\mathcal{D}_{23}} + \frac{z_2^2 c_2}{\mathcal{D}_{13}} + \frac{z_3^2 c_3}{\mathcal{D}_{12}}\right)}{\left(\frac{c_1}{\mathcal{D}_{12}\mathcal{D}_{13}} + \frac{c_2}{\mathcal{D}_{12}\mathcal{D}_{23}} + \frac{c_3}{\mathcal{D}_{13}\mathcal{D}_{23}}\right)} . \tag{2-33}$$

Conclusions

The macroscopic transport equations derived for a mixture of two binary molten salts with a common ion provide a consistent framework for the description of mass transfer of electrolytes of this type in free solutions or in porous media. The analysis also provides rational definitions for the transport properties that characterize the system behavior. The results presented, together with information on electrode kinetics, can be used to predict the time-dependent and position-dependent behavior of electrolyte concentration, porosity, current, and reaction rate within porous electrodes.

3. TRANSIENT BEHAVIOR OF POROUS ELECTRODE WITH HIGH EXCHANGE CURRENT DENSITIES

Introduction

Many porous electrodes in commerically important batteries have high values for the product of the electrochemically active specific interfacial area and the exchange current density. This permits operation at high superficial current densities without excessive surface overpotentials that would lower the energy efficiency of the system.

Previously, the distributions of current and electrochemical reaction in porous electrodes have been considered under various special conditions.[14,18] Mass transport of reactants and the effective conductivities of the matrix and solution phases have a strong influence on electrode behavior. The current distribution becomes nonuniform for large values of active surface area, exchange current density, electrode length, and current density and for small conductivities.

Particular attention has been paid to the electrodes of the lead-acid battery,[19-22] and several of the proposed models make the assumption of reversible kinetics.[21,22] With this assumption, it has been shown that highly nonuniform reaction distributions can be obtained, especially for high rate discharges.[21] This can result in an increase in internal cell resistance because local changes in electrolyte composition lower the electrolyte conductivity. Under some circumstances the electrode could become totally passivated. It has also been shown that, in principle, a fraction of the total reaction will be restricted to the electrode/separator interface.[21]

Another study allows all the current to penetrate the electrode, and concludes that models with reversible kinetics are inferior because they cannot take proper account of transport of external acid into the electrode pores.[22]

This chapter considers the nature of the current and reaction distributions for electrode processes with high, but not infinite, exchange current densities. A simplified model is developed in order to give an analytic solution to the governing differential equations. The results obtained illustrate the important features that would be observed with a more sophisticated approach. The method used in this study complements a computer solution which is able to account for many complications not considered here, but which cannot easily clarify the highly nonuniform reaction distribution at moderately short times that results from a high value of the exchange current density. The model can also be used to assess quantitatively the validity of the assumption of reversible kinetics for a particular electrode system.

Analysis

The system considered is a porous electrode in contact with an inert porous separator. The electrode is treated as two superposed continua which represent the solution and matrix phases independently. The actual geometric details of the pores have been disregarded and only variations of parameters in a direction normal to the electrode face are considered. Each phase is taken to be electrically neutral, and consequently the divergence of the total current density is zero.

The analysis is restricted to a single electrode reaction with stoichiometry represented by:

$$\sum_i s_i M_i^{z_i} \rightarrow ne^- . \tag{3-1}$$

A polarization equation of the form

$$j = ai_o\left[e^{\alpha_a F(\Phi_1-\Phi_2)/RT} - e^{-\alpha_c F(\Phi_1-\Phi_2)/RT}\right] \tag{3-2}$$

can be used to express the dependence of the reaction rate at any point in the electrode on the local potential jump at the matrix/solution interface. The potential of the pore solution Φ_2 is measured with a reference electrode of the same kind as the working electrode. The composition dependence of the exchange current density can be assumed to have the form:

$$i_o = i_{oR} \prod_i \left(\frac{c_i}{c_{iR}}\right)^{\gamma_i} , \tag{3-3}$$

where i ranges over the ionic species. Solid phase activities are taken as constant, and initial concentrations are used for the reference condition, R. The possibility of homogeneous chemical reactions is not considered, and double layer charging effects are ignored. To simplify the analysis further, it is assumed that transport properties and pore structure do not change as the reaction proceeds. Under these circumstances, the major concentration changes are caused by electrochemical reaction and by diffusion of electrolyte. Therefore, a nonsteady state material balance for species i becomes:

$$\varepsilon \frac{\partial c_i}{\partial t} = \frac{B}{F} j + \varepsilon D \frac{\partial^2 c_i}{\partial y^2} . \tag{3-4}$$

For times over which equation (4) is to be applied, the parameter B is taken as a constant, dependent on the system considered. Relationships for B, for the positive plate of a lead-acid battery and for the negative electrode in a high temperature LiAl/LiCl, KCl/FeS_x battery, are derived in Appendix A. The molecular diffusion coefficient D can be characterized by

$$D = D_\infty/\zeta^2 . \tag{3-5}$$

Also, it is assumed that the tortuosity factor ζ is directly related to porosity by:[23]

$$\zeta = \varepsilon^{(1-q)/2} , \tag{3-6}$$

where the constant q is taken as 1.5.

The driving force for the current can be specified in terms of the potential in the pore solution Φ_2 measured with a reference electrode. With this definition, a modified Ohm's law for the pore electrolyte is

$$\frac{\underline{i}_2}{\kappa} = -\nabla\Phi_2 + \frac{RT\ W}{F} \nabla \ln c_i , \tag{3-7}$$

where the second term on the right includes the diffusion potential. In this analysis, the parameter W is regarded as a constant, dependent on the electrode studied (see Appendix A). The effective conductivity κ is estimated from

$$\kappa = \varepsilon\kappa_{\infty}/\zeta^2 , \tag{3-8}$$

together with Eq. (6).

The movement of electrons in the matrix phase is governed by Ohm's law. However, it is assumed that the matrix conductivity is large ($\sigma/\kappa >> 1$) so that the matrix potential can be taken to be uniform. With this condition, the initial electrode reaction will be confined to a region adjacent to the electrode/separator interface. This reaction zone can be characterized with a penetration depth L which, for linear kinetics and constant matrix potential, is defined as:[10]

$$L = \left(\frac{\kappa RT}{(\alpha_a + \alpha_c) a i_{oR} F}\right)^{1/2} , \tag{3-9}$$

where i_{oR} is evaluated at the initial composition.

When the discharge process begins there is a rapid and substantial change in current distribution, caused by changes in composition. Nevertheless, the concentrations have only altered significantly from the standpoint of concentration overpotential, and the ratio c_i/c_{iR} has not changed enough to affect appreciably the exchange current density given by Eq. (3). In this restricted range of investigation it is appropriate to define a set of dimensionless variables

$$\tau = Dt/L^2, \quad J = jL/I, \quad \eta = \kappa(\Phi_1 - \Phi_2)/IL, \quad \theta_i = F\varepsilon D(c_i - c_i^o)/ILB ,$$

that have values of order unity. After these definitions have been substituted into the governing equations, it becomes possible to identify those terms which can be neglected as i_o becomes large.

When the exchange current density, or the product ai_o, is large, the local surface overpotential for a specified superficial current density I is expected to be low. Consequently, it is reasonable to reduce Eq. (2) to the form

$$\frac{J}{\eta} = \prod_i \left(1 + \frac{ILB\theta_i}{\varepsilon DFc_i^o}\right)^{\gamma_i} . \tag{3-10}$$

As the exchange current density is raised, the penetration depth decreases and, for $\theta_i = 0(1)$, the right side of Eq. (10) approaches unity. Under these circumstances, Eq. (10) can be simplified further to give

$$J = \eta . \tag{3-11}$$

It might appear that Eq. (11) can be obtained directly from Eq. (2) provided that $(\Phi_1 - \Phi_2)F/RT << 1$. However, the analysis above emphasizes that it is necessary to verify that the composition dependence of the exchange current density does not alter this result.

For small concentration changes, it becomes valid to linearize the concentration dependent term in Eq. (7). Combination of Eqs. (7) and (11) then gives, on differentiation:

$$J = \frac{d^2J}{dY^2} + Q\,\frac{d^2\theta}{dY^2} \qquad (3\text{-}12)$$

where $Y = y/L$ and

$$Q = \frac{\kappa_\infty\, RT\, BW}{D_\infty c_i^o F^2}\ . \qquad (3\text{-}13)$$

In Appendix A, it is shown that only one concentration variable is required for Eq. (7), and, therefore, the subscript on the dimensionless variable θ_i can be dropped.

The material balance, Eq. (4), can be rewritten in dimensionless form

$$\frac{\partial\theta}{\partial\tau} = J + \frac{\partial^2\theta}{\partial Y^2}\ . \qquad (3\text{-}14)$$

The governing differential equations (12) and (14), are subject to the initial condition

$$\theta(Y,0) = 0\ , \qquad (3\text{-}15)$$

and the boundary conditions

(i) $\theta(Y,\tau) \rightarrow 0$ as $Y \rightarrow \infty$,

(ii) at the electrode/separator interface $(Y = 0)$;

a) $i_2 = -I$,

b) θ continuous, (3-16)

c) $\left(\varepsilon D\,\frac{\partial\theta}{\partial Y}\right)_{os} = \left(\varepsilon D\,\frac{\partial\theta}{\partial Y}\right)_{oe}$.

For condition (i), the electrode is assumed to be considerably thicker than the penetration depth so that its length can be regarded as infinite. The last boundary condition assumes that the reaction rate is not a Dirac δ function at the origin.

Equations (12) to (16) define the dependence of concentration and transfer current on time and distance through the porous electrode for a constant current discharge. The reaction zone is restricted to the region immediately adjacent to the separator, and this limits the applicability of the results, as discussed below. The equations refer to systems with high exchange current densities or small penetration depths, but it should be emphasized that the macrohomogeneous model on which the analysis is based will breakdown if the reaction zone is significantly smaller than the characteristic dimensions of the microscopic porous structure.

Results and Discussion

In terms of Laplace transforms, the solution to the stated problem may be written as:

$$\bar{J}(Y,s) = Ae^{-EY} + \frac{1}{E\sqrt{s}}\left(1 - \frac{As}{E}\right)e^{-Y\sqrt{s}/E} , \qquad (3\text{-}17)$$

where the variable s is defined by:

$$f(s) = \int_0^\infty e^{-s\tau}F(\tau)\, d\tau . \qquad (3\text{-}18)$$

The parameters A and E are related by the imposed requirement that integration of Eq. (17) across the electrode gives the superficial current density, viz:

$$\int_0^\infty \bar{J}(Y,s)\,dY = \frac{1}{s}\,. \tag{3-19}$$

Equations (5), (6), (15), (16), and (19) may be combined to specify the coefficient A and E as

$$A = -\frac{1}{s}\left[\frac{(1 - E^2)(1 + P\sqrt{s}/E)}{(1 - s/E^2)(1 + PE)} - 1\right]^{-1}, \tag{3-20}$$

and

$$E = \left(\frac{2s}{1 + s + Q + [(1 + s + Q)^2 - 4s]^{1/2}}\right)^{1/2}, \tag{3-21}$$

where

$$P = (\varepsilon_s/\varepsilon)^{2.5(q-1)}\,. \tag{3-22}$$

Equation (18), together with the definitions of τ and L, indicates that the variable s is inversely proportional to the exchange current density. Consequently, inversion of Eq. (17) in the limit as $s \to 0$ should give a moderate time solution for the dimensionless transfer current. Two terms in the inverse Laplace transform for Eq. (17) are

$$J = \sqrt{1 + Q}\,\lambda e^{-\sqrt{1+Q}\,Y} + \frac{1 - \lambda}{\sqrt{\pi(1 + Q)\tau}}\,e^{-\eta^2}, \tag{3-23}$$

where

$$\lambda = \frac{P\sqrt{1 + Q} + 1}{P\sqrt{1 + Q} + 1 + Q} \tag{3-24}$$

and

$$\eta = Y/2\sqrt{(1 + Q)\tau} \ . \qquad (3-25)$$

The variables Y and η can be regarded as inner and outer perturbation parameters, respectively. In the region $Y \lesssim 0(1)$, Eq. (23) describes the reaction zone immediately adjacent to the separator, whereas in the region $\eta \gtrsim 0(1)$ it describes the progressive penetration of the reaction through the electrode. The first term in the equation represents a time-independent spike in J which is largest at the separator and which penetrates a relatively short distance into the electrode. The factor $\sqrt{1 + Q}$ in the exponent reflects the influence of diffusion on the spike shape.

The fraction of the total current associated with the spike, λ , is an important parameter in the description of an electrode process with a high exchange current density. If λ is small, most of the current will be progressively distributed through the electrode whereas, as λ approaches unity, it becomes more acceptable to disregard the time-dependent term in equation (23) and to assume that the reaction is restricted to the spike alone. The spike is sharper for larger exchange current densities, and in the limit of infinite exchange current density it will become a Dirac δ function (with area λI) at the electrode/separator interface. Consequently, in electrode models that neglect the surface overpotential (reversible kinetics, $i_o = \infty$), only a fraction $(1 - \lambda)$ of the total current should be distributed through the electrode.

Two examples have been chosen to illustrate these concepts; the positive plate of a lead-acid battery and the negative electrode of a $LiAl/FeS_x$ high temperature cell with molten LiCl, KCl electrolyte. For the lead-acid system, it is assumed that the electrolyte dissociates completely. The reaction for discharge of the lead dioxide electrode is then

$$\frac{1}{2}\,PbO_2 + 2H^+ + \frac{1}{2}\,SO_4^{--} + e^- = \frac{1}{2}\,PbSO_4 + H_2O \;. \qquad (3\text{-}26)$$

The stoichiometric coefficients defined in accordance with Eq. (1) are, $s_+ = -2$, $s_- = -\frac{1}{2}$, $s_0 = 1$, and $n = 1$. With the electrode parameters given in Table 1, the model proposed indicates that 39% of the superficial current density is associated with the time-independent spike in Eq. (23). Alternatively, if incomplete dissociation of electrolyte were assumed, it would be necessary to change the stoichiometric coefficients for the electrode reaction, the cation transference number, and the activity coefficient for the electrolyte in a consistent manner.

The reaction at the LiAl electrode of the high temperature battery is

$$LiAl \rightarrow Al + Li^+ + e^- \qquad (3\text{-}27)$$

and therefore, $s_+ = -1$, $s_- = 0$, $s_0 = 0$ and $n = 1$. Table 1 lists system parameters for discharge with an electrolyte of eutectic composition. The analysis shows that 85% of the total current is in the spike. Figure 1 gives the dependence of the dimensionless transfer

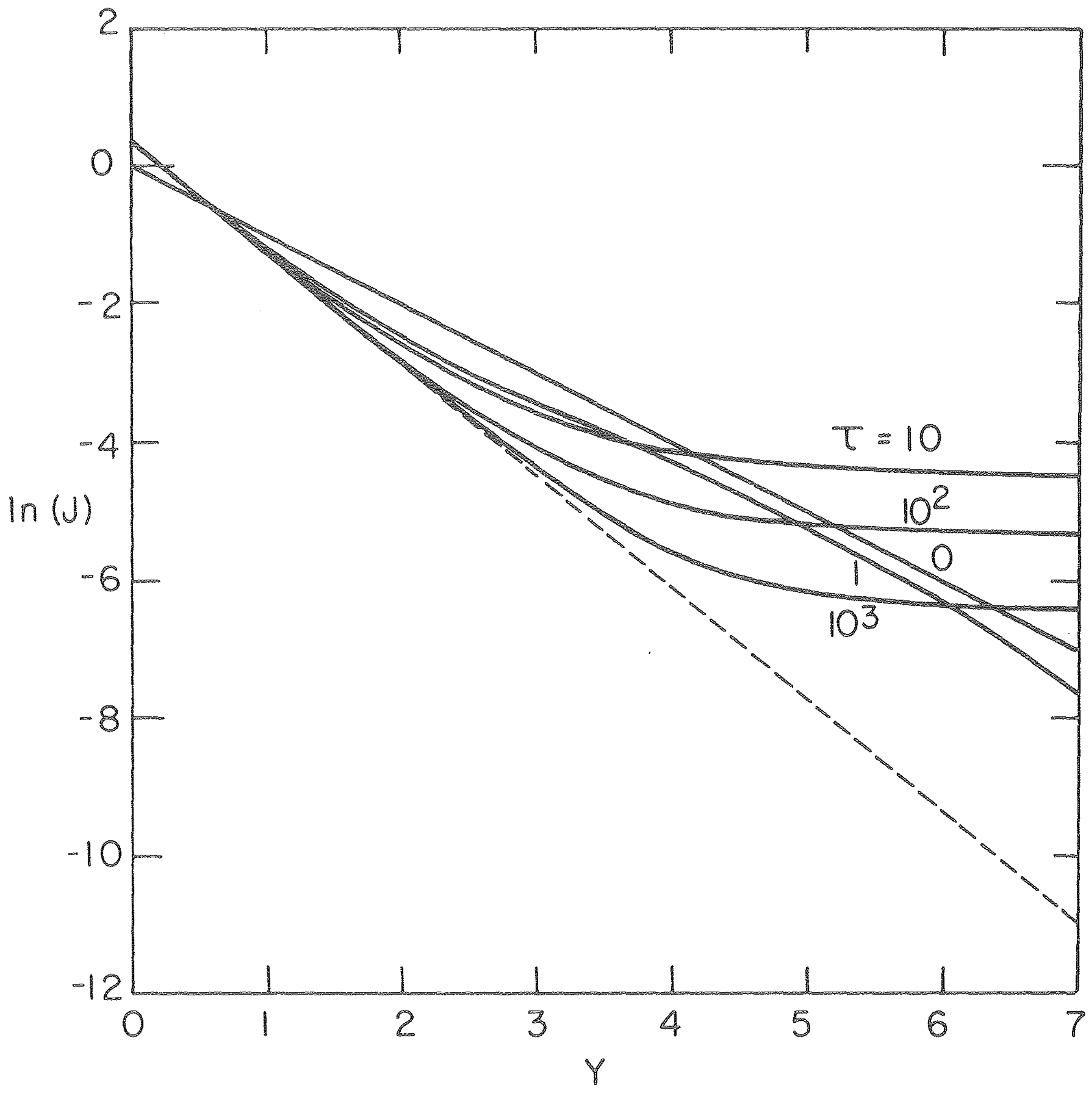

XBL7810-6071

Fig. 3-1. Solution in the inner region for the dimensionless transfer current at different times, τ, for the LiAl electrode, as predicted with Eq. (23). The solution at $\tau = 0$ is from Eq. (28).

----- time-independent spike.

Table 3-1. Typical parameters for PbO_2 and LiAl electrodes

Parameter	PbO_2	LiAl	Parameter
κ_∞(mho/cm)	0.91	1.75	κ_∞(mho/cm)
$D_\infty x10^5(cm^2/s)$	3.03	3.33	$D_\infty x10^5(cm^2/s)$
T(K)	298.15	723.15	T(K)
ε_s^o	0.56	0.75	ε_s^o
ε^o	0.52	0.20	ε^o
$\alpha_a = \alpha_c$	0.50	0.50	$\alpha_a = \alpha_c$
$10^3 c_e^o (mol/cm^3)$	5.00	0.58	x_A^o
$\rho(g\ /cm^3)$	1.29	33.92	$\tilde{V}(cm^3/mol)$
$1 + \frac{d \ln \gamma}{d \ln m}$	2.30	1.92	$1 + \frac{d \ln \gamma_A}{d \ln x_A}$
t_+^o	0.73	0.29	t_1^*
P	1.10	5.22	P
Q	6.17	1.60	Q
λ	0.39	0.85	λ
L(cm)	0.42	1.32×10^{-3}	L(cm)

current on the inner perturbation parameter Y for the LiAl electrode. For small values of Y, the major contribution to J is from the time-independent term in Eq. (23), and the distance over which the spike is dominant increases with time for $\tau \gtrsim 10$. At progressively larger times the reaction penetrates further into the electrode, and J falls locally in response to the requirement of constant total current. Eventually the material closest to the separator will become depleted of reactant, and the narrow reaction zone will then move through the electrode as the available material is consumed. At this stage, the analysis presented here will no longer be valid. Additional complications can arise if local changes in composition significantly affect the exchange current density through Eq. (3). For example, if i_o is most sensitive to the reactant concentration, it is expected that the spike will become more diffuse as the reaction proceeds. This is not accounted for by the model, although concentration changes are included in the nonsteady state material balance, Eq. (14).

The zero time solution of Eq. (17),

$$J = e^{-Y} , \qquad (3\text{-}28)$$

is also shown in Fig. 1 in order to emphasize how the reaction distribution becomes separated into two components that correspond to the two terms in Eq. (23). The apparent agreement between the zero time solution and the reaction distribution at $\tau = 1$ is coincidental; the moderate time solution cannot be extended to $\tau < 1$ and, moreover, an assessment of the influence of higher order terms not shown in Eq. (23) is needed to establish its validity at $\tau = 1$.

Figure 2 shows the inner solution at moderate times for the PbO_2 electrode. The different values for the parameters Q and λ, in comparison with the LiAl electrode, both make the penetration of the spike smaller and hence reduce the contribution of this term to the total transfer current at a given position in the electrode. The penetration depth for the PbO_2 system, as calculated with Eq. (9), is approximately 0.4 cm, which is considerably larger than the corresponding value for the LiAl electrode (see Table 1). Since the assumption, $L << 1$, is used in the high current density analysis for the PbO_2 electrode, the results should be treated with caution and, in particular, the assumption of reversible kinetics that has been used previously[21,22] requires some justification.

The outer solution for J for the LiAl electrode at moderate times is given in Fig. 3 in terms of the outer perturbation parameter, η. The incomplete curves show the contribution of the time-dependent term in Eq. (23). The intercepts of these parabolae represent inner limits of the outer expansion, given by $(1-\lambda)/\pi\sqrt{(1+Q)\tau}$. This is also seen in Fig. 1 as the magnitude of J in the region where the current associated with the spike is negligible. The dimensionless distance within which half the current that penetrates is to be found is given by $0.98\sqrt{(1+Q)\tau}$. This dependence indicates that the process is dominated by diffusion but that interactions between diffusion and reaction modify the current distribution.

The reaction rate distribution at very short times is obtained as a power series expansion in τ, by inversion of Eq. (17) in the limit as $s \to \infty$. It is found that

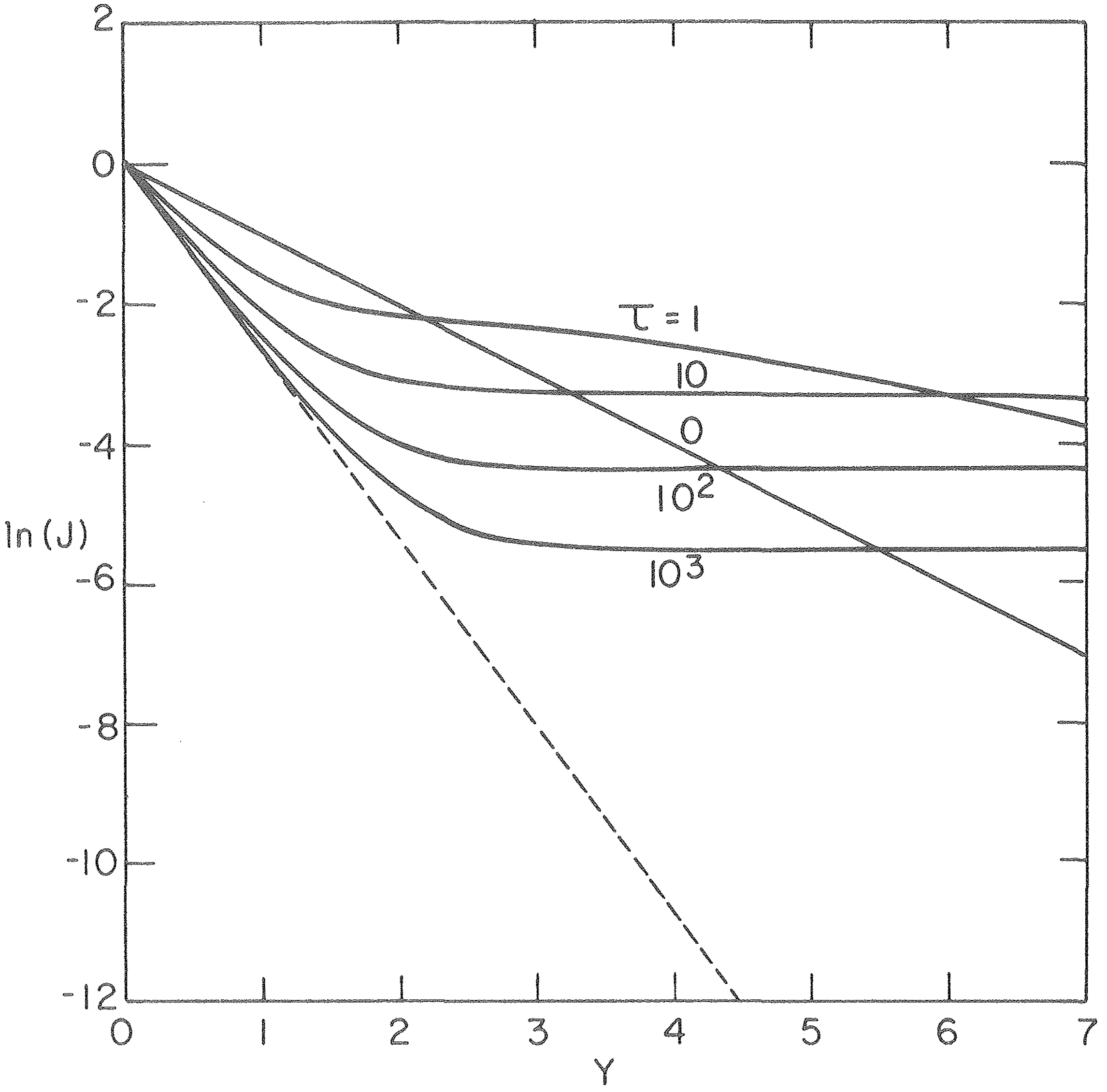

XBL 7810-6072

Fig. 3-2. Solution in the inner region for the dimensionless transfer current at different times, τ, for the PbO_2 electrode, as predicted with Eq. (23). The solution at $\tau = 0$ is from Eq. (28).
------ time-independent spike.

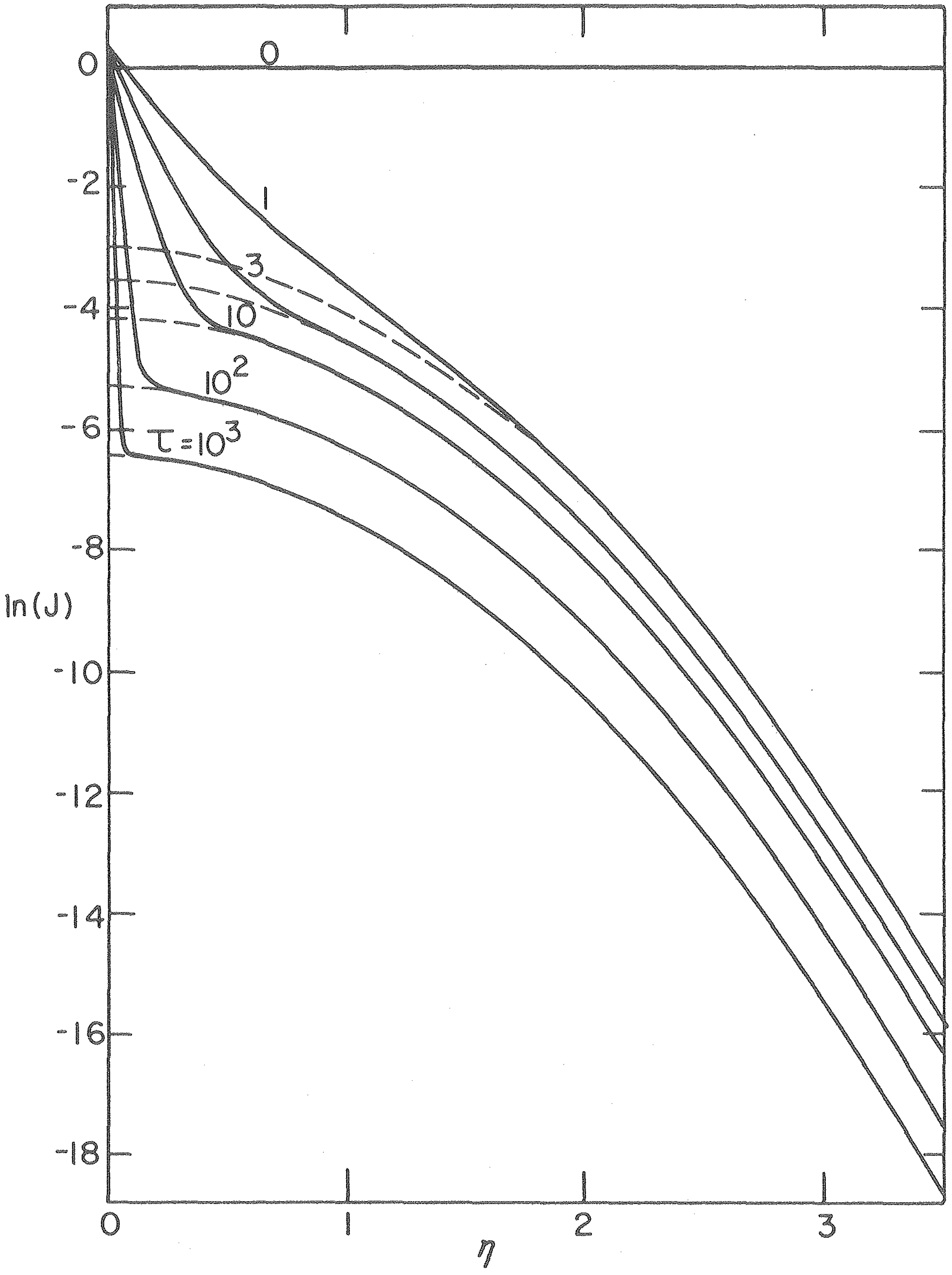

XBL 7810-6073

Fig. 3-3. Solution in the outer region for the dimensionless transfer current at different times, τ, for the LiAl electrode as predicted with Eq. (23). The solution at $\tau = 0$ is from Eq. (28).
----- time-dependent term in Eq. (23).

$$J = e^{-Y}\left[I_o(\alpha) - \frac{Q\tau}{\alpha} I_1(\alpha) - \frac{2\sqrt{2}\ PQ}{1+P}\left(\frac{\tau}{\alpha}\right)^{3/2} I_{3/2}(\alpha)\right] + \left(\frac{PQ}{1+P}\right)\tau\left[(1+2z^2)\ \mathrm{erfc}(z) - \frac{2z}{\sqrt{\pi}}\ e^{-z^2}\right] + \left(\frac{8Q}{1+P}\right)\tau^{3/2}\left[\frac{(1+z^2)}{6\sqrt{\pi}}\ e^{-z^2} - \frac{z}{4}\left(1+\frac{2z^2}{3}\right)\mathrm{erfc}(z)\right] \tag{3-29}$$

where $\alpha = \sqrt{2Q\tau Y}$, $z = \sqrt{1+Q}\ \eta$, and $I_\nu(\alpha)$ is a modified Bessel function of the first kind and of order ν .

For short times, e.g. $\tau < 0(10^{-2})$, J can be predicted adequately by the zero time solution, Eq. (28). At first sight, the e^{-Y} term in Eq. (29) would seem to be equivalent to the spike observed in the moderate time solution. Numerically, however, the clear distinction between the two contributions at moderate times has not developed at the short times for which Eq. (29) is valid. This range of validity can be assessed by a comparison of the first order, short-time approximation for J with the approximations accurate to orders τ and $\tau^{3/2}$ (J_1, J_2, J_3 respectively). Figure 4 shows that, for the LiAl electrode, the validity of Eq. (29) becomes questionable for $\tau > 0.1$. At $\tau = 0.1$, inclusion of the $\tau^{3/2}$ term causes a relatively minor shift in J_2 . At $\tau = 0.5$, the difference between J_2 and J_3 indicates that higher order terms are needed to obtain a satisfactory solution. For the PbO_2 electrode, the range of validity of Eq. (29) is restricted to even smaller values for τ because the parameter Q is significantly larger than for the LiAl system (see Table 1).

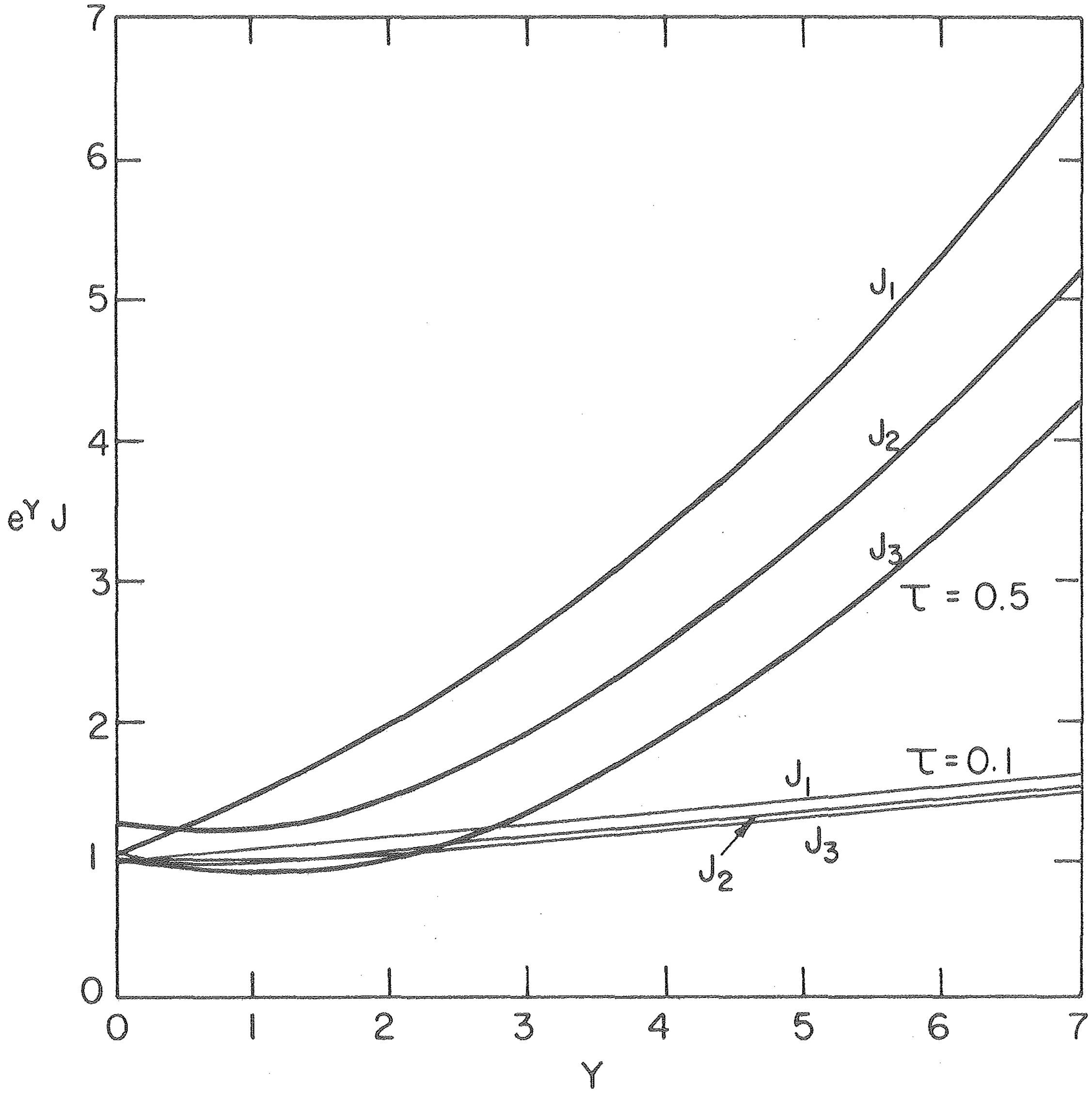

XBL 7810-6074

Fig. 3-4. Reaction rate distribution for LiAl electrode at short times, as predicted with Eq. (29). J_1, J_2, J_3, are first, second, and third order approximations, respectively.

The distinct differences in short and moderate time behavior predicted by Eqs. (23) and (29) preclude the formation of a combined perturbation expansion that would provide an acceptable link between the two time regions. A more general inversion of the solution in Laplace space, Eq. (17), is needed to be able to predict this intermediate behavior.

Conclusions

A simplified macrohomogeneous model can be used to elucidate the transient behavior of porous electrodes with high exchange current densities. The highly nonuniform initial reaction distribution changes at moderately short times due to the influence of concentration overpotential. The analysis presented can be used to predict the magnitude of these changes and to characterize the time-dependent and time-independent components of the transfer current at a given position within the electrode. The results show clearly the association between high exchange current densities and nonuniform reaction distributions which can, in turn, have a significant impact on battery performance.

4. GALVANOSTATIC DISCHARGE BEHAVIOR OF THE LITHIUM-ALUMINUM, IRON SULFIDE CELL

Introduction

The LiAl/LiCl,KCl/FeS_x high temperature battery is a candidate for off-peak electrical energy storage and for electric vehicle propulsion. A mathematical model is needed to predict the operational characteristics of the system and to assess the influence of changes in design parameters on the cell performance.

Many models have been proposed to describe the behavior of flooded porous electrodes, and current and reaction distributions in a direction perpendicular to the separator have been considered in great detail.[10] The electrode can be regarded as a homogeneous mixture of matrix and electrolyte[14] or as a single pore, provided that proper averages are taken over a cross-section.[11,24]

The macrohomogeneous model has been applied to several specific battery electrodes. An analysis of the constant current discharge behavior of electrodes with sparingly soluble reactants, such as the Ag-AgCl and Cd-$Cd(OH)_2$ couples, has elucidated the relative importance of different failure modes in these systems.[11] Transient and failure analyses have also been made of the zinc electrode[12] and the lead dioxide electrode.[21,22] An assessment of steady-state composition profiles in lithium/sulfur battery analogues has been made, but the results are restricted to non-porous systems.[25]

Far less effort has been directed towards modeling complete cells and, up until now, only the lead-acid cell has been considered in detail.[19,26-28] In this chapter, a one-dimensional model is presented for the LiAl/FeS system, which is currently being developed at the Argonne National Laboratory.[3] A whole prismatic cell is considered, consisting of negative electrode, separator, electrolyte reservoir, and positive electrode (see Fig. 1). The model can be used to identify system limitations and to help guide experimental research.

Model Development

The analysis is based on the macroscopic theory of porous electrodes in which the solution and matrix phases are treated as superposed continua without regard for the actual geometric details of the pores.[14] With this approach, one can obtain a consistent framework for the description of isothermal transport processes in the molten salt electrolyte (see chapter 2).

A material balance for species i is given by

$$\frac{\partial(\varepsilon c_i)}{\partial t} = aj_{in} - \nabla\cdot\underline{N}_i \ , \tag{4-1}$$

where $\underline{N}_i$ is the flux of species i in the pore solution averaged over the cross-sectional area of the electrode and where aj_{in} represents the transfer rate of species i from the solid phases to the pore solution per unit electrode volume. In addition, the superficial current density in the pore solution is due to the movement of charged species:

$$\underline{i}_2 = F \sum_i z_i\underline{N}_i \tag{4-2}$$

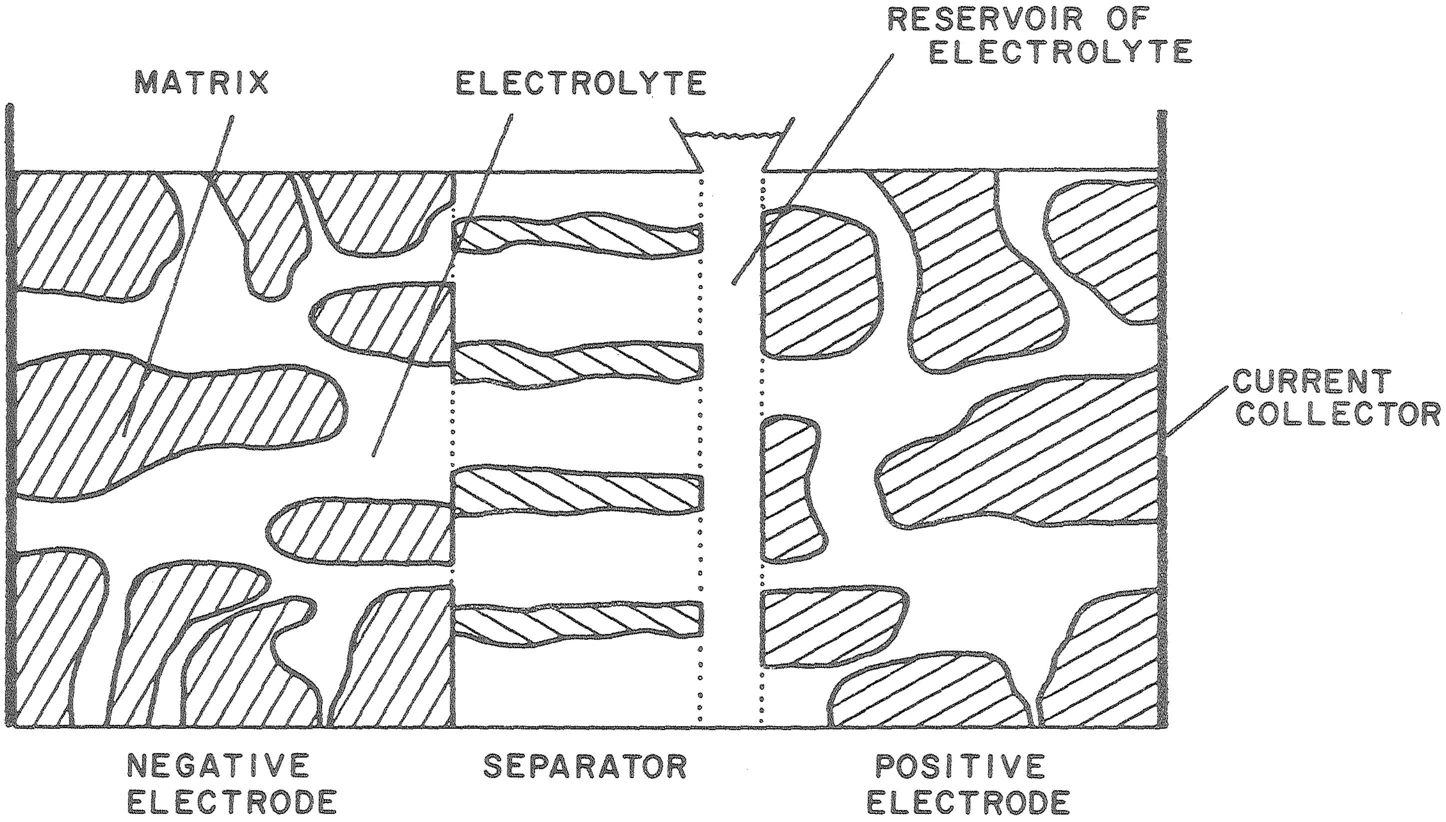

XBL 7910-12435A

Fig. 4-1. Schematic diagram of LiAl/FeS cell.

and, as a consequence of the condition of electrical neutrality, the divergence of the total current density is zero:

$$\nabla\cdot\underline{i}_1 + \nabla\cdot\underline{i}_2 = 0 \ . \tag{4-3}$$

For j simultaneous reactions of the form

$$\sum_i s_{ij} M_i^{z_i} \rightarrow n_j e^- \ , \tag{4-4}$$

Faraday's law can be expressed as

$$a j_{in} = - \sum_j \frac{s_{ij}}{n_j F} a i_{nj} - \frac{1}{\tilde{V}_k} \frac{\partial \varepsilon_{pk}}{\partial t} \ , \tag{4-5}$$

provided that double layer charging can be ignored. The last term on the right hand side of Eq. (5) represents the removal of species i from the electrolyte as a result of precipitation of salt k . The transfer current per unit electrode volume $\nabla\cdot\underline{i}_2$ is related to the individual average transfer current densities by

$$\nabla\cdot\underline{i}_2 = \sum_j (a i_n)_j \ . \tag{4-6}$$

A material balance on the solid phases indicates how the electrode porosity changes with the extent of reaction at each location within the electrode:

$$\frac{\partial(\varepsilon+\varepsilon_p)}{\partial t} = \sum_j \sum_{\substack{\text{solid}\\ \text{phases}}} \frac{s_{ij}\tilde{V}_i}{n_j F} (a i_n)_j \ , \tag{4-7}$$

where $\varepsilon_p = \sum_k \varepsilon_{pk}$.

The flux of mobile species in the electrolyte can be attributed to the combined effects of diffusion, migration, and convection. For the LiCl - KCl electrolyte, the fluxes of lithium and potassium ions are given by (see Eq. (2-13)):

$$\underline{N}_1 = - \frac{\varepsilon D}{\tilde{V}} \nabla x_A + \frac{t_1^{\star} \underline{i}_2}{F} + x_A (c_A + c_B) \underline{v}^{\star} \qquad (4\text{-}8)$$

$$\underline{N}_2 = - \frac{\varepsilon D}{\tilde{V}} \nabla x_B + \frac{t_2^{\star} \underline{i}_2}{F} + x_B (c_A + c_B) \underline{v}^{\star} \quad . \qquad (4\text{-}9)$$

These relationships can be substituted into Eq. (1) to give, respectively,

$$\frac{\partial (\varepsilon x_A / \tilde{V})}{\partial t} + \nabla \cdot [x_A \underline{g} + (x_B t_1^{\star} - x_A t_2^{\star}) \frac{\underline{i}_2}{F} - \frac{\varepsilon D}{\tilde{V}} \nabla x_A] = a j_{in} \qquad (4\text{-}10)$$

$$\frac{\partial (\varepsilon x_B / \tilde{V})}{\partial t} + \nabla \cdot [x_B \underline{g} + (x_A t_2^{\star} - x_B t_1^{\star}) \frac{\underline{i}_2}{F} - \frac{\varepsilon D}{\tilde{V}} \nabla x_B] = a j_{2n} \quad , \qquad (4\text{-}11)$$

where

$$\underline{g} = \frac{\underline{v}^{\star}}{\tilde{V}} + (t_1^{\star} + t_2^{\star}) \frac{\underline{i}_2}{F} \quad . \qquad (4\text{-}12)$$

For the special case where $t_1^{\star} = x_A/2$ and $t_2^{\star} = x_B/2$, the direct dependence of Eq. (10) and (11) on current density is removed. The molar average velocity has been chosen as the reference frame because physical data for LiCl-KCl mixtures are often correlated with the mole fraction (see Appendix B).

The movement of electrons in the matrix phase is governed by Ohm's law

$$\underline{i}_1 = -\sigma \nabla \Phi_1 \ , \tag{4-13}$$

where σ is the effective conductivity of the matrix. In the electrolyte, the variation in solution potential is given by

$$\frac{\underline{i}_2}{\kappa} = -\nabla \Phi_2 - \frac{1}{F}\left[\left(\frac{s_1}{n} + t_1^c\right)\frac{1}{x_B} - \frac{s_3 x_A}{n x_B}\right]\nabla \mu_A \ , \tag{4-14}$$

where Φ_2 is measured with a reference electrode that has stoichiometric coefficients s_i and number n of electrons transferred, and μ_A is the chemical potential of LiCl (see Appendix B). Equations (13) and (14) may be combined to obtain variations in the overpotential $\eta = \Phi_1 - \Phi_2$ directly.

Polarization equations are needed to express the dependence of the local rate of each reaction on the various concentrations and on the potential difference driving force at the reaction interface. Electrode kinetics do not follow fundamental laws that can be expressed as reliably as Ohm's law or the law of conservation of matter. Consequently, the polarization relationships will be subject to further refinement, as one tries to account not only for the mechanism of the charge transfer process but also for the morphology of the electrode, the formation of covering layers, and the transport of species to and from the reaction site.

It is common to begin with a polarization equation of the form

$$i_{nj} = i_{oj} \left[e^{\alpha_{aj} F \eta_{sj}/RT} - e^{-\alpha_{cj} F \eta_{sj}/RT} \right] \tag{4-15}$$

where η_{sj} is the local value of the surface overpotential, $\eta_{sj} = \eta - U_{j,o}$, and where the exchange current density i_{oj} can be written as

$$i_{oj} = i_{oj,ref} \prod_{i} \left(\frac{c_{i,o}}{c_{i,ref}} \right)^{\gamma_i} \prod_{k} a_k^{\gamma_k} \; . \tag{4-16}$$

The theoretical open circuit cell potential for reaction j is given by[29]

$$U_{j,o} = U_j^{\theta} - U_{re}^{\theta} + \frac{RT}{n_{re}F} \sum_i s_{i,re} \ln a_{i,re} - \frac{RT}{n_j F} \sum_i s_{i,j} \ln a_{i,o} \, . \tag{4-17}$$

The discharge reaction in the negative electrode is

$$\mathrm{LiAl} \rightarrow \mathrm{Li}^+ + \mathrm{Al} + e^- \; . \tag{I}$$

In the fully charged state, it is assumed that the negative matrix consists of non-porous, spherical particles of β-LiAl. On discharge, the outermost region of a particle reacts first and a layer of α-Al is established which thickens gradually, at the expense of β-LiAl, as the reaction proceeds. The Butler-Volmer equation (15) should be modified to include the diffusional overpotential for mass transport of lithium across the α-phase to the solid-electrolyte interface.

The parameter

$$S = \frac{3.87(1-\varepsilon) I}{nF \bar{c}_{Li}^{\beta} L a^2 D_{\alpha}} \tag{4-18}$$

can be used as a criterion to assess the importance of solid state diffusion within a LiAl particle.[30] Small values of S indicate that the time required for diffusion is much shorter than the time needed for complete utilization of the particle. Even though $S \sim O(0.1)$ for this system, the influence of solid state diffusion may be appreciable at high current densities or with low specific interfacial areas, particularly towards the end of discharge. However, for $S < 1$, it is reasonable to invoke the pseudo-steady state approximation to evaluate the composition profile within the α-phase. With this assumption, and with unit activity coefficients, the surface concentration of lithium can be written as (see Appendix C):

$$\frac{(c^{\alpha}_{Li})_o}{(c^{\alpha}_{Li})_{sat}} = 1 - \frac{\nabla \cdot \underline{i}_2}{(\nabla \cdot \underline{i}_2)_{lim}} . \tag{4-19}$$

The diffusion-limited transfer current is given by

$$(\nabla \cdot \underline{i}_2)_{lim} = \frac{4\pi N F D_{\alpha} (c^{\alpha}_{Li})_{sat}}{(1 - \bar{x}^{\alpha}_{Li})\left(\frac{1}{r_{\beta}} - \frac{1}{r_{\alpha}}\right)} , \tag{4-20}$$

where r_{α} and r_{β} can be related to the state of charge. Combination of Eq. (6), (15), (19), and (20) gives

$$\nabla \cdot \underline{i}_2 = \frac{e^{\alpha_a F\eta/RT} - e^{-\alpha_c F\eta/RT}}{\dfrac{1}{4\pi N r_{\alpha}^2 \, i_{o,ref} \left(\dfrac{x_A}{x_{A,ref}}\right)^{\gamma_{Li^+}}} + \dfrac{e^{\alpha_a F\eta/RT}}{(\nabla \cdot \underline{i}_2)_{lim}}} , \tag{4-21}$$

where η is measured with a reference electrode of the same kind as the working electrode, but with a fixed lithium activity corresponding to saturated β-phase (see Table 1). Implicit in Eq. (21) are the assumptions that there is no more reaction after the β-LiAl is completely transformed to α-Al and that there are no variations in electrolyte composition between the center of a pore and the adjacent solid surface.

The complicated discharge processes in the positive electrode are represented by two simultaneous reactions:

$$2FeS + 2Li^+ + 2e^- \rightarrow Li_2FeS_2 + Fe \qquad \text{IIA}$$

$$Li_2FeS_2 + 2Li^+ + 2e^- \rightarrow 2Li_2S + Fe \qquad \text{IIB}$$

Equation (15) is used to describe the rate of each reaction and the reference electrode is taken to be the same kind as reaction IIB (see Table 1). More sophisticated models for the positive electrode kinetics could include additional intermediate reactions, diffusion of reactants and products to and from reaction sites, and crystallization overpotentials for the formation of solid products. However, the detailed mechanism of the reactions and the juxtaposition of the different phases have not yet been formally established and are the subject of a separate study.[32] At the high operating temperatures of the lithium/iron sulfide system, and with the relatively high concentration of lithium ions in the electrolyte, the rate of reaction is expected to be high and, therefore, the simplified kinetic analysis may be adequate.

Table 4-1. Kinetic parameters used in model

Negative Electrode		Positive Electrode	
Parameter	Value	Value	Parameter
$\alpha_a = \alpha_c$	0.5	1.0	$\alpha_{aj} = \alpha_{cj}$
n	1.0	2.0	n_j
s_1	-1.0	-2.0	$s_{1,j}$
s_3	0.0	0.0	$s_{3,j}$
$(x_A)_{ref}$	0.58	1.0	$(x_A)_{ref}$
γ_{Li^+}	0.5	1.0	γ_{Li^+}
i_o(A/cm^2)	2.8	2.0×10^3	$(ai_o)_j$ (A/cm^3)
D_α(cm^2/s)[31]	4.0×10^{-10}	0.0326	$U_{IIA,o}$ (V)
$\bar{x}^{\alpha}_{Li}$	0.05	0.0	$U_{IIB,o}$ (V)

The governing differential equations for the lithium-aluminum/iron sulfide system are subject to the following boundary conditions (see Fig. 1):

(i) at the current collectors;

$$\begin{aligned}&\text{(a)}\quad \underline{N}_i = 0\ ,\\ &\text{(b)}\quad \underline{g} = 0\ ,\\ &\text{(c)}\quad \underline{i}_2 = 0\ ,\end{aligned} \tag{4-22}$$

(ii) at the negative electrode/separator interface;

$$\begin{aligned}&\text{(a)}\quad \underline{i}_2 = I\ ,\\ &\text{(b)}\quad x_A,\ \underline{v}^{\star}\ \text{continuous}\ ,\\ &\text{(c)}\quad \left(\varepsilon D\,\frac{\partial x_A}{\partial y}\right)_s = \left(\varepsilon D\,\frac{\partial x_A}{\partial y}\right)_e\ ,\end{aligned} \tag{4-23}$$

(iii) at the positive electrode/reservoir interface;

$$\begin{aligned}&\text{(a)}\quad \underline{i}_2 = I\ ,\\ &\text{(b)}\quad x_A\ \text{continuous}\ ,\\ &\text{(c)}\quad \frac{V_R}{A}\,\frac{\partial x_{AR}}{\partial t} = \left(\varepsilon D\,\frac{\partial x_A}{\partial y}\right)_e - \left(\varepsilon D\,\frac{\partial x_A}{\partial y}\right)_s\ ,\end{aligned} \tag{4-24}$$

where V_R/A can be estimated from

$$\frac{\partial (V_R/A)}{\partial t} = \underline{v}_s^{\star} - \underline{v}_e^{\star} + \frac{V_R}{A}\,\frac{d\ln\tilde{V}}{dx_A}\,\frac{\partial x_A}{\partial t}\ . \tag{4-25}$$

The electrolyte composition is assumed to be uniform across the reservoir. It should also be noted that alternative formulations can be used for the boundary conditions at the front of the electrodes. These choose control volumes for the material balances that avoid the need for separate evaluation of the composition gradients at the interfaces (see Appendix D). In the separator, the governing equations can be simplified in accordance with:

$$\begin{aligned} &\text{a)}\quad \underline{i}_2 = I, \\ &\text{b)}\quad \nabla\cdot\underline{i}_2 = 0, \\ &\text{c)}\quad \varepsilon = \varepsilon_s \quad . \end{aligned} \tag{4-26}$$

The initial conditions are taken as:

$$\begin{aligned} &\text{(i)}\quad x_A = x_A^o , \\ &\text{(ii)}\quad \varepsilon_e = \varepsilon_e^o , \\ &\text{(iii)}\quad \nabla\cdot(\tilde{V}\underline{g}) = \bar{V}_A a j_{1n} + \bar{V}_B a j_{2n} - \frac{\partial \varepsilon}{\partial t} + \frac{\varepsilon}{\tilde{V}}\frac{\partial \tilde{V}}{\partial T}\frac{\partial T}{\partial t} + \tilde{V}\nabla\cdot\left(\frac{\varepsilon D}{\tilde{V}}\nabla x_A\right) , \end{aligned} \tag{4-27}$$

where Eq. (27(iii)) is derived from Eq. (10) and (11).

During discharge the temperature is assumed to be uniform throughout the cell sandwich, but it can change with time in response to reversible heat effects, Joule heating, overpotentials associated with electrode reactions, and precipitation or dissolution of electrolyte. The first law of thermodynamics gives

$$\frac{m\ C_p}{A}\frac{dT}{dt} = [U_o - V - T_o \frac{\partial U_o}{\partial T}]\ I - h_o(T - T_A) + \sum_k \frac{L_k}{\tilde{V}_k} \int_o^{L_T} \frac{\partial \varepsilon_{pk}}{\partial t}\, dy\ , \quad (4\text{-}28)$$

where the transfer coefficient h_o is based on estimated heat losses for a battery module.

The LiAl/LiCl,KCl/FeS system can be described by the local variables x_A, ε, $\underline{i}_2$, $\underline{g}$, and η, and by the governing Eqs. (7), (10), (11), (14), and (15), subject to the specified boundary conditions. These relationships constitute a set of coupled, ordinary, nonlinear differential equations at each time step which are cast into finite difference form accurate to $O(h^2)$, and solved simultaneously by a numerical technique.[6] Each nonlinear equation is linearized properly to assure convergence, and each time-dependent equation is programmed symmetrically between the old time step and the present one, in order to attain stability.

Results and Discussion

Electrolyte Composition

Figure 2 shows composition profiles across the cell sandwich for several times during a constant current discharge of 41.6 mA/cm^2. A lithium-rich electrolyte is used, and the dimensions and capacities of the fully charged electrodes correspond to those of the Argonne National Laboratory Mark 1A cell.[3] When the discharge is started, lithium ions are introduced into the electrolyte at the negative electrode and transported across the porous separator to the positive electrode, where they can react cathodically to form Fe and Li_2FeS_2 or Li_2S.

Fig. 4-2. Position dependence of mole fraction of LiCl at different discharge times. Dashed line represents saturation limit for LiCl at 450°C. Simulation parameters: $N = 1.1 \times 10^8$ cm^{-3}; Table 4-1; Table B-1.

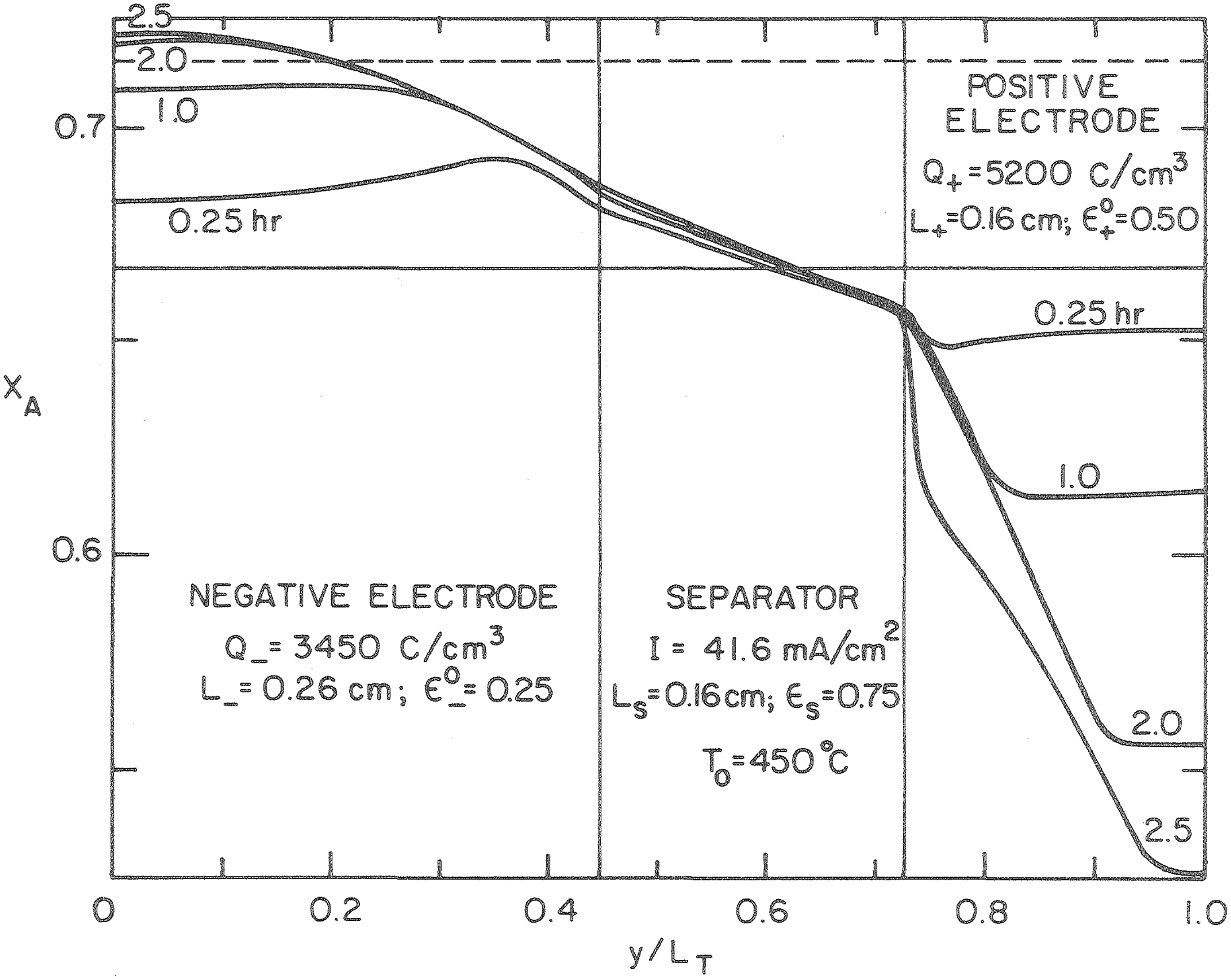

Fig. 4-2.

XBL 7910-7169A

Since the transference number of Li^+ is not unity, a concentration profile develops, and diffusion aids migration in the transport of lithium ions. An almost constant composition gradient is established across the separator that corresponds to the flux of lithium ions needed for the specified current density. The presence of the reservoir attenuates composition changes at the front of the positive, but, within the electrode, the composition variations are accentuated by local porosity changes.

The details of the composition variations can be attributed to the combined effects of diffusion, migration, convection, and electrochemical reaction. The contribution of convection, which arises primarily from the influx or squeezing out of electrolyte as the porosity alters, is expected to be small for this system ($\underline{v}^* \sim O(10^{-5})$ cm/s). However, convection is included in the analysis to ensure that the accuracy of the electrolyte material balances is retained.

The importance of $\underline{v}^*$ was tested by repeating the simulation in Fig. 2, with the temperature dependence of the electrolyte molar volume included in a manner that caused oscillation in $\underline{v}^*$, without adversely affecting the material balances. The results differed by less than 0.2%, except in the region with KCl precipitation, where the largest error in ε_p was 5%. The sensitivity of precipitation to temperature and composition indicates that a significant proportion of this error should be associated with changes in $\tilde{V}$, rather than $\underline{v}^*$.

If the cell temperature remains constant, the model predicts that the electrolyte composition in the negative electrode would cross the solubility limit for LiCl (indicated by the dashed line) after 1.5 hours. However, the average temperature rises by approximately 15°C during this period, and therefore precipitation of LiCl is avoided. Nevertheless, at about 54% depth of discharge, the composition has fallen markedly in the positive electrode and precipitation of KCl is predicted. This is illustrated in Fig. 3, which shows the variations in maximum and minimum electrolyte concentrations during the discharge, in comparison with the saturation compositions. The prediction of large variations in electrolyte composition during discharge emphasizes the need for inclusion of variable physical properties in the theoretical analysis.

The fraction of active material utilized within the negative electrode is shown in Fig. 4, at several discharge times. The large electrode surface area and the high operating temperature help to create fast reaction kinetics. As a result, a highly nonuniform reaction distribution, dominated by ohmic effects, is obtained. Initially, the sharp reaction front is restricted to the electrode/separator interface because an infinite matrix conductivity has been assumed for the simulation (see chapter 3). This reaction zone gradually moves through the electrode as active material is consumed and the potential required for the reaction becomes more positive. At the back of the electrode, the transfer current rises slowly in response to the composition dependent term in the Ohm's law relationship for the electrolyte.

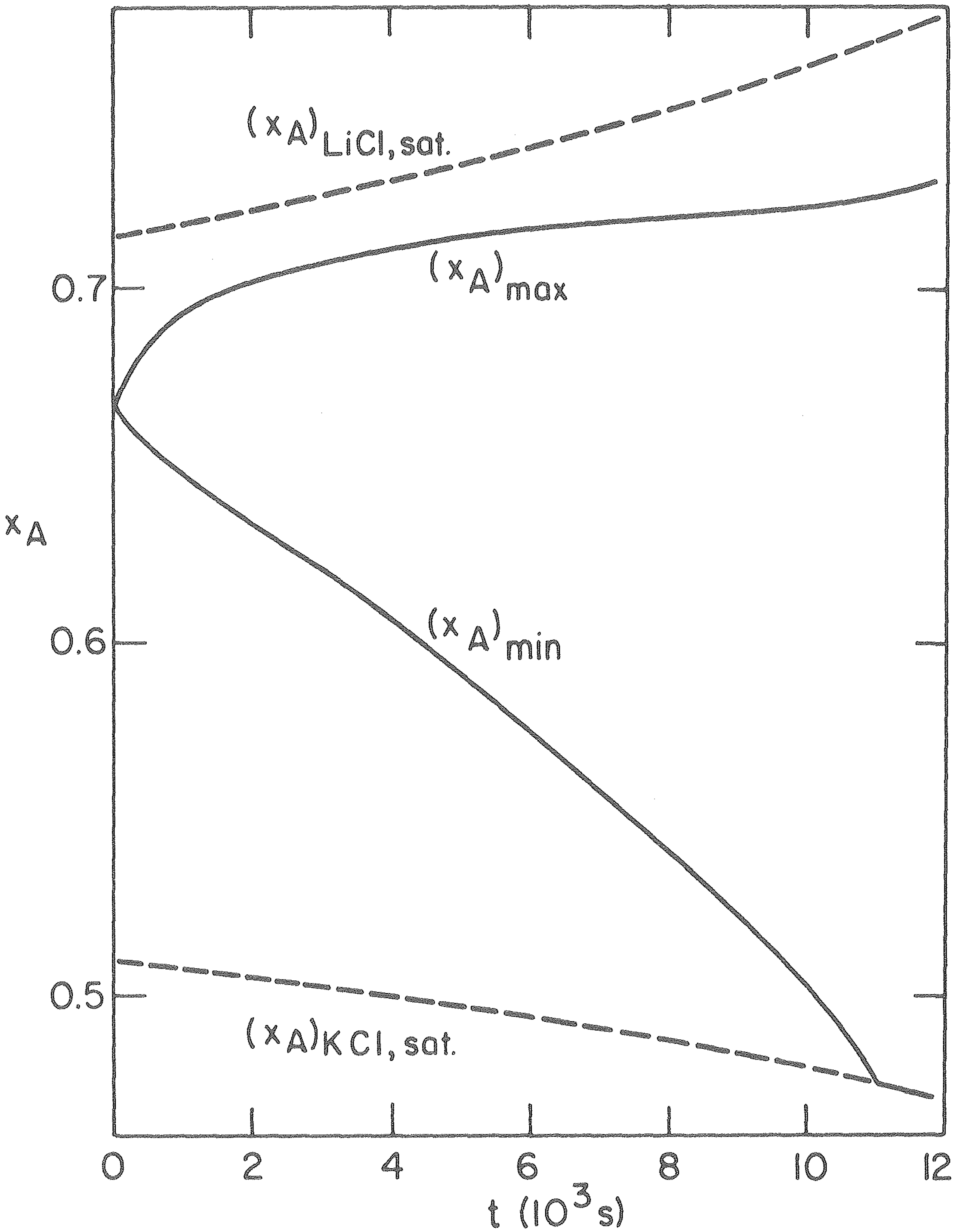

XBL7912-14577

Fig. 4-3. Comparison of variations in saturation limits for LiCl & KCl and maximum & minimum electrolyte concentrations. Parameters as in Fig. 4-2.

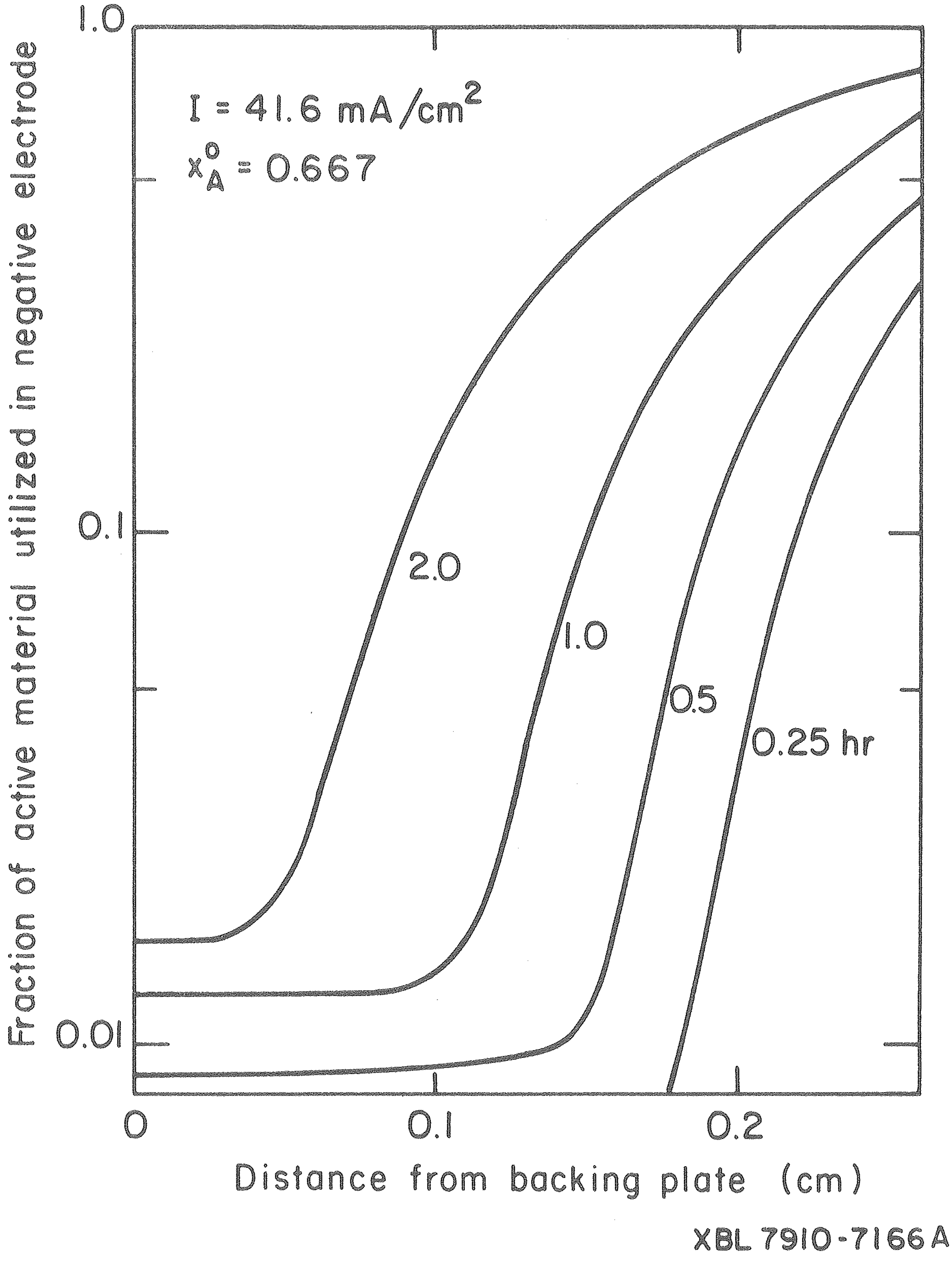

Fig. 4-4. Fraction of active material utilized in negative electrode at different discharge times. Parameters as in Fig. 4-2.

The complementary reaction distributions for the positive electrode are presented in Fig. 5. Reaction IIA starts first, and after two hours it has proceeded about two-thirds of the way through the electrode. The FeS is fully converted to Li_2FeS_2 behind this reaction front, which is itself relatively narrow. Subsequently, a front for reaction IIB begins to move through the electrode, and its influence on the composition can be seen in Fig. 2 at 2.5 hours.

The distance that the first reaction penetrates the electrode before onset of the second front is dependent on the operating conditions. Table 2 indicates that the distance between the fronts is smaller, and hence the reactions are less distinct, with higher current densities or with lower initial electrolyte compositions.

The microstructure in the positive shortly after the second reaction has begun is shown in Fig. 6. In this example, the initial composition is that of the eutectic, 58 mole percent LiCl, and precipitation of KCl occurs at a relatively low depth of discharge. Precipitation is responsible for the extremely small value of the porosity ε at a distance of about 0.075 cm which effectively blocks off the back portion of the electrode. In this isolated region, self-discharge reactions can take place as a result of composition variations in the electrolyte and potential gradients in the matrix. The diagram shows that, in the depth of the electrode, reaction IIA has occurred to some extent, producing a certain volume fraction ε_X of Li_2FeS_2 and slightly decreasing the porosity from its initial value of 0.5. Behind the central reaction front, there is a plateau for

Table 4-2. Characteristics of reaction fronts in positive electrode.

x_A^o	0.58		0.667	
$I(A/cm^2)$	0.0416	0.1	0.0416	0.1
L_{gap}/L_+	0.40	0.18	0.63	0.30
$100t_{f2}/t_f$	22.7	12.2	33.6	17.7

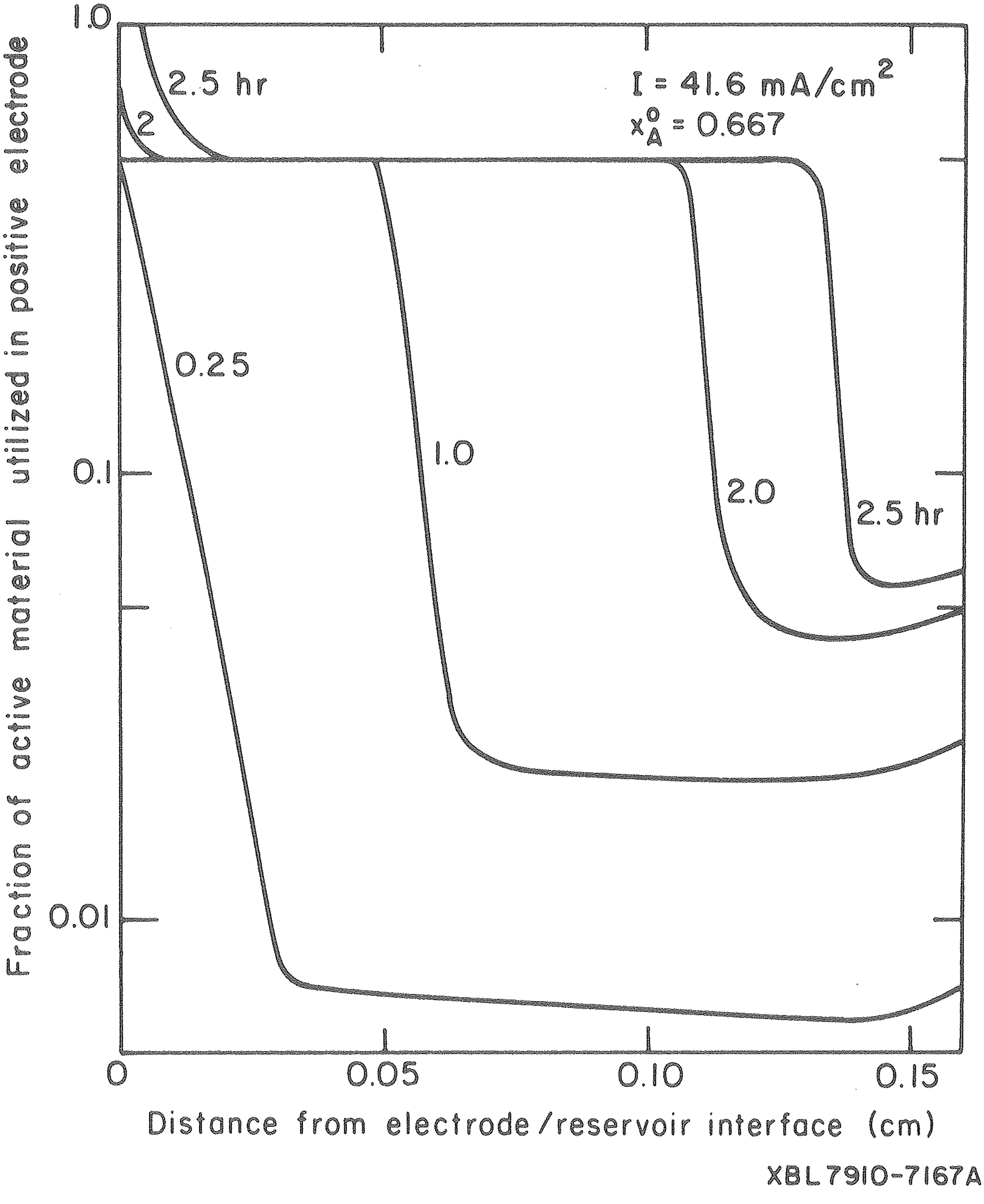

Fig. 4-5. Fraction of active material utilized in positive electrode at different discharge times. Parameters as in Fig. 4-2.

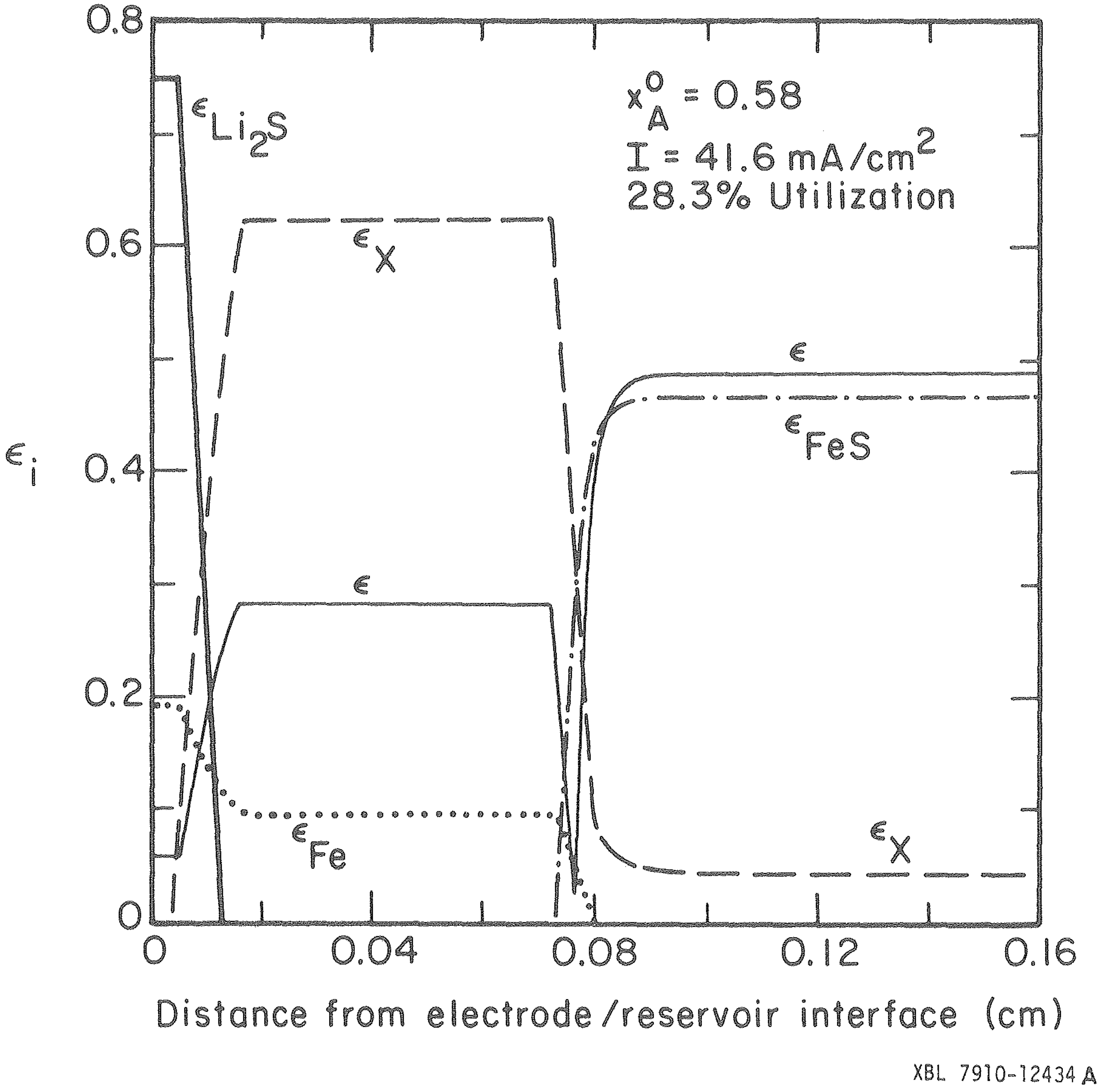

Fig. 4-6. Volume fractions of solid phases and electrolyte in positive electrode. Parameters as in Fig. 4-2, except as indicated.

the values of ε_X, ε, and ε_{Fe} that corresponds to completion of reaction IIA. At distances less than 0.01 cm the consequence of reaction IIB can be seen; Li_2FeS_2 is consumed, Li_2S is produced, and the porosity drops to a small value.

As the first reaction front moves back through the positive electrode, the precipitated region does so also, and it remains as a sharp spike located in the region of highest transfer current. With the progression of the second reaction, the region of precipitation spreads to affect a larger part of the electrode. The local reductions in porosity that result from the large molar volume of the Li_2S and the precipitation of KCl lead to a reduction in local electrolyte conductivity in accordance with Eq. (3-8). Consequently, a significant potential drop can develop across the low porosity region that may severely limit utilization of the electrode. The plugging of porous electrodes has been cited as a possible cause of failure in other electrodes.[12,33] In the zinc electrode, for example, a large volume fraction of ZnO can be produced at the front face early in a discharge, particularly if the reaction distribution is highly nonuniform.

Initial Electrolyte Composition

An important consideration in the development of the LiAl/LiCl, KCl/FeS battery is the choice of initial electrolyte composition, x_A^o. The dependence of composition changes on x_A^o is illustrated in Fig. 7, at two different depths of discharge. The difference between the maximum and minimum electrolyte compositions is larger for smaller x_A^o, and this effect becomes magnified as the discharge proceeds. The

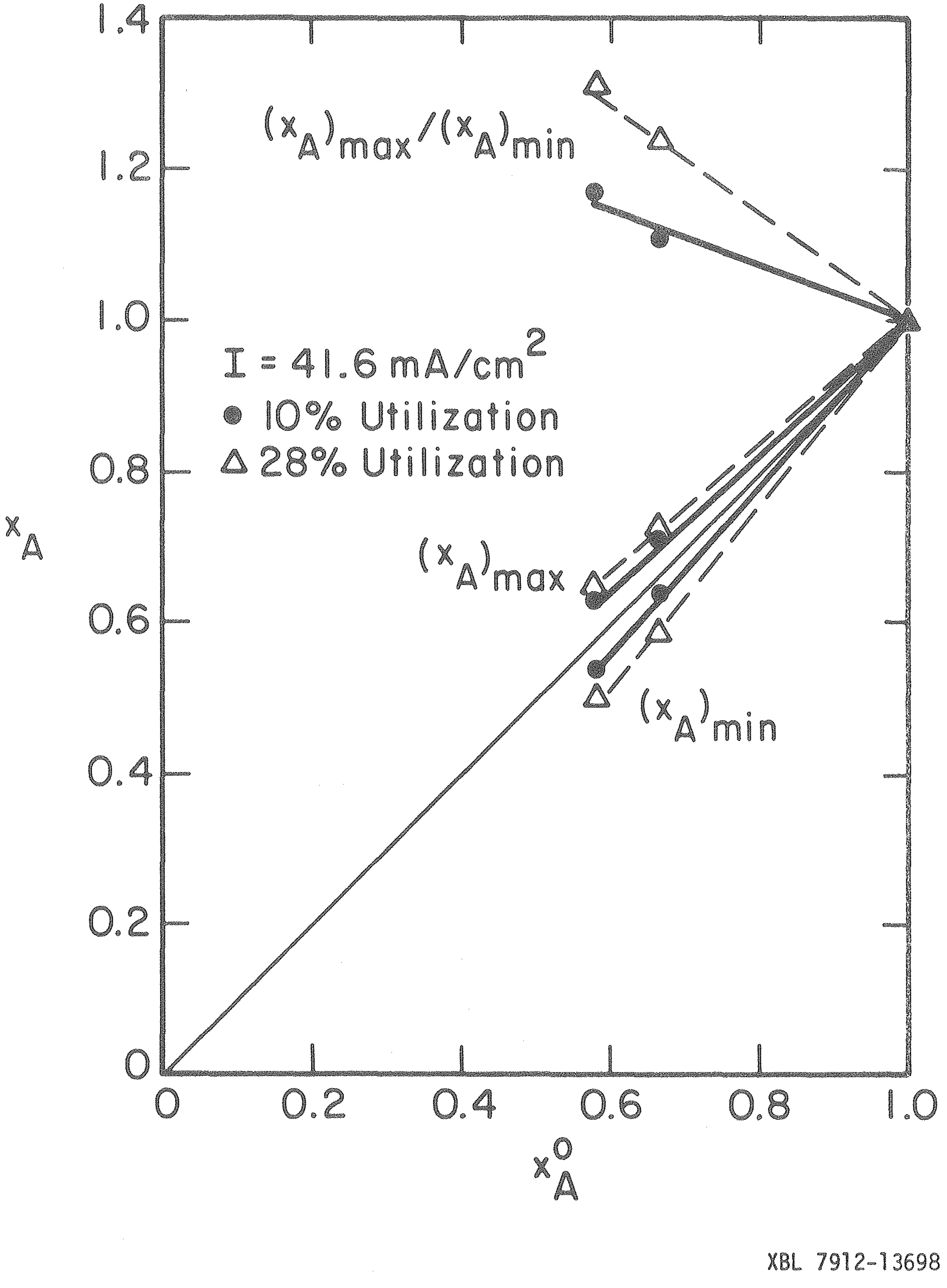

XBL 7912-13698

Fig. 4-7. Dependence of composition variations on initial electrolyte concentration. Parameters as in Fig. 4-2, except as indicated.

composition changes have a direct influence on the extent of precipitation and on the Nernst relationship for the cell potential.

With pure LiCl, there is no concentration polarization, but the minimum operating temperature would be 609°C. For molten salt mixtures with Li^+ as a common ion, the composition changes in the Li/FeS cell are expected to be small. The transport theory developed in chapter 2 can be applied directly to binary electrolytes such as LiCl-LiF. It also applies to more complicated mixtures, such as LiCl-LiF-LiBr, provided that it is reasonable to assume that, from a mass transport standpoint, the anions can be lumped together to give only a single independent composition variable.

If the anions do not participate in the electrode reactions, the production term in the material balance Eq. (2-22B) is given by

$$R_A = \tilde{V} a j_{3n} \left(\frac{c_2 t_1^r}{\nu_2^B \nu_3^A} - \frac{c_1 t_2^r}{\nu_1^A \nu_3^B} \right) . \qquad (4\text{-}29)$$

For electrolytes with unit stoichiometric coefficients, and for transference numbers that are directly proportional to concentration, Eq. (29) reduces to $R_A = 0$ and, therefore, the electrolyte composition is constant. In practice, R_A is still expected to be small even with transference numbers not exactly proportional to concentration, and successful cell operation may be possible at temperatures much closer to the melting point than are permissible with the LiCl-KCl electrolyte.

Discharge curves

An important capability of the model is to predict the dependence of total cell voltage on state of charge. Discharge curves for the Argonne Mark 1A cells are presented in Fig. 8, for several different operating conditions. The upper curves are for a current density of 41.6 mA/cm^2, and the highest of these is for a lithium-rich electrolyte, which has a larger bulk electrolyte conductivity than the eutectic mixture. Two curves are shown for the eutectic, which is the composition actually used in the Mark 1A cell design. Curve A takes account of precipitation of either component of the electrolyte, whereas curve B does not. For all three curves, the sharp reduction in cell voltage can be attributed to the localized porosity reductions in the fully reacted region of the positive electrode. Precipitation reduces the porosity still further, and the decline in voltage is correspondingly more acute. In practice, the porosity changes may not be quite so dramatic because it is possible for the electrodes to swell. Expansion may occur by compaction of the separator and displacement of the can walls during the formation cycles of the cell, or by motion of the electrodes relative to one another during a particular charge or discharge. The extent to which swelling can take place will depend on the stresses generated within the cell and the physical restraints on the container.

At the high current density, the initial cell voltage is considerably reduced as a result of the finite grid resistance (see Appendix B). Also, the cell voltage declines more rapidly since there

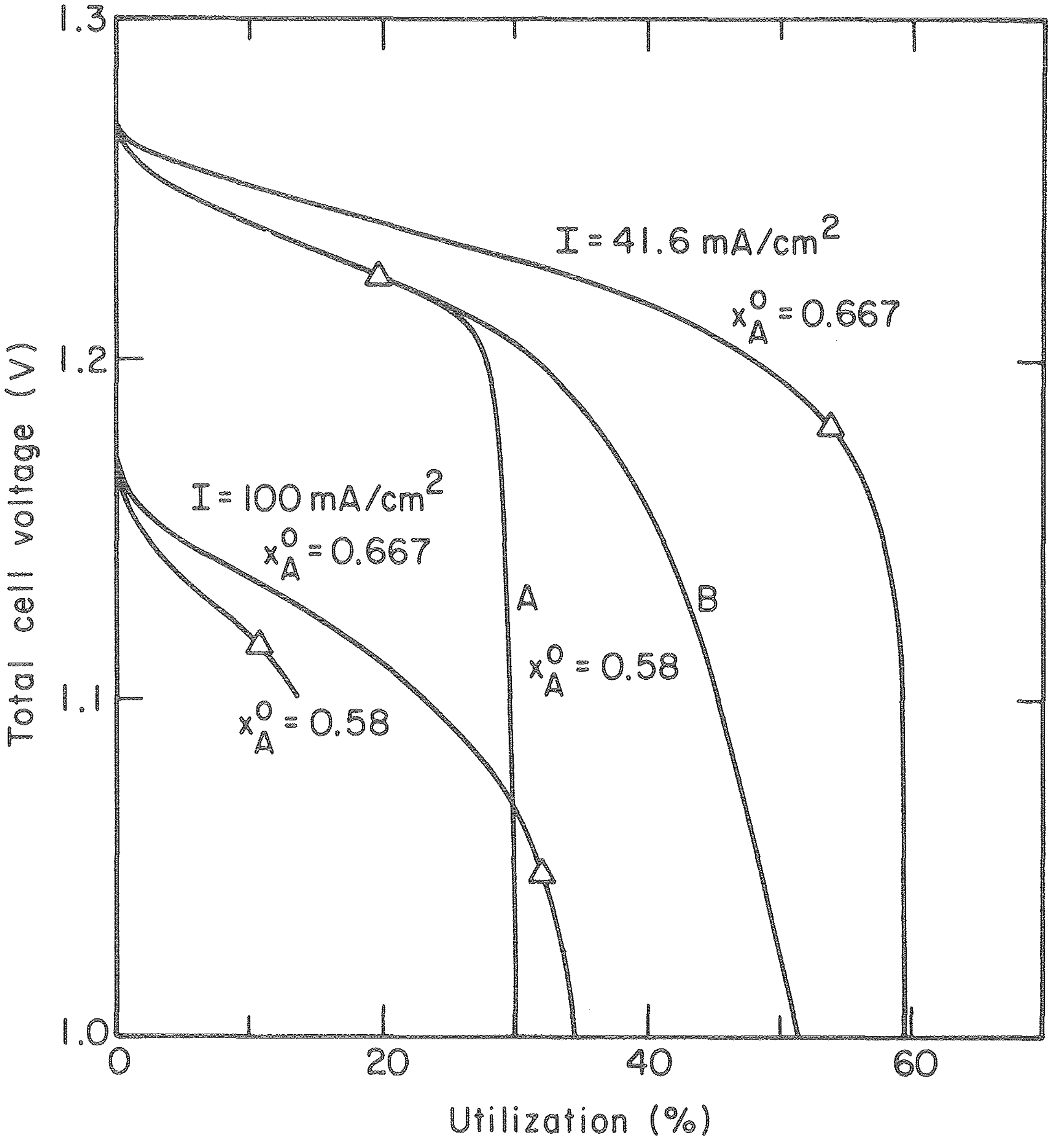

XBL 7910-12253 A

Fig. 4-8. Theoretical discharge curves for Argonne National Laboratory Mark 1A Cells. Parameters as in Fig. 4-2, except as indicated.

is less time available for diffusional processes to take place, and because the reaction distribution in the positive electrode is less uniform (see Table 2).

The triangles in Fig. 8 indicate the onset of precipitation of KCl. They show that, at lower I or higher x_A^o, precipitation is delayed. The exact time when precipitation begins is largely dependent on the details of the heat balance used to estimate the average cell temperature, Eq. (28). Small changes in the rate of heat loss from the battery module, or slight differences in initial cell temperature, could have a significant impact on the extent of precipitation and, possibly, on the cell performance. In the examples shown, precipitation of LiCl is not predicted, even though the maximum composition is close to the solubility limit (see Fig. 3).

Careful consideration of precipitation is needed for several additional reasons. The rate of mass transport from the electrolyte in the bulk of the pores to the matrix surface may influence the rate at which precipitation takes place. This has been included in previous studies of electrodes with sparingly soluble reactants,[34-36] but the effects may not be so important in molten salt systems because the salt concentrations are generally much higher. The morphology of the precipitate may be important, particularly if it forms as a passivating layer over the active material. Furthermore, local thermal effects may influence the extent and nature of precipitation; heat generated as precipitate forms will tend to retard the precipitation process.

In Fig. 9, an experimental discharge curve is compared with theoretical predictions obtained at a similar current density. The experiment was done with a bicell (2 negative electrodes with a central positive plate) that was built with electrodes designed for the Mark 1A battery program.[37] The computer simulation is based on the electrode capacities specified in Fig. 8, but it is assumed that the positive and negative electrodes have expanded 12.5% and 23%, respectively. It is also assumed that the heat transfer coefficient h is twice as large as the value assumed for the Mark 1A battery model. The ambient temperature used in the model remains at 25°C, whereas it may be closer to 450°C in the experiments.

The two theoretical curves in Fig. 9 indicate the influence of initial cell temperature on the predicted system behavior. The cell temperatures rise by 18°C and 26°C during the discharge, for low and high T_o, respectively. Even with high operating temperatures and swollen electrodes, the maximum predicted utilization is still considerably below the experimental observations. Two possible reasons for this discrepancy are:

a) Additional expansion of the positive electrode either during the formation cycles or on discharge.

b) Reduction in amount of precipitation due to: (i) high local temperatures; (ii) mass transport limitations; (iii) modification of the equilibrium solubility limit by the presence of sparingly soluble species in the electrolyte or due to supersaturation; (iv) circulation of electrolyte caused by free convection.

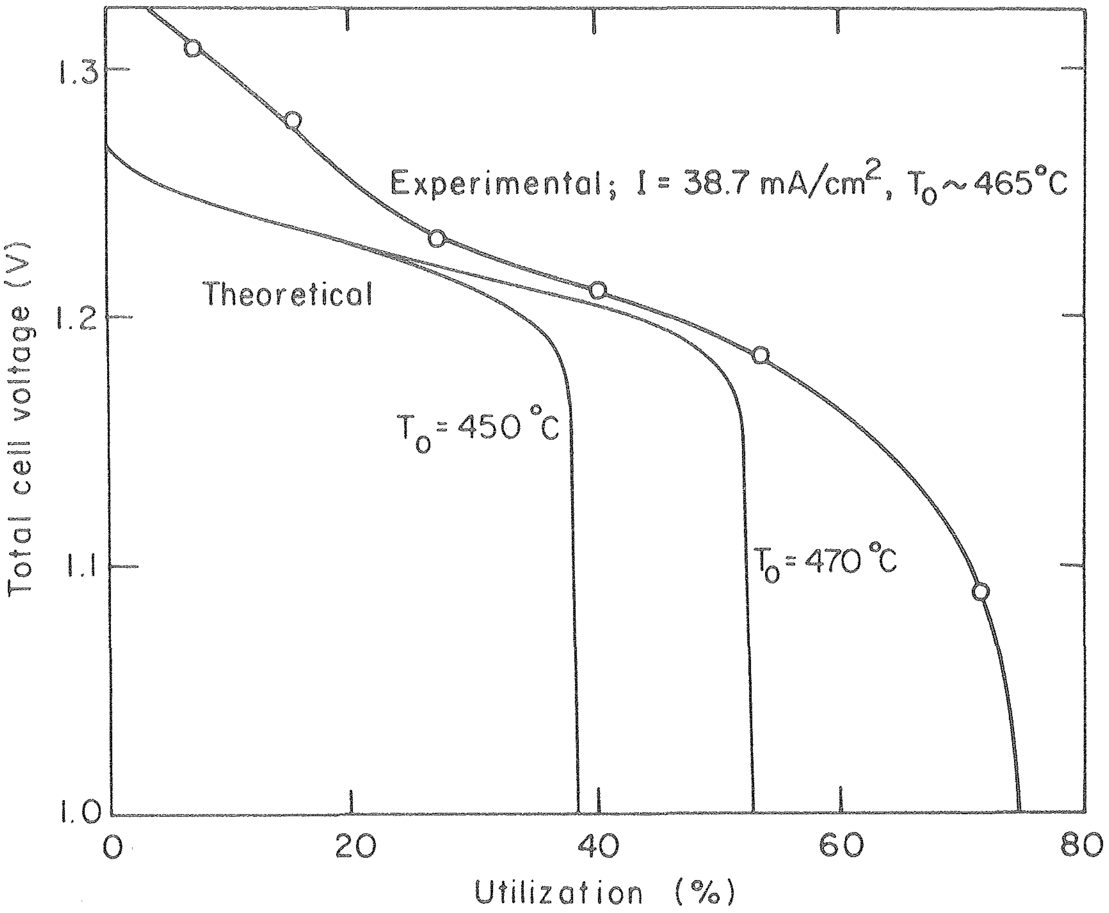

XBL 7912-14571

Fig. 4-9. Comparison of theoretical and experimental[37] discharge curves. Simulation parameters: $Q_- = 2800$ C/cm^3, $Q_+ = 4630$ C/cm^3, $L_- = 0.32$ cm, $L_s = 0.16$ cm, $L_+ = 0.18$ cm, $\varepsilon_-^o = 0.39$, $\varepsilon_s^o = 0.75$, $\varepsilon_+^o = 0.555$, $x_A^o = 0.58$, $I = 41.6$ mA/cm^2, $N = 5.5 \times 10^7$ cm^{-3}, $h_o = 8.25 \times 10^{-2}$ W/m^2.K.

A separate study may be needed to establish the detailed composition variations across the cell under closely controlled experimental conditions.

One can also speculate on the reasons for the differences between experiment and theory shown in Fig. 9, at low utilizations. The experimental curve rises more sharply than the model predictions at depths of discharge below approximately 25%. This can be attributed, at least in part, to the presence of about 15% Cu_2S in the positive electrode. Copper sulfide was added to the Mark 1A electrodes to minimize the formation of an intermediate sulfide, $LiK_6Fe_{24}S_{26}Cl$ (J-phase), which can adversely affect cell performance.[38] There is now evidence to suggest that J-phase can also be suppressed by the use of lithium-rich electrolytes and increased operating temperatures.[39] Elimination of Cu_2S from the positive would be advantageous because gross movement of Cu_2S to the separator, with subsequent cell shorting, can take place.[40]

Small quantities of lithium are sometimes added to the negative to augment the electrode capacity. As with Cu_2S, addition of lithium tends to raise the total cell voltage. However, the lithium activity is increased and this may cause operational difficulties, such as displacement of potassium from the electrolyte, dendrite formation, shift of charge range in cycling, or failure to achieve full charge.

The small discrepancy between experiment and theory at approximately 30% utilization could result, amongst other reasons, from uncertainty in the estimation of the current collector and terminal resistance (see Appendix B). The finite conductance of the grid will also lead to nonuniform current and potential distributions across the face of an electrode, which are not included explicitly in the one-dimensional cell model. A separate study has been made of ohmic drop in current collectors in order to help provide a rational basis for scale-up of cells.[5]

An analysis of local variations in potential across the cell sandwich can provide additional insight into the behavior of the individual electrodes. Figure 10 shows potentials at different positions across the cell described in Fig. 9, relative to a saturated β-LiAl/LiCl,KCl reference electrode placed at the front face of the negative. The separator potential Φ_s is almost unchanged throughout the discharge, in keeping with the constancy of the composition profile across the separator (see Fig. 2). The open circuit potential difference $(\Phi_s)_{I=0}$, that would be measured by a reference electrode at the front face of the positive electrode, indicates the influence of concentration polarization, which is characterized by the composition dependent term in Ohm's law, Eq. (14). The curves marked $\Phi_{+,cc}$ and $\Phi_{-,cc}$ represent the potentials of the positive and negative current collectors, respectively. The difference between these potentials and their open circuit counterparts are the resistances of the individual electrodes. In the negative electrode, there is assumed to be no potential difference in the matrix phase, and, in the positive electrode, the matrix potential difference is too small to be discernable in Fig. 10 because the effective matrix conductivity

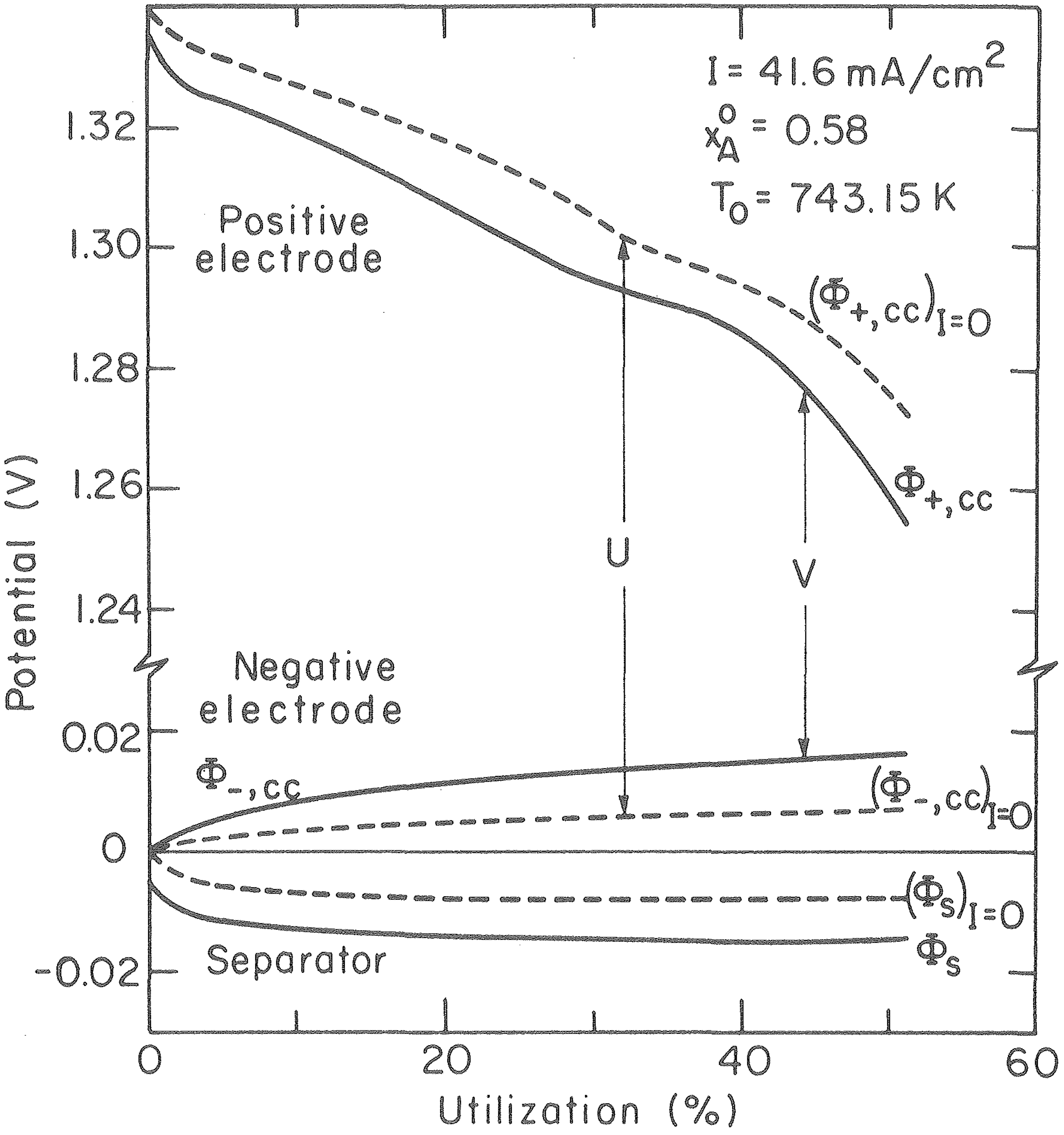

XBL7912-14568

Fig. 4-10. Theoretical potential variations at different locations across the cell sandwich. Parameters as in Fig. 4-9. Dashed lines represent open circuit potentials.

calculated with Eq.(B-7) is large ($\sigma \sim 0(10^4)$), throughout the discharge.

The components of the potential for the experimental cell depicted in Fig. 9 are presented in Fig. 11.[37] Both experimental and theoretical results indicate that changes in total cell voltage are largely dependent on the variations in apparent open circuit cell potential U, and that changes in electrode resistances are relatively small. The experimental results show that the positive is polarized more strongly than the negative electrode, but that the negative electrode potential rises more sharply towards the end of discharge. This could be interpreted as a negative electrode 'limitation', although this term has not been carefully defined. In this context, it is not possible to distinguish between limitations caused by inherent electrochemical factors or by changes in the useable capacity of an electrode over a number of cycles. It might be expected that, with a sufficient increase in excess capacity in the negative electrode, the positive would limit cell performance on both charge and discharge.

For both electrodes, the model predicts resistances that are smaller than the observed values. This could be caused by overestimation of electrochemically active interfacial areas, exchange current densities, or matrix conductivities. Contact resistance or partial loss of electrical connectivity between electrode particles can lead to conductivities below those calculated from Eq. (B-7), which is based on the concept of parallel conduction paths. Separate experiments may be needed to establish the conductivity of each

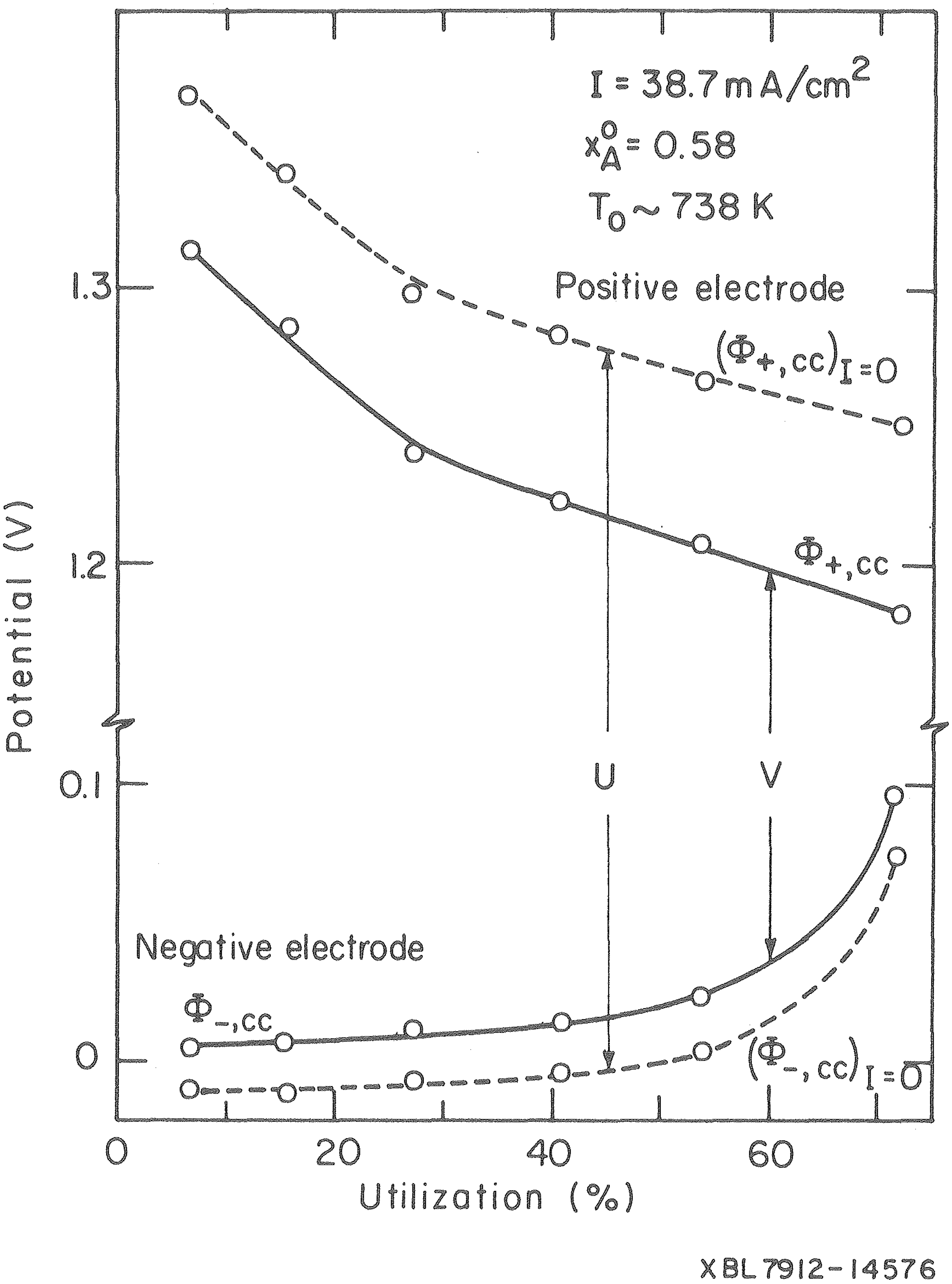

Fig. 4-11. Potentials at different locations across a cell sandwich measured with a reference electrode placed at the edge of the separator.[37] Dashed lines represent open circuit potentials, 15 s after current interruption.

electrode matrix as a function of state of charge. Contact resistances are not expected to be significant in the positive electrode during discharge because the large volume of solid products tends to increase the internal electrode pressure. Furthermore, the presence of Li_2S at the front of the positive electrode may not influence cell behavior markedly, since all the current will be carried in the electrolyte across the fully reacted region. However, the formation of a poorly conducting layer adjacent to the current collector could have a more profound effect on the potential distribution.

Despite the underestimates for the electrode resistances, the model still gives voltages that lie below the experimental results in Fig. 9. This is directly associated with the estimated value of the current collector resistance R_g, which is only included in the model to improve the accuracy of the heat balance. The estimate of R_g could be refined with more precise experimental data for the polarization conductance Y of a cell element. This parameter (Y) could be obtained directly in a small, open test cell with current collectors large enough to ensure insignificant current and potential variations across the face of a plate and with voltage taps placed in direct contact with the current collectors.

Additional experiments may also be needed to elucidate the reasons for the observed rise in potential of the negative electrode towards the end of discharge (see Fig. 11). The theoretical calculations indicate that the increase in porosity as the discharge proceeds more than compensates for the additional distance the current must penetrate the electrode, and that the current collector potential approaches a constant (see Fig. 10). The discrepancy between theory and experiment may result from:

(a) reduction in negative electrode porosity caused by expansion of the positive,

(b) gross morphology changes in the negative electrode,

(c) reduction in the available electrode capacity and uncertainty in the state of charge caused by

  (i) segregation of active material from the bulk

  (ii) cumulative coulombic losses,

(d) nonuniform initial distribution of reactants.

Agglomeration would reduce the electrochemically active interfacial area and increase the diffusion overpotential for transport of lithium atoms across the α-Al. A computer simulation with the initial particle size r_o^o increased by a factor of 4.5 shows an increased electrode resistance at a particular depth of discharge but, contrary to observations, the open circuit potential $(\Phi_{-,cc})_{I=0}$ does not alter appreciably. The influence of the initial variation in state of charge across the negative electrode could be investigated by comparing potential distributions obtained during two experiments; one where a considerable time interval was introduced between the discharge of interest and the previous charge, and the other where the discharge followed the charge immediately, but the overall initial state of charge matched the first experiment.

It should also be noted that a considerable quantity of lithium can be retained in the α-Al after the β-phase has been completely utilized. For the example with highest utilization in Fig. 9, the characteristics of particles at the front of the electrode when the cutoff voltage is reached are: $r_\beta = 0.474 \times 10^{-3}$ cm, $r_\alpha = 1.115 \times 10^{-3}$ cm, and $(c^\alpha_{Li})_o/(c^\alpha_{Li})_{sat} = 0.78$. This indicates that the reaction is not limited by diffusion of lithium across the α-Al and that a minimum of approximately 7.8% of the total theoretical capacity could be stored in the α-Al when no β-LiAl remains. Consequently, the available capacity in the negative electrode may be significantly lower than the theoretical estimate, and this could contribute to the apparent limitation observed in this electrode.

Polarization Characteristics

In many applications it is important to know the effect of discharge rate and depth of discharge on the useable capacity of the cell. Figure 12 shows polarization curves that represent a voltage sweep of a cell that has been discharged at a specified constant current density for a given period of time. It should be emphasized that this is not simply a cross-plot of a number of constant current discharges. Before discharge begins, there is a single current-potential curve, but the polarization characteristics will alter during the discharge in a manner that depends on the total applied current. In general, polarization is greater at larger depths of discharge, and for higher current densities at a given depth of discharge.

Fig. 4-12. Effect of state of charge on theoretical cell polarization behavior. Simulation parameters as in Fig. 4-9, $T_o = 470°C$.

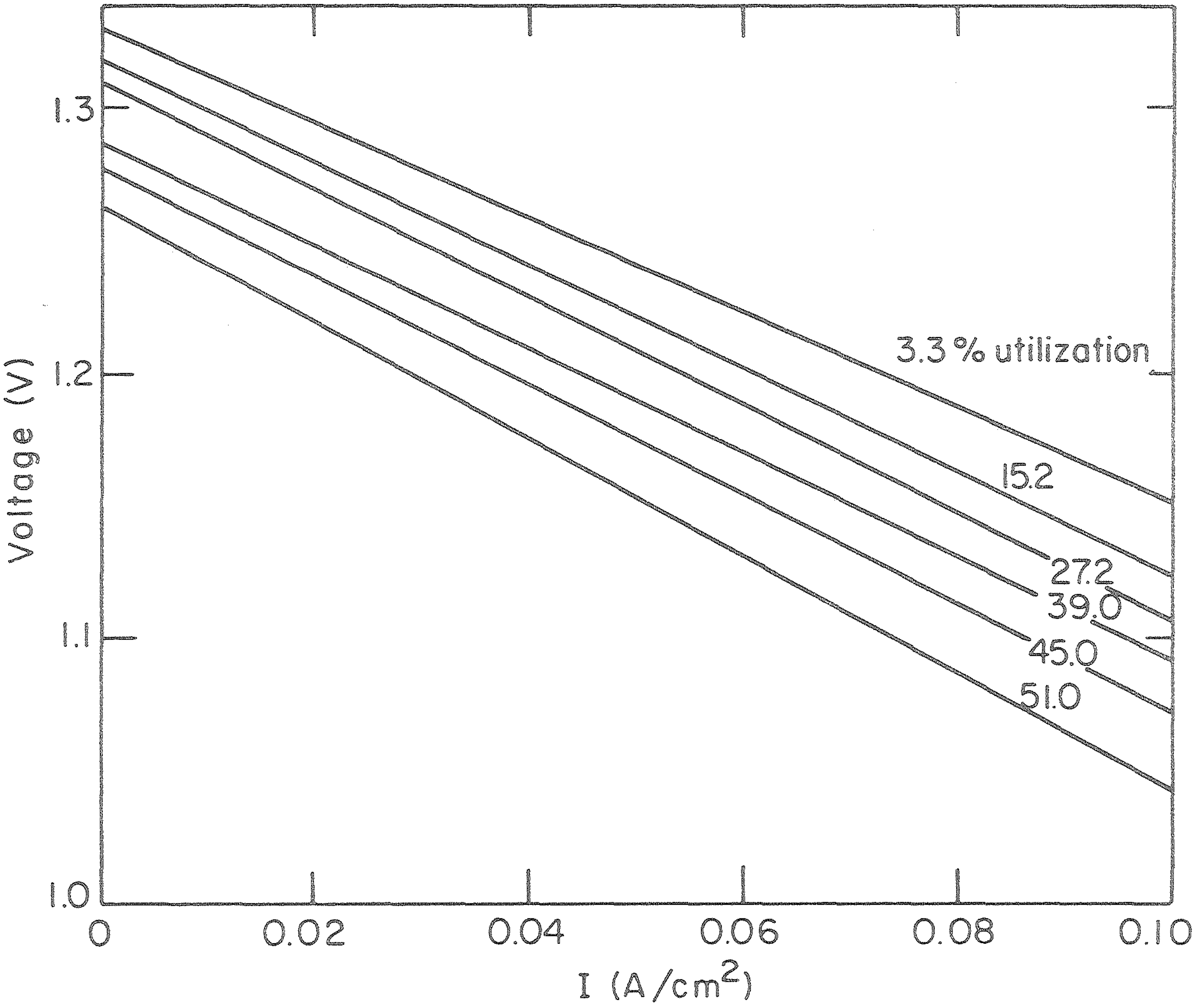

Fig. 4-12.

XBL7912-14572

An important feature of the curves in Fig. 12 is that they are substantially straight, and there is little error in approximating them by the equation

$$I = Y(U - \Phi_+ - \Phi_-) \quad , \tag{4-30}$$

where Y is the polarization conductance, given by the reciprocal of the slope of the lines, and U is the apparent open circuit cell potential, given by the ordinate intercept. In this way, the polarization characteristics of the LiAl/FeS cell can be summarized by the dependence of U and Y on the operating conditions.

Figure 13 shows the dependence of electrochemical resistance on state of charge for several different current densities. Each curve shows that, in an overall sense, the resistance increases as more active material is consumed. However, for $I = 0.1$ A/cm^2, there is an almost discontinuous reduction in 1/Y at a time that corresponds to the onset of reaction IIB ($X + 2Li^+ + 2e^- \rightarrow 2Li_2S + Fe$) in the positive electrode. At lower current densities the drop in resistance is neither as marked nor as abrupt, and it occurs later in the discharge (see Table 2). At each current density, the resistance rises again as porosity variations in the positive electrode lower the effective electrolyte conductivity. In practice, there is much less distinction between the intermediate reaction steps in the positive electrode. Consequently, it is not expected that the sharp changes in resistance predicted with the model, will be observed experimentally. It should also be emphasized that the model does not include the

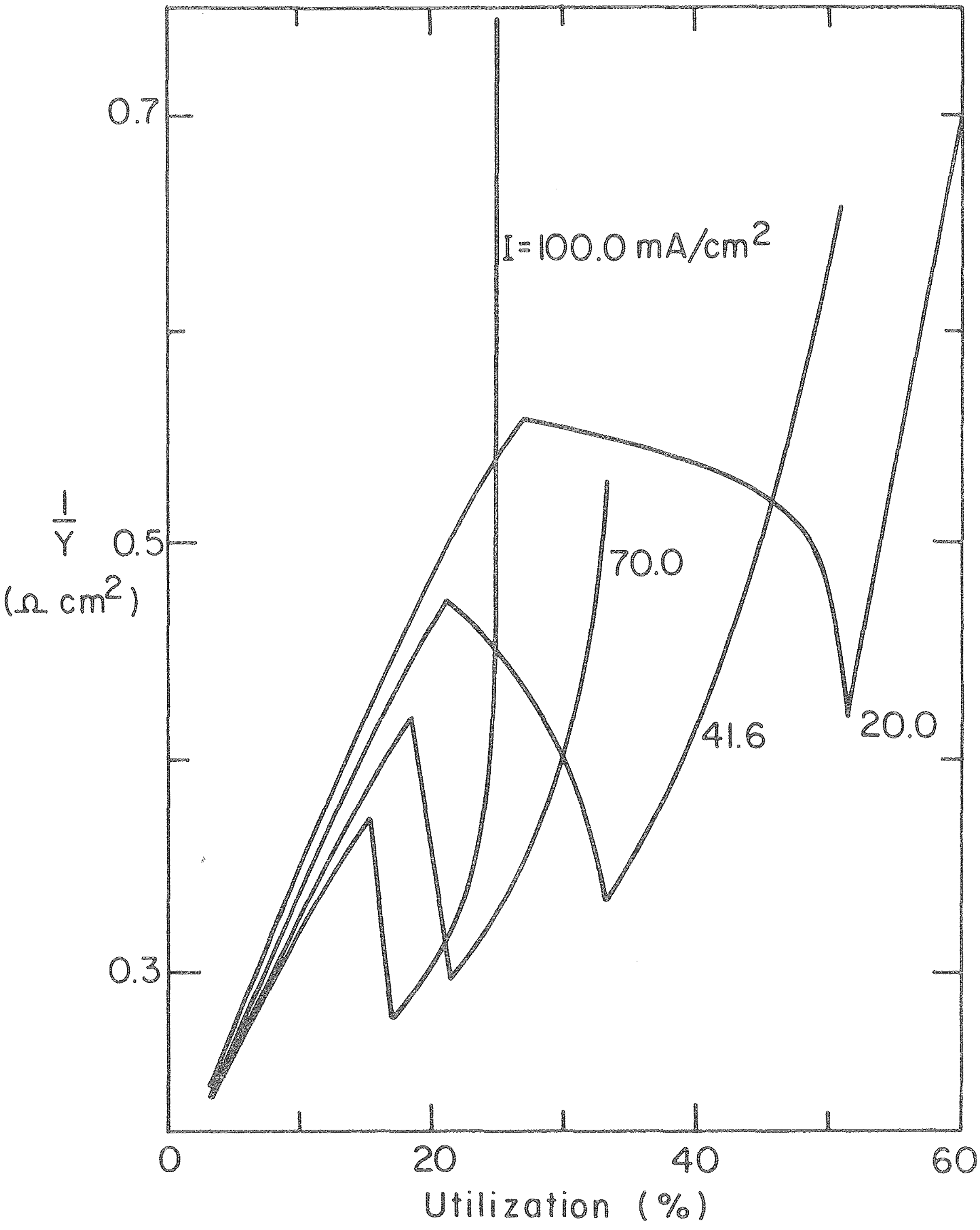

XBL7912-14573

Fig. 4-13. Predicted dependence of polarization resistance on utilization at different discharge rates. Parameters as in Fig. 4-9, T_o = 470°C.

possibility for reaction of additives such as Cu_2S or CoS_2, or for additional intermediates, such as J-phase, in the conversion of FeS to Li_2S and Fe.

The dependence of the apparent open current cell potential on state of charge and discharge current density is presented in Fig. 14 and Fig. 15, for theory and experiment, respectively. In both cases, the value of U drops markedly during the discharge. The experimental results lie above the model predictions as a consequence of the presence of additives, such as Cu_2S, which raise the equilibrium open circuit cell potential. For less than about 30% utilization, the experimental curves show no systematic dependence on current density. At greater depths of discharge, U changes more markedly at higher I, as predicted in Fig. 14.

The reduction in U during the discharge can be associated with concentration polarization caused by nonuniform utilization of active material. In the negative, lithium is preferentially removed from the front of the electrode first, as illustrated in Fig. 4, and a maximum in electrolyte composition can develop part of the way through the electrode. At open circuit, the region with highest electrolyte composition becomes cathodic with respect to the rest of the electrode, and local concentration cells are set up which act in a manner that tends to reduce the composition variations. These variations can be more substantial at higher discharge rates, for a given state of charge, and, consequently, the open circuit resistance can be higher in the negative electrode, leading to smaller values for U.

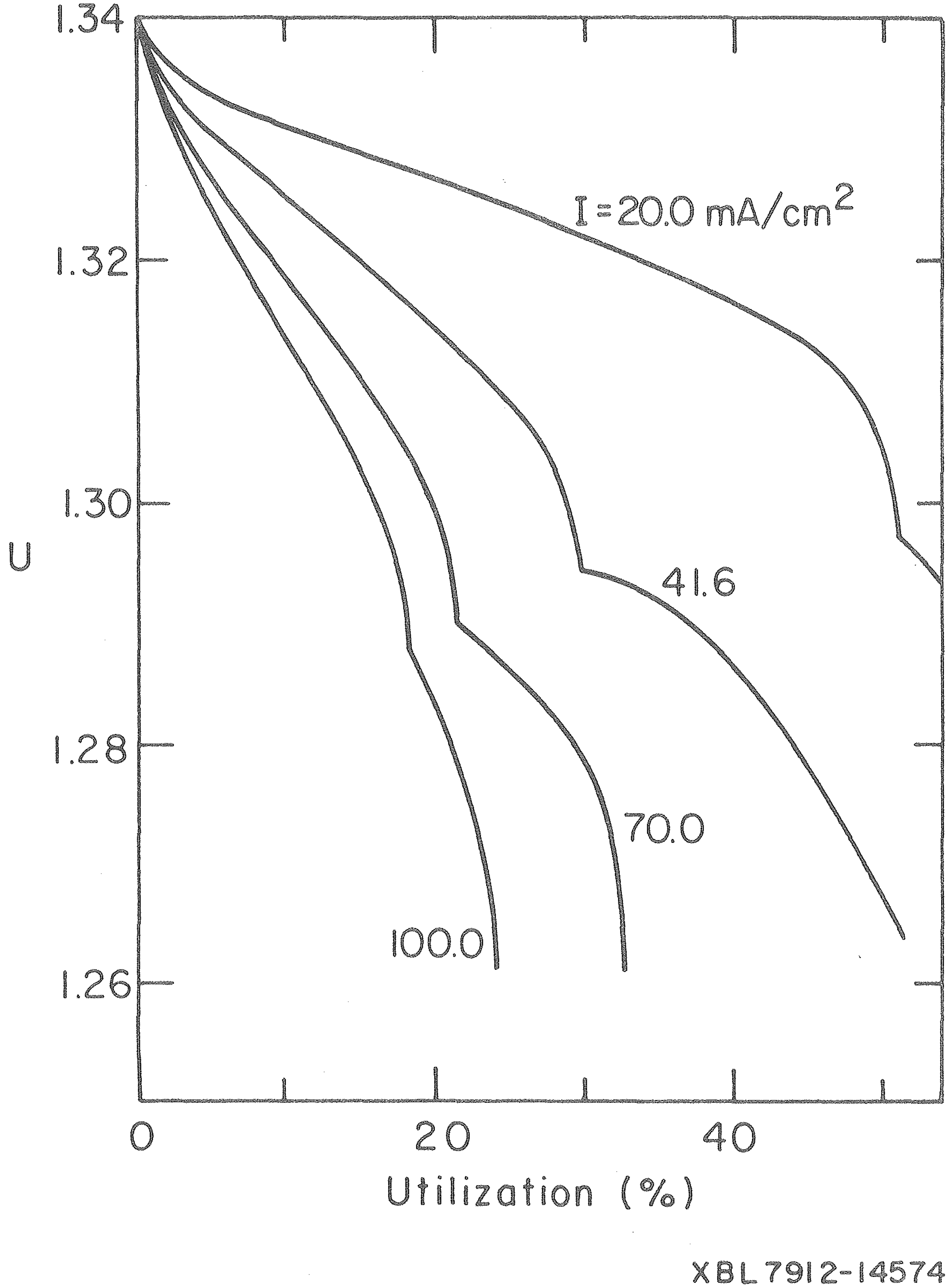

Fig. 4-14. Effect of discharge rate and state of charge on the theoretical apparent open circuit cell potential. Parameters as in Fig. 4-9, T_o = 470°C.

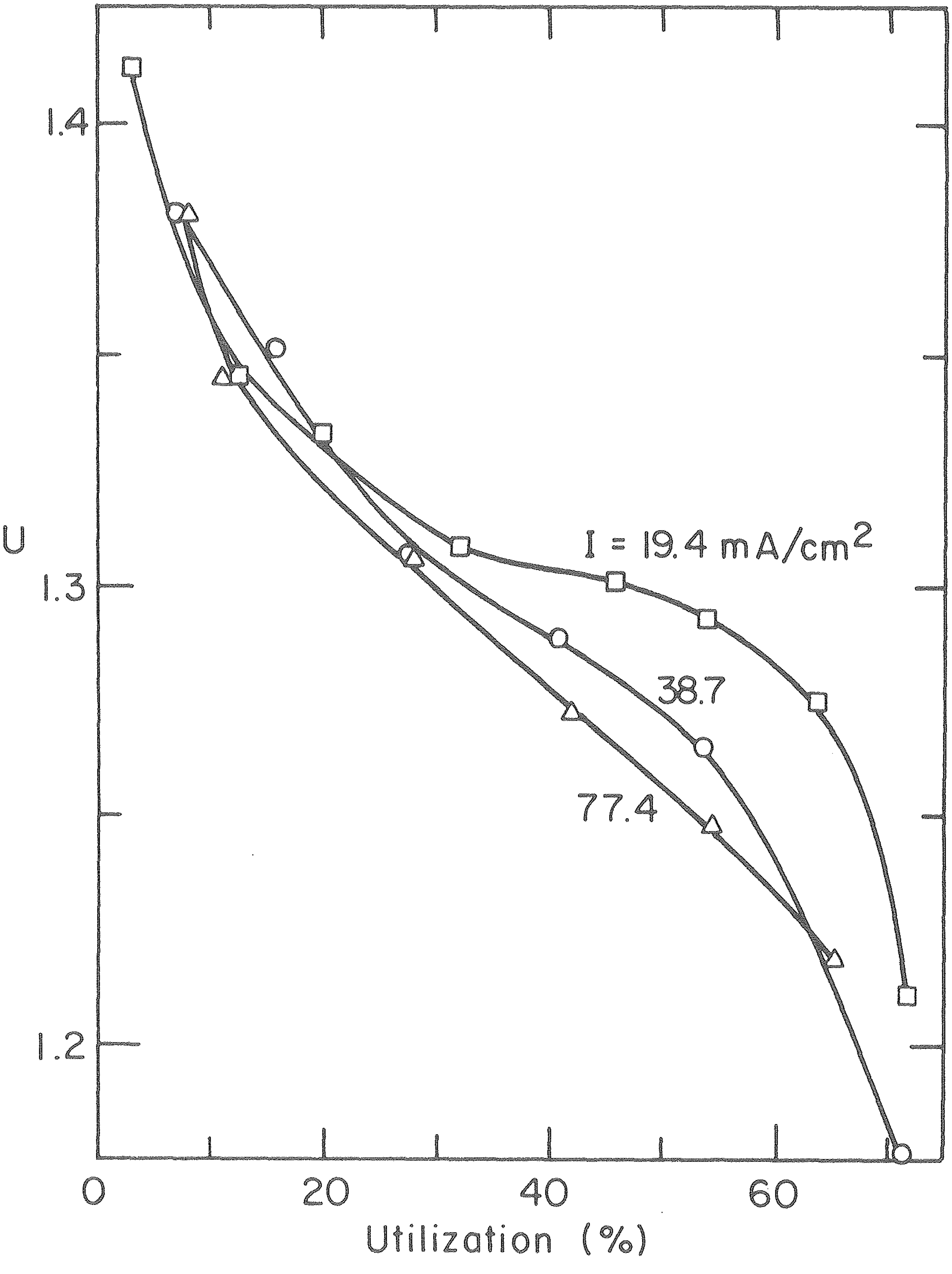

XBL 7912-14570

Fig. 4-15. Variation in experimental apparent open circuit cell potential with discharge current density and utilization. Measurements taken 15 s after current interruption.[37]

In the positive electrode, the situation is complicated by the possibility of simultaneous reactions. Before reaction IIB begins, $(\Phi_{+,cc})_{I=0}$ is controlled by local concentration cells that result from electrolyte composition variations, in much the same way as described for the negative electrode. When reactions IIA and IIB both occur, a corrosion potential can be established on open circuit, which corresponds to cathodic formation of Li_2FeS_2 in the back of the electrode, and anodic formation of Li_2FeS_2, towards the front. These reactions would be observed on current interruption, even in the absence of a composition gradient in the electrolyte. As the second reaction (IIB) progresses, the mixed corrosion potential shifts towards the equilibrium potential $U_{IIB,o}$.

The positive electrode behavior is the major factor that leads to the predicted reduction in U. At higher current densities, reaction IIB begins earlier in the discharge and therefore U declines more rapidly. The less marked dependence of U on current density observed experimentally is further evidence to suggest that there is less distinction between the positive electrode reactions in practice.

Conclusions

A mathematical model has been developed that can describe the time-dependent and position-dependent behavior of a complete LiAl/LiCl,KCl/FeS cell. Composition and reaction distributions can be predicted, as well as variations in volume fractions of individual phases and electric potential within the electrodes. The results of the theoretical analysis show many of the general trends in discharge behavior that are observed experimentally. The model predicts that high internal resistance can develop in the positive electrode as a result of low local porosities which are, in turn, caused by large volume reaction products or precipitated KCl. This implies that, with the electrode capacities currently being considered for electric vehicle applications, swelling may be a prerequisite for successful operation and thermal management of battery modules may also be important. Furthermore, an investigation of the potential distribution across the cell sandwich indicates that, before porosity reductions become critical, variations in total cell voltage are controlled more by changes in apparent open circuit cell potential than by changes in resistance across the individual electrodes.

5. THE INFLUENCE OF RELAXATION TIME ON THE CHARGING CHARACTERISTICS OF THE LITHIUM-ALUMINUM, IRON SULFIDE CELL

Introduction

The mathematical model developed in Chapter 4 can also be used to investigate the behavior of the LiAl/FeS cell during relaxation and charging. The changes that take place under these conditions could influence the dependence of cell performance on the number of completed cycles.

In the laboratory, current interruption techniques can be used to assess the resistance within the electrodes, separator, and grids. Furthermore, in some experiments, such as post-mortem cell examinations, a period of relaxation may be needed before the temperature is low enough to begin the analyses. Current interruption may also be important in modules for electric vehicle propulsion, where it is anticipated that there will be significant periods when the battery is not in use. Cell behavior on charge can control the overall energy efficiency of the system and may also directly affect the nature of the subsequent cell discharge.[34,36] For these reasons, it is necessary to identify the factors that can limit the system during the relaxation and charging modes of operation.

The governing differential equations presented in chapter 4 can be used directly in the analysis, and it is only necessary to modify the model for negative electrode kinetics (see Appendix C) and to replace the initial conditions, Eq. (4-27(i)) and (4-27(ii)), with the appropriate composition and porosity distributions.

Results and Discussion

Relaxation

Figure 1 shows composition profiles across the cell sandwich for several times after interruption of the current at the end of a discharge with $I = 41.6\ \mathrm{mA/cm^2}$. The concentration variations diminish in both electrodes and, after 2 hours, the electrolyte composition is practically uniform. In the negative, the region with highest x_A, at the back of the electrode, becomes cathodic with respect to the front portions. Local concentration cells, with the reaction

$$\mathrm{LiAl} \rightleftharpoons \mathrm{Li^+} + \mathrm{Al} + e^- \ , \qquad \mathrm{I}$$

are established that reduce the initial composition variations. However, there is no driving force for equalization of the local state of charge within the α-Al, β-LiAl alloy, and the reactions that take place to give a uniform electrolyte composition accentuate the nonuniform utilization of reactants. The magnitude of this effect is dependent on the composition profile and the depth of discharge before current interruption.

In the positive electrode, the situation is complicated by the possibility of simultaneous reactions and by precipitation of electrolyte. Initially, the electrolyte concentration is almost uniform across the majority of the electrode due to precipitation of KCl as two spikes adjacent to the reaction fronts, and self-discharge

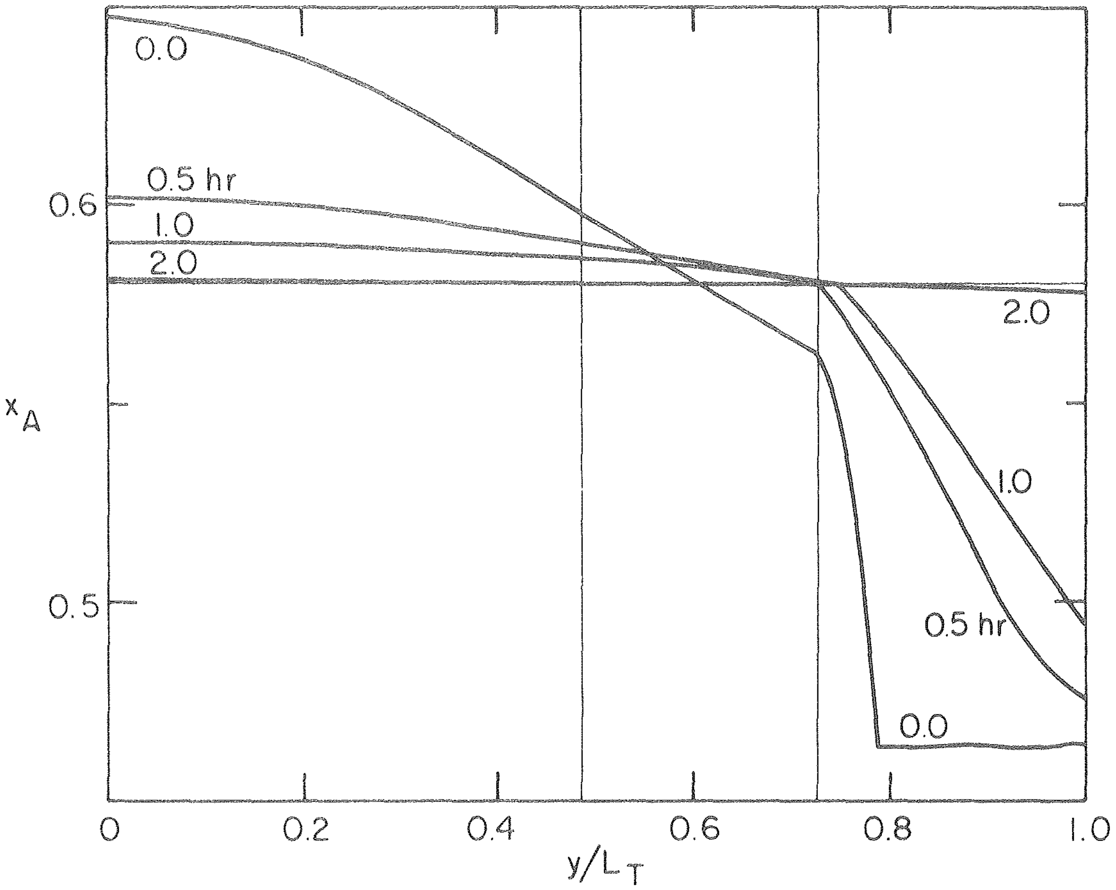

XBL 7912-14569

Fig. 5-1. Position dependence of mole fraction of LiCl at different times after current interruption. Simulation parameters: $Q_- = 2800$ C/cm^3, $Q_+ = 4630$ C/cm^3, $L_- = 0.32$ cm, $L_s = 0.16$ cm, $L_+ = 0.18$ cm, $N = 5.5 \times 10^7$ cm^{-3}, $h_o = 8.25 \times 10^{-2}$ W/m^2.K, $R_g = 1.55\ \Omega$ cm^2, $h = 0.004$ cm, $\omega = 0$, $\bar{c}^{\beta}_{Li}/(c^{\beta}_{Li})_{sat} = 1.0$, $D_\beta = 4 \times 10^{-8}$ cm^2/s. Parameters at start of previous discharge: $\varepsilon^o_- = 0.39$, $\varepsilon_s = 0.75$, $\varepsilon^o_+ = 0.555$, $T_o = 470$°C, $I = 41.6$ mA/cm^2, $x^o_A = 0.58$. Initial state of charge, $\lambda(t{=}0) = 47.9\%$. Additional parameters specified in Table 4-1 and Table B-1.

reactions in the isolated regions behind the spikes. Adjacent to the current collector, FeS reacts with lithium ions according to

$$2FeS + 2Li^+ + 2e^- \rightleftharpoons Li_2FeS_2 + Fe \qquad IIA$$

whereas, near the front of the electrode, Li_2S reacts anodically with iron, thus:

$$2Li_2S + Fe \rightleftharpoons Li_2FeS_2 + 2Li^+ + 2e^- \; . \qquad IIB$$

The transformation of Li_2S and FeS to the intermediate sulfide reduces the local variations in state of charge although, once all the FeS has been removed, it is not possible for the remainder of the Li_2S to react further. Consequently after approximately 1 hour, there are no more reactions in the positive, and the composition now relaxes under the influence of diffusion alone.

Characteristic times for other relaxation processes can also be identified from the composition profiles. In Fig. 1, the electrolyte concentration changes by less than 1% across the separator after 1.3 hours, whereas the 1% condition is achieved in the negative electrode after only 0.8 hours. This reflects, to some extent, the influence of the electrochemical reaction on the relaxation time. However, the 1% criterion is rather arbitrary and, even though the composition is fairly uniform at 0.8 hours, the concentration in the negative still needs to drop by another 2.5%, as diffusion takes place across the separator. In the positive, an additional characteristic time can be distinguished. Self-discharge reactions take place in the region where Li_2FeS_2 is only partially converted to Li_2S. Here, the portion closest to the front of the electrode becomes preferentially cathodic and, after approximately 4 minutes, a sharp reaction front for the second reaction has been formed.

Heat is not generated in the cell during relaxation, and the temperature falls in accordance with the specified rate of heat transfer to the surroundings. As a result, the saturation concentration for KCl can rise faster than the minimum electrolyte concentration and, under these circumstances, the total volume of precipitate becomes greater than the value at current interruption. However, the reduction in minimum composition soon dominates and, in this example, all the KCl has dissolved after 1500 s.

Figure 2 shows the variations in total cell voltage that take place after the current is switched off, for the two simulations described in Fig. 4-9. Curve A is for the example that had a temperature of 450°C at the start of discharge, and that achieved 39.2% utilization before the cutoff voltage was reached. The second example had a higher initial temperature (470°C), and a greater utilization was attained before the termination of discharge. In both cases, there is an initial instantaneous rise in cell voltage. The magnitude of this step change can, in principle, be used as a basis for estimation of cell resistance. However, the numerical predictions cannot be used directly because the effects of double layer capacity are not included in the model, and because the final total cell voltage, prior to interruption, can be much lower than expected in practice, due to the acute

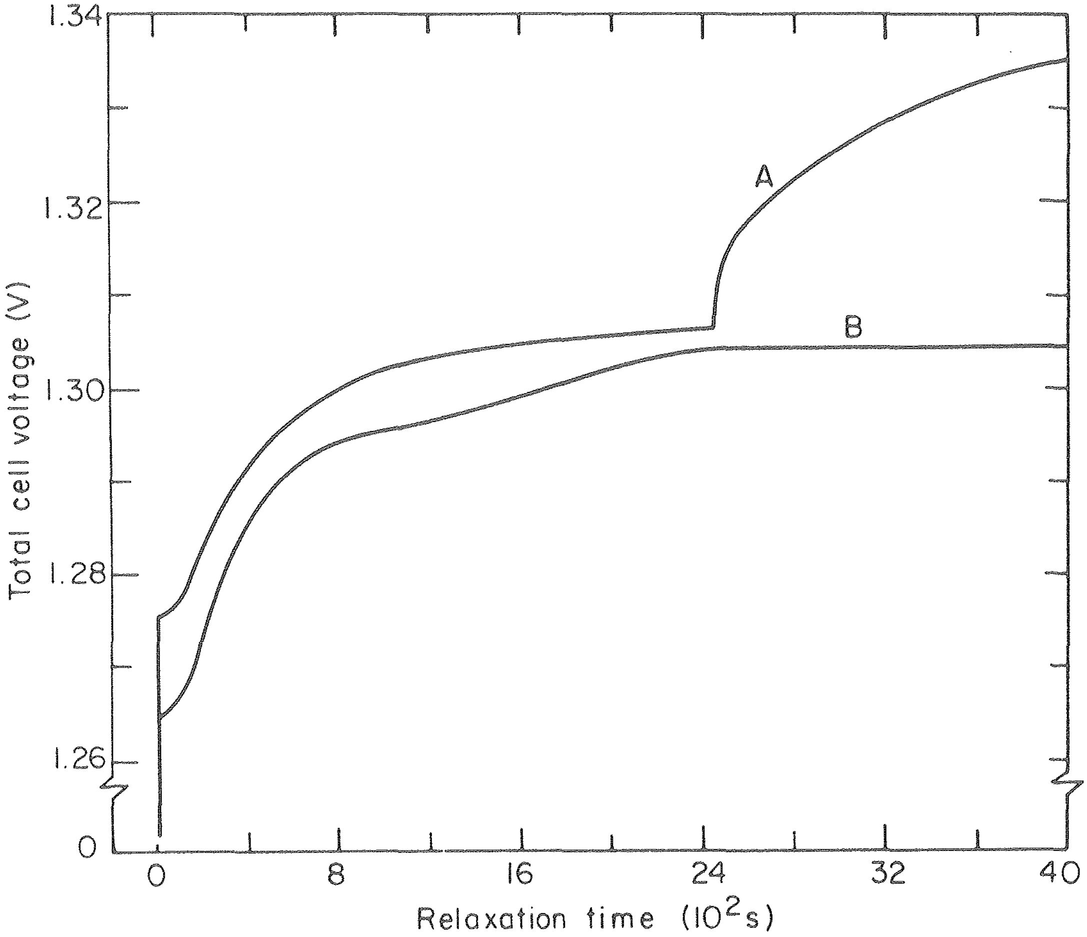

XBL7912-14563

Fig. 5-2. Dependence of total cell voltage on relaxation times simulation parameters as in Fig. 5-1, except as indicated.
Curve A: $\lambda(t=0) = 60.8\%$, $R_I = 0.15\ \Omega\ cm^2$, $T(t=0) = 468.2°C$, T_o (at start of previous discharge) = 450.0°C.
Curve B: $\lambda(t=0) = 47.9\%$, $R_I = 0.14\ \Omega\ cm^2$, $T(t=0) = 496.2°C$, T_o (at start of previous discharge) = 470°C.

nature of the predicted failure mechanism. Therefore, separate calculations are necessary to estimate the interrupter resistance.

At the instant of interruption, there is no change in the composition profile. The potential profile retains the same shape within the negative electrode, and the potential difference $\Phi_1-\Phi_2$ in the positive is constrained to maintain the same value because of the double layer capacity. Consequently, at any point in the system, Ohm's law gives

$$\frac{\underline{i}_1}{\sigma} - \frac{\underline{i}_2}{\kappa} = -\nabla\eta = \frac{\underline{i}_1^o}{\sigma} - \frac{\underline{i}_2^o}{\kappa} \ , \tag{5-1}$$

where the superscript refers to conditions just before interruption. Since $\underline{i}_1 + \underline{i}_2 = 0$ and $\underline{i}_1^o + \underline{i}_2^o = I$, one may write

$$\underline{i}_1 - \underline{i}_1^o = -\frac{I\sigma}{\sigma+\kappa} \ , \tag{5-2}$$

which indicates that the resistance of matrix and solution are effectively in parallel, even though each segment of the electrode is in series. Combination of Eq. (2) and Ohm's law for the matrix phase gives the change in cell voltage, $\Delta(V-V^o)$, as

$$\frac{\Delta(V-V^o)}{I} = \int_o^{L_T} \frac{dy}{\sigma+\kappa} \ , \tag{5-3}$$

where the left hand side represents the interrupter resistance, R_I. In the computer calculations, R_I is dominated by the resistance across the separator because the matrix conductivity is assumed to be infinite in the negative and high in the positive electrode. The separator resistance changes only slightly during operation of the cell, in response to variations in electrolyte conductivity.

It should be emphasized that the theoretical models for the LiAl/FeS cell[5] do not include double layer effects since they are not generally regarded as being significant in the normal operation of a cell. Therefore, for the purpose of measuring the cell polarization characteristics (i.e. Y and U in Eq. (4-30)), one may prefer the resistance to be measured after charging of the electric double layer has been completed. For this system, the double layer relaxation time, from point to point within an electrode, is estimated as approximately 50 ms,[5] whereas relaxation of concentration profiles by diffusion and reaction is on the order of 3000 s (see above).

After interruption, the voltage gradually approaches the equilibrium open circuit cell potential. The shape of the curves is determined by the details of the reactions that occur in the individual electrodes. In particular, a corrosion potential is established in the positive by reactions IIA and IIB. In example A, all the Li_2S has been converted to Li_2FeS_2 after approximately 2450 s, and the voltage rises sharply to the open circuit value, $U_o = 1.34$ V. Curve B does not show this effect because some Li_2S still remains when reactions IIA and IIB are completed. In this case, the voltage slowly approaches the open circuit potential, $U_o - U_{IIA,o} = 1.3074$ V, as the electrolyte composition becomes more uniform. It should also be noted that the small initial rate of rise of cell voltage shown in the examples is atypical, and it results from potential drop across the sharp spike of precipitate that was responsible for the rapid decline in cell voltage before current interruption. Both theoretical and experimental results indicate that the initial voltage rise is more rapid when the current is interrupted before the cutoff voltage is reached.[37]

Charging

Figure 3 shows simulated composition profiles at different stages of a constant current charge. A relaxation time of two hours was included between the initial discharge and the start of the charging process. The parameter λ represents the overall state of charge; when the cutoff voltage of 1.65 V is reached, 89.3% of the total theoretical capacity is available for the next discharge.

In contrast to discharge, lithium ions are now introduced into the electrolyte at the positive electrode and transported across the separator to the negative electrode, where they are incorporated into the LiAl alloy. The composition profiles represent the combined effects of diffusion, migration, and electrochemical reaction. An almost constant composition gradient is established across the separator, but the electrolyte concentration in the reservoir rises significantly during the charge. The model predicts that the electrolyte composition is almost uniform behind each reaction front.

The variations in electrolyte concentration in Fig. 3 can be compared with those in Fig. 4, for the same cell, but without relaxation

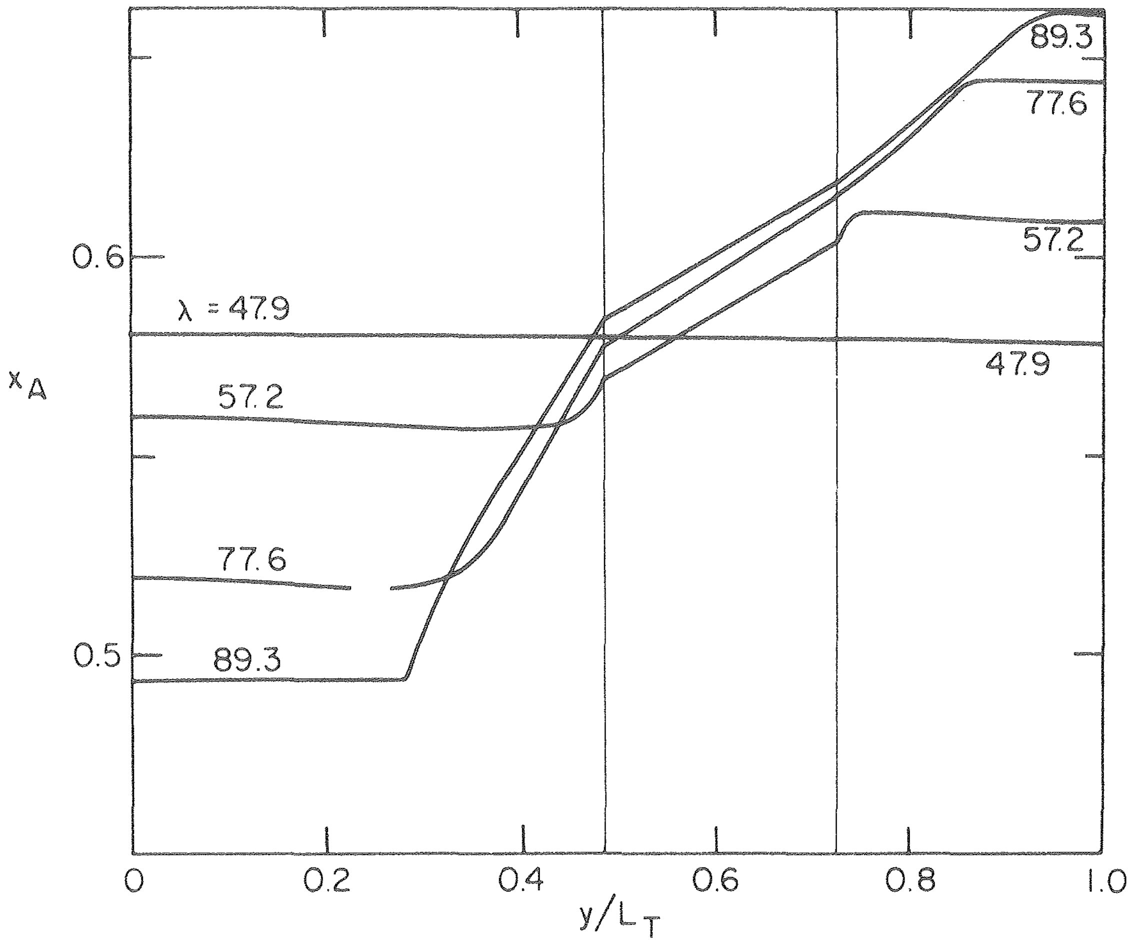

XBL 7912-14567

Fig. 5-3. Position dependence of mole fraction of LiCl at different states of charge for a constant current charge of -41.6 mA/cm^2. A relaxation time of 2 hours is included between the end of the previous discharge and the beginning of the charging process. Simulation parameters: T(t=0) = 480.4°C, see also Fig. 5-1.

between discharge and charge. At $\lambda = 77.6$, the profiles are very similar in the two cases, and there is little trace of the composition profile before the charge was started.

The average cell temperature in Fig. 3 falls from 753.5 to 740.0 K during the charge, as a result of reversible heat effects and heat transfer to the surroundings. Consequently, the saturation limit for KCl rises, and precipitation begins at the reaction front in the negative electrode when $\lambda = 85.9$. The temperature of the cell in Fig. 4 also falls, but over the range 769.4 to 751.6 K, and precipitation is delayed until $\lambda = 91.1$. For this reason, 93.7% of the theoretical capacity can be recovered before the resistance across the precipitated region becomes excessive, and the cutoff voltage is reached.

The difference in charging behavior caused by the temperature drop during relaxation emphasizes the need for careful thermal management of battery modules. At lower charging current densities the temperature falls even more dramatically, but the maximum and minimum concentrations are smaller at a given state of charge, and precipitation of KCl no longer controls the final value of λ. For the cell characteristics used in the simulations, a current density of -70 mA/cm^2 is needed to keep the average cell temperature reasonably constant.

Figures 5 and 6 show the fraction of active material utilized within the negative electrode, at several overall states of charge, for the examples in Fig. 3 and Fig. 4, respectively. A comparison of the curves at $\lambda = 47.9$ $(t=0)$, shows the increase in nonuniform utilization of reactants that results from relaxation of the electrolyte

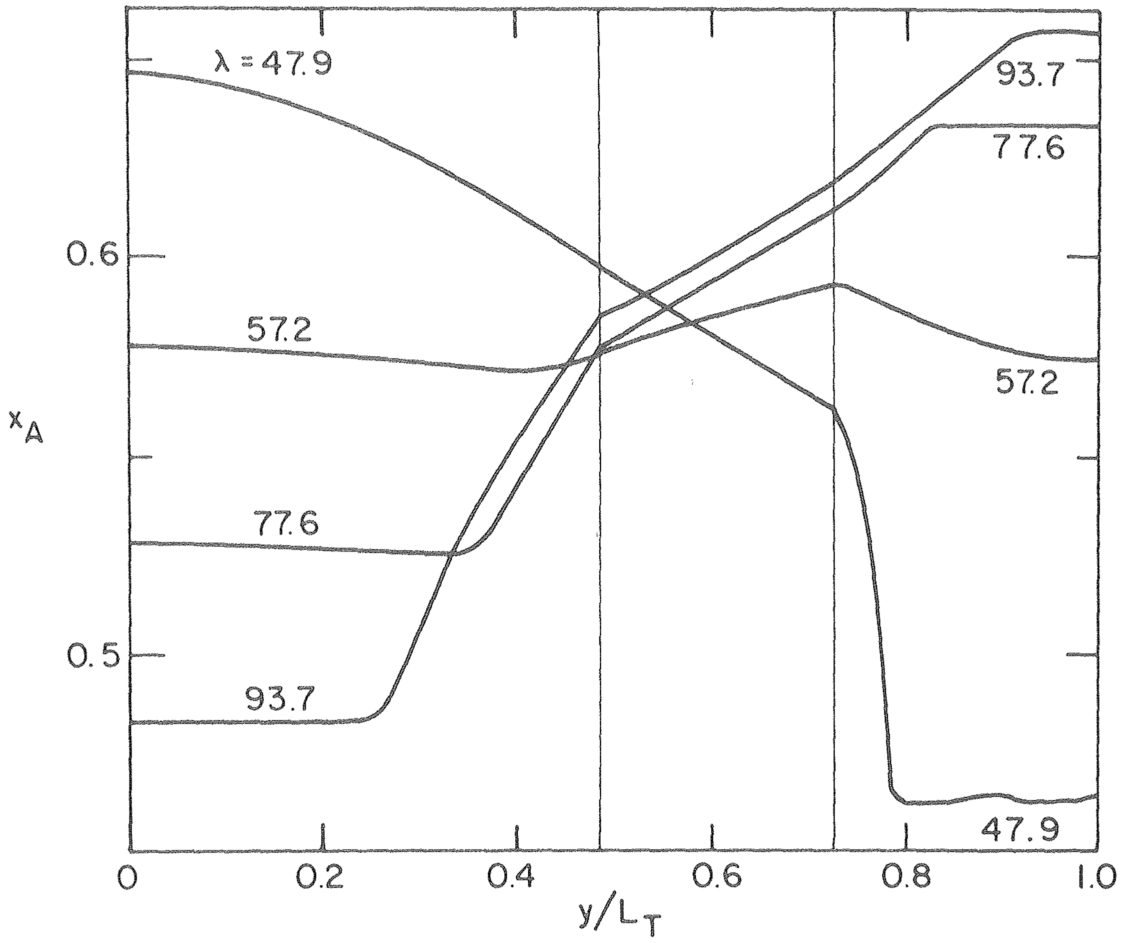

XBL 7912-14566

Fig. 5-4. Position dependence of mole fraction of LiCl at different states of charge for a constant current charge of -41.6 mA/cm^2. No relaxation between the end of the previous discharge and the start of the charging process. Simulation parameters: T(t=0) = 496.2°C, see also Fig. 5-1.

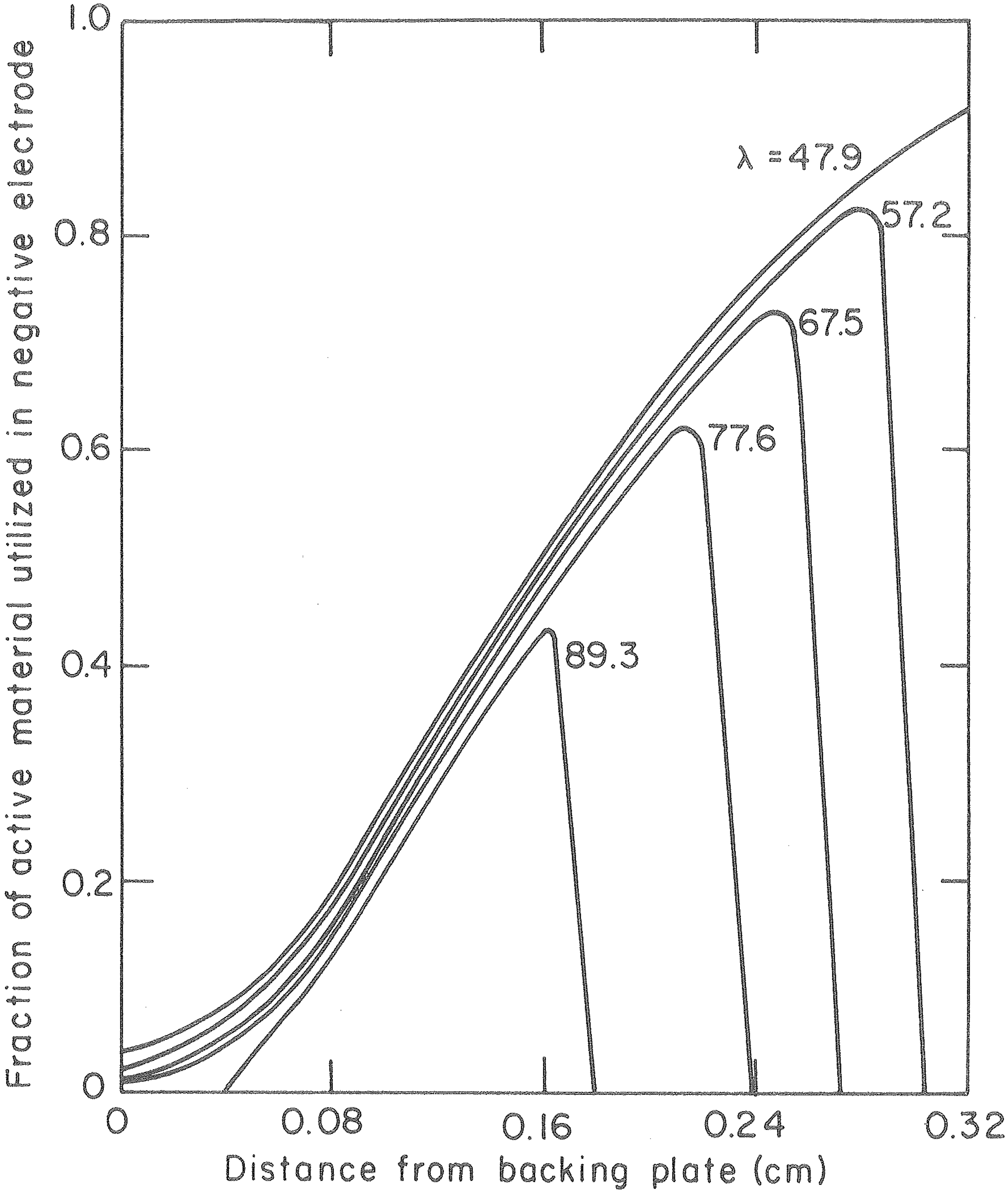

XBL7912-14565

Fig. 5.5. Fraction of active material utilized in negative electrode at different overall states of charge during a constant current charge of $-41.6\ \mathrm{mA/cm^2}$. A relaxation time of 2 hours is included between the end of the previous discharge and the beginning of the charging process. Simulation parameters as in Fig. 5-1.

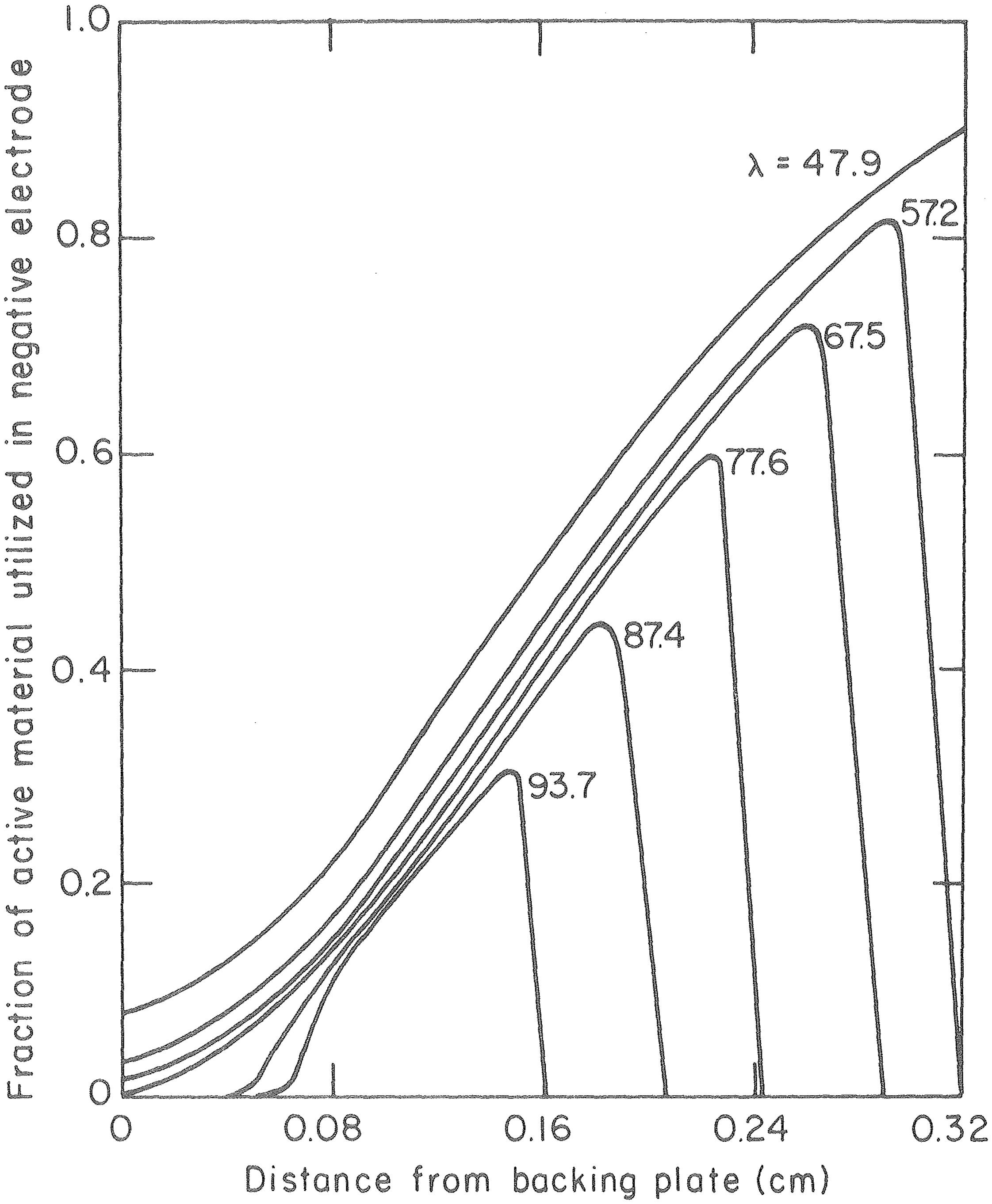

XBL 7912-14564

Fig. 5-6. Fraction of active material utilized in negative electrode at different overall states of charge during a constant current charge of -41.6 mA/cm^2. No relaxation between the end of the previous discharge and the start of the charging process. Simulation parameters as in Fig. 5-1.

composition. The general charging mechanism is similar in the two cases: the region closest to the electrode/separator interface is recharged first, and the reaction front moves back through the electrode as the alloy is completely reconverted to β-LiAl. Further reaction of the β-LiAl is not included in the model because the necessary increase in overpotential of 0.3 V cannot be obtained with the specified cutoff voltage. Diffusion of lithium in the β-phase is considerably faster than in α-Al, and only very small concentration differences are predicted across the outer β-LiAl layer (see Appendix C).

The complementary reaction distributions for the positive electrode are presented in Fig. 7 and Fig. 8. The results at $\lambda = 47.9$ show explicitly the equalization in local state of charge that takes place during relaxation. Figure 7 shows that reaction IIA occurs preferentially at the front of the electrode, adjacent to the reservoir, and that a sharp reaction front moves through the electrode as Li_2FeS_2 is consumed. This mechanism also predominates in Fig. 8, although the final distribution of unreacted material is shifted from the back of the electrode. Figure 8 also indicates that, early in the charge and at a distance of approximately 0.14 cm, FeS reacts cathodically to form X-phase, in accordance with reaction IIA. This self-discharge process corresponds, in part, to the charge equalization predicted during relaxation. The effect is more pronounced at lower current densities.

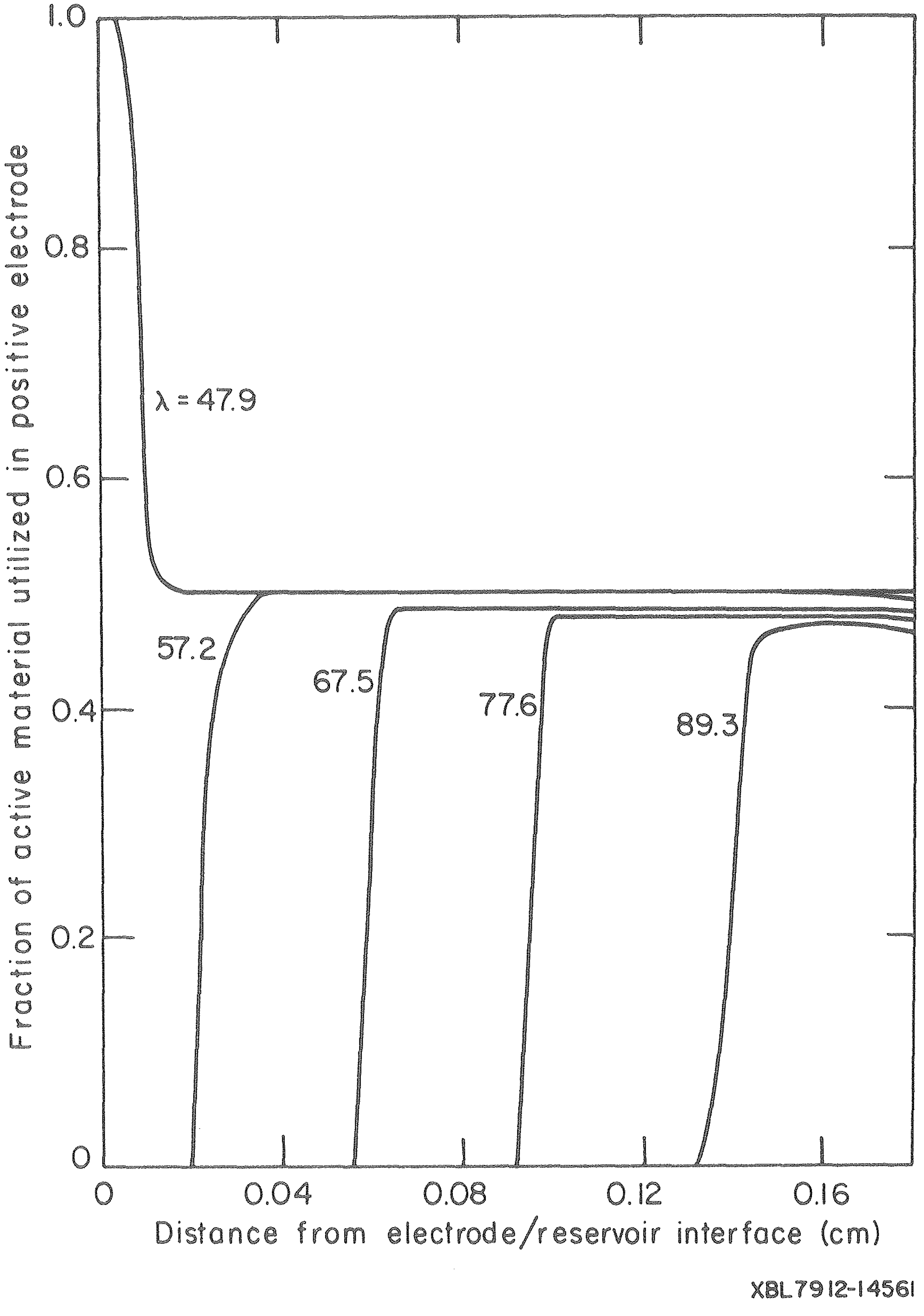

Fig. 5-7. Fraction of active material utilized in positive electrode at different overall states of charge during a constant current charge of $-41.6\ mA/cm^2$. A relaxation time of 2 hours is included between the end of the previous discharge and the beginning of the charging process. Simulation parameters as in Fig. 5-1.

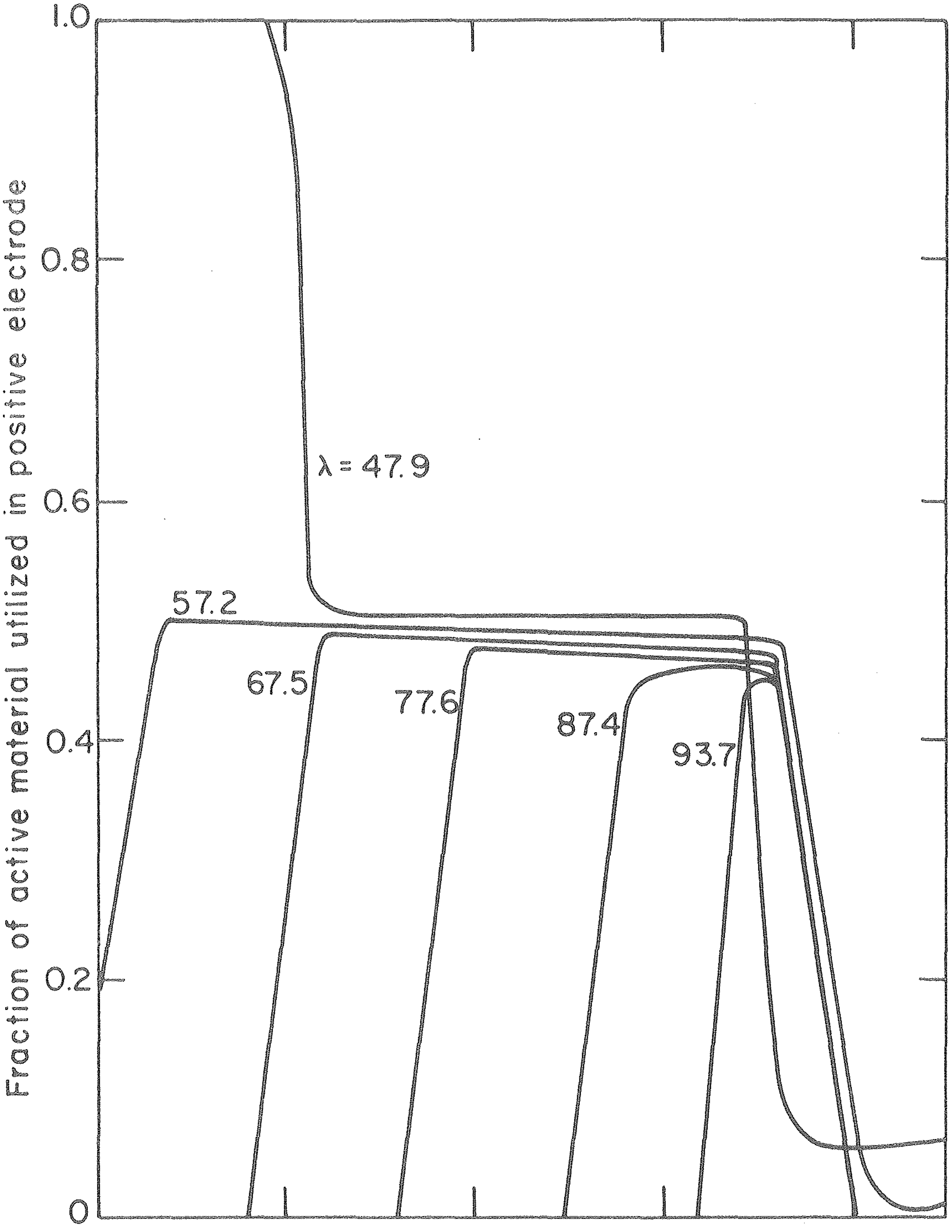

XBL 7912-14562

Fig. 5-8. Fraction of active material utilized in positive electrode at different overall states of charge during a constant current charge of -41.6 mA/cm^2. No relaxation between the end of the previous discharge and the start of the charging process. Simulation parameters as in Fig. 5-1.

The variations in total cell voltage for several constant current charges are presented in Fig. 9. In each case, there is a relatively sharp rise in electrode potential when reaction IIB is completed in the positive electrode. Also, precipitation of KCl in the negative electrode is predicted, and the local reduction in electrolyte conductivity that results causes a sharp increase in resistance at the higher current densities. At $I = -20\ \mathrm{mA/cm^2}$, charging is completed before precipitation effects dominate. The time for onset of precipitation is sensitive to the cell temperature, and this is largely responsible for the lower final states of charge that are predicted when a period of relaxation is included in the operating cycle.

Experiments on the charging behavior of LiAl/FeS cells[37] show that the positive electrode current collector potential, measured relative to a reference electrode placed adjacent to the separator, can rise sharply towards the end of charge. The rate of change of this potential can be larger than that of the negative electrode current collector, and this might be interpreted as a positive electrode limitation on charging. There are several possible reasons for this apparent discrepancy between experiment and theory:

(a) reduction in positive electrode porosity caused by expansion of the negative,

(b) reduction in available electrode capacity and uncertainty in state of charge,

(c) development of high matrix resistance in the positive electrode due to poor electrical connectivity of the phases or large contact resistances.

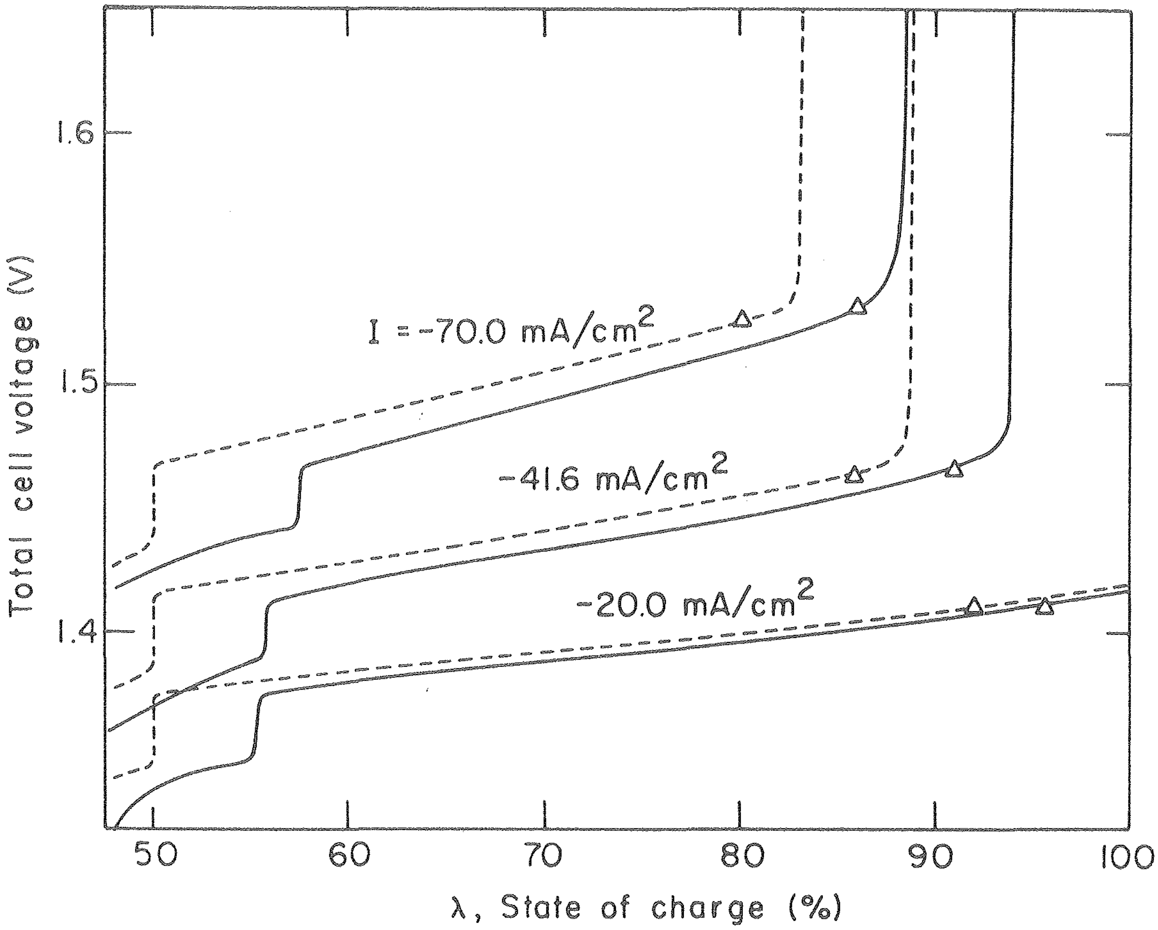

XBL 7912-14578

Fig. 5-9. Dependence of total cell voltage on state of charge during constant current charges. Simulation parameters as in Fig. 5-1 and $\lambda(t=0) = 47.9\%$.

———: charge begins immediately after discharge, $T(t=0) = 480.4°C$.

------: 2 hours relaxation between discharge and charge, $T(t=0) = 496.2°C$.

Δ : onset of precipitation of KCl in negative electrode.

Additional experiments may be needed to obtain a clearer picture of the factors that limit the charging behavior and to assess the validity of the numerical predictions. The nature of overcharge reactions, and the potentials at which they become thermodynamically feasible, may also need to be investigated.

Conclusions

A mathematical model of the LiAl/FeS cell has been used to investigate the influence of relaxation on the charging characteristics of the system. The analysis indicates that composition variations become less pronounced during relaxation, but the local state of charge within the electrodes can become more nonuniform. The concentration changes induced on charging mask the effects of current interruption and the effect of relaxation on cell temperature can be more important. The model shows that precipitation of KCl in the negative electrode can cause a rapid rise in applied potential towards the end of charge, but that the effect is not critical at low current densities. The results obtained are sensitive to the details of the heat balance used in the calculation, and this reflects a need for precise thermal management of LiAl/FeS battery modules.

NOMENCLATURE

a	interfacial area per unit electrode volume (cm^{-1})
a_k	relative activity of species k
A	variable in s domain defined by Eq. (3-20)
A	cross-sectional area of electrode (cm^2)
A_o	parameter defined by Eq. (D-4)
B	parameter in Eq. (3-4)
c_i	concentration of species i (mol/cm^3)
c_T	total ionic concentration (mol/cm^3)
C_p	specific heat (J/g.K)
D	diffusion coefficient (cm^2/s)
$\mathcal{D}$	effective diffusion coefficient of electrolyte in porous medium for thermodynamic driving force (cm^2/s)
$\mathcal{D}_{ij}$	transport coefficient for binary interactions (cm^2/s)
E	variable in s domain defined by Eq. (3-21)
F	Faraday's constant (96487 C/equiv)
$\underline{g}$	variable defined by Eq. (4-12)
G	parameter defined by Eq. (3-39)
h	mesh size (cm)
h_o	heat transfer coefficient ($W/m^2.K$)
i_o	exchange current density (A/cm^2)
$\underline{i}_1$	superficial current density in matrix phase (A/cm^2)
$\underline{i}_2$	superficial current density in pore phase (A/cm^2)
i_{nj}	total current density due to reaction j (A/cm^2)
I	superficial current density to an electrode (A/cm^2)

j	$= \nabla \cdot \underline{i}_2$, transfer current per unit electrode volume (A/cm^3)
j_{in}	pore wall flux of species i (mol/cm^2.s)
J	dimensionless transfer current
$\bar{J}$	dimensionless transfer current in s domain
L	electrode thickness (cm)
L	penetration depth (cm)
L_k	latent heat of fusion of salt k
L_T	width of cell sandwich (cm)
m	mass of cell (kg)
m	molality of electrolyte (mol/kg)
M_i	symbol for the chemical formula of species i
M_i	molecular weight of species i (g/mol)
n	number of components in electrolyte solution
n_j	number of electrons transferred in electrode reaction j
N	number of LiAl particles per unit electrode volume (cm^{-3})
$\underline{N}_i$	superficial flux of species i (mol/cm^2.s)
P	parameter defined by Eq. (3-22)
q	parameter defined by Eq. (3-6)
Q	parameter defined by Eq. (3-13)
Q	parameter defined by Eq. (2-19)
r_i	radius of β-LiAl in LiAl pellet (cm)
r_o	radius of LiAl pellet (cm)
r_{AB}	parameter defined by Eq. (2-24)
R	universal gas constant (8.3143 J/mol.K)

R_A	parameters defined by Eqs. (2-22), (2-23), and (2-33)
R_{AB}	
R_B	
R_g	grid resistance (Ω cm^2)
s	variable defined by Eq. (3-18)
s_{ij}	stoichiometric coefficient of species i in electrode reaction j
S	parameter defined by Eq. (4-18)
S_A^r	parameters defined by Eqs. (2-26) and (2-27)
S_B^r	
t	time(s)
t_f	final time(s)
t_{f2}	time between start of discharge and onset of reaction IIB in positive electrode (s)
t_i	transference number of species i with respect to the mass average velocity
t_i^r	transference number of species i with respect to reference frame, r
t_i^o	transference number of species i relative to solvent velocity
T	absolute temperature (K)
T_A	temperature of surroundings (K)
T_o	initial temperature
U	apparent open circuit cell potential (V)
$U_{j,o}$	theoretical open-circuit potential for reaction j at the composition prevailing locally at the electrode surface, relative to a reference electrode of a given kind (V)
U_j^θ	standard electrode potential for reaction j (V)

U_o	open circuit cell potential (V)
$\underline{v}$	mass average velocity (cm/s)
$\underline{v}_3$	velocity of common ion in molten salt mixture (cm/s)
$\underline{v}^{\star}$	molar average velocity (cm/s)
$\underline{v}^{\blacksquare}$	superficial volume average velocity (cm/s)
$\tilde{V}$	molar volume (cm^3/mol)
$\bar{V}_i$	partial molar volume of species i (cm^3/mol)
$\bar{V}_k$	partial molar volume of salt k (cm^3/mol)
V_R	reservoir volume (cm^3)
w	reservoir width (cm)
W	parameter defined by Eq. (3-7)
x_k	mole fraction of salt k
y	distance through electrode measured from separator (cm)
Y	dimensionless distance through porous electrode measured from separator
Y	polarization conductance (Ω^{-1} cm^{-2})
z_i	valence or charge number of species i

Greek Letters

α_a	transfer coefficient in anodic direction
α_c	transfer coefficient in cathodic direction
γ	mean molal activity coefficient
γ_i	exponent in Eq. (3-3) and Eq. (4-16)
γ_k	activity coefficient of salt k
ε	porosity or void volume fraction

ε_i	volume fraction of species i
ε_p	total volume fraction of precipitate
ε_{pk}	volume fraction of precipitate of salt k
ζ	tortuosity defined by Eq. (3-6)
η	outer perturbation parameter defined by Eq. (3-25)
η	dimensionless surface overpotential
η	$\Phi_1-\Phi_2$
θ	dimensionless concentration
κ	effective solution conductivity (mho/cm)
λ	parameter defined by Eq. (3-24)
λ	state of charge (%)
λ_k^o	property that expresses the secondary reference state for salt k
μ_e	chemical potential of electrolyte (J/mol)
μ_i	electrochemical potential of species i (J/mol)
μ_k	chemical potential of salt k (J/mol)
ν^k	total number of ions produced by dissociation of a mole of salt k
ν_i^k	number of ions of species i produced by dissociation of a mole of salt k
ρ	density (g/cm^3)
σ	effective matrix conductivity (mho/cm)
τ	dimensionless time
Φ_1	electric potential in the matrix (V)
Φ_2	electric potential in the solution (V)
ω_i	mass fraction of species i
ω_k	mass fraction of salt k

Subscripts

A	salt A, e.g. lithium chloride
B	salt B, e.g. potassium chloride
cc	current collector
e	electrolyte; electrode
i	species i (numbered 1, 2, 3)
j	reaction j
k	salt A or B
lim	limiting value
m-1	previous time step
o	at the electrode surface
o	solvent
os	in separator at electrode/separator boundary
oe	in electrode at electrode/separator boundary
ref	reference electrode
R	reference condition
s	separator
s	saturation value
α	α-Al
β	β-LiAl
+	positive electrode
−	negative electrode
∞	bulk solution property

Superscripts

A	salt A, e.g. LiCl
B	salt B, e.g. KCl
c	relative to common ion reference velocity
o	initial value
r	relative to reference frame r
α	α-Al
β	β-LiAl
$\blacksquare$	relative to volume average reference velocity
$\bigstar$	relative to molar average reference velocity
$\bar{\ }$	average value

REFERENCES

1. A. R. Landgrebe, Proceedings of Symposium and Workshop on Advanced Battery Research and Design, Argonne National Laboratory, Argonne, Illinois, March 1976, p. A-19.
2. E. J. Cairns and J. S. Dunning, Ibid., p. A-81.
3. P. A. Nelson *et al.*, "High-Performance Batteries for Electric-Vehicle Propulsion and Stationary Energy Storage," Progress Report for the period 11/78-3/79, ANL 79-39, Argonne National Laboratory (May 1979).
4. E. J. Cairns and H. Shimotake, Science, 164, 1347 (1969).
5. J. Newman and R. Pollard in "High Performance Batteries for Electric-Vehicle Propulsion and Stationary Energy Storage," Progress Report for the Period 4/78-10/79, ANL 79-94, Argonne National Laboratory (November 1979).
6. J. Newman, "Electrochemical Systems," Prentice-Hall, Englewood Cliffs, N. J. (1973).
7. J. Newman, D. Bennion, and C. W. Tobias, Ber. Bunsenges. Physik. Chem. 69, 608 (1965). For corrections, see ibid., 70, 493 (1966).
8. J. Newman, Adv. in Electrochem. Electrochem. Eng. 5, 87 (1967).
9. D. G. Miller, J. Phys. Chem. 71, 616 (1967).
10. J. Newman and W. Tiedemann, AIChE Journal, 21, 25 (1975).
11. J. S. Dunning, Dissertation, University of California, Los Angeles (1971).
12. W. G. Sunu, Dissertation, University of California, Los Angeles (1978).

13. C. E. Vallet, H. R. Bronstein, and J. Braunstein, J. Electrochem. Soc. 121, 1429 (1974).

14. J. Newman and C. W. Tobias, Ibid. 109, 1183 (1962).

15. J. Newman and T. Chapman, AIChE Journal 19, 343 (1973).

16. M. Blander in "Molten Salt Chemistry," M. Blander, Editor, pp. 127-238, Interscience (1964).

17. R. B. Bird, W. E. Stewart, and E. N. Lightfoot, "Transport Phenomena," pp. 554-572, J. Wiley & Sons, New York (1960).

18. J. Newman, Internal tech. report, NOLC project, Dept. of Chem. Eng., Univ. of California, Berkeley (1962).

19. K. Micka and I. Rousar, Electrochim. Acta 21, 599 (1976).

20. D. Simonsson, J. Appl. Electrochem. 3, 261 (1973).

21. W. Stein, Ph.D. thesis, Rheinisch-Westfalischen Techn. Hochschule, Aachen (1959).

22. K. Micka and I. Rousar, Electrochim. Acta 18, 629 (1973); Ibid., 19, 499 (1974).

23. J. Newman and W. Tiedemann, "Advances in Electrochemistry and Electrochemical Engineering," Vol. 11, H. Gerischer and C. W. Tobias, Editors, Wiley-Interscience, (1977).

24. A. Winsel, Z. Elektrochem. 66, 287 (1962).

25. C. E. Vallet and J. Braunstein, J. Electrochem. Soc. 125, 1193 (1978).

26. W. Tiedemann, J. Newman, and F. De Sua, Power Sources, 6, 15 (1977).

27. W. Tiedemann and J. Newman, Proc. Symp. Battery Design and Optimization, S. Gross (Ed.), Princeton: The Electrochemical Society, Inc., 1979, page 23.

28. W. Tiedemann and J. Newman, Ibid., page 39.

29. R. White, Dissertation, University of California, Berkeley (1977).

30. W. Tiedemann and J. Newman, J. Electrochem. Soc. 122, 1482 (1975).

31. C. A. Melendres, Ibid. 124, 650 (1977).

32. R. Pollard and J. Newman, unpublished work.

33. D. Gidaspow and B. S. Baker, J. Electrochem. Soc. 120, 1005 (1973).

34. J. S. Dunning, D. N. Bennion, and J. Newman, Ibid. 118, 1251 (1971).

35. J. S. Dunning, D. N. Bennion, and J. Newman, Ibid. 120, 906 (1973).

36. H. Gu, D. N. Bennion, and J. Newman, Ibid., 123, 1364 (1976).

37. L. Redey and D. R. Vissers, personal communication.

38. D. R. Vissers, K. E. Anderson, C. K. Ho, and H. Shimotake, Proc. Symp. Battery Design and Optimization, S. Gross (Ed.), Princeton: The Electrochemical Society, Inc., 1979, page 416.

39. M. L. Saboungi and A. E. Martin, The Electrochem. Soc. Mtg., Pittsburgh, Oct. 15-20, 1978, Extended Abstract No. 339.

40. N. C. Otto and J. E. Battles in, "High Performance Batteries for Electric Vehicle Propulsion and Stationary Energy Storage," Progress Report for the period 11/78-3/79, ANL 79-39, Argonne National Laboratory (May 1979), page 50.

41. S. V. Karpachev, A. G. Stromberg, and V. N. Podchainova, Zh. Obshchei Khim., 5, 1517 (1935).

42. E. R. van Artsdalen and I. S. Yaffe, J. Phys. Chem. 59, 118 (1955).

43. J. Richter, U. Gasseling, and R. Conradt, E. Acta 23, 1165 (1978).

44. C. T. Moynihan and R. W. Laity, J. Phys. Chem. 68, 3312 (1964).

45. E. Aukrust, B. Bjorge, H. Flood, and T. Førland, Annals N. Y. Acad. Sci. 79, 830 (1960).

46. B. Chu and J. J. Egan, Annals N. Y. Acad. Sci. 79, 908 (1960).

47. J. Lumsden, "Thermodynamics of Molten Salt Mixtures," Academic Press, 1966.

48. T. J. Edwards, J. Newman, and J. M. Prausnitz, Ind. Eng. Chem. Fund. 17, 264 (1978).

49. M. Hansen, "Constitution of Binary Alloys," Metallurgy and Metallurgical Engng. series, 2nd Ed., McGraw-Hill, N.Y. (1958).

50. J. P. Suchet, "Crystal Chemistry and Semiconduction in Transition Metal Binary Compounds," Academic Press (1971).

APPENDIX A

Derivation of Parameters for Analytic Model of Porous Electrodes with High Exchange Current Densities

Positive plate of lead-acid battery

In the PbO_2 electrode, a nonsteady state material balance for species i may be combined with Faraday's law to give

$$\frac{\partial(\varepsilon c_i)}{\partial t} = -\nabla\cdot\underline{N}_i - \frac{s_i}{nF}\, j \tag{A-1}$$

for a single electrode reaction.[10] For a concentrated binary electrolyte, the superficial flux of species i can be expressed in terms of the superficial volume average velocity $\underline{v}^{\blacksquare}$:[10,15]

$$\underline{N}_i = -\varepsilon D\nabla c_i + \frac{t_i^o}{z_i F}\,\underline{i}_2 + c_i\underline{v}^{\blacksquare} \ . \tag{A-2}$$

Substitution into Eq. (1) and comparison with Eq. (3-4) defines the parameter B as

$$B = \frac{\nu_i c_o \bar{V}_o}{n}\left[\frac{s_o c}{c_o} - \left(\frac{s_+ t_-^o}{\nu_+} + \frac{s_- t_+^o}{\nu_-}\right)\right] . \tag{A-3}$$

Ohm's law can be used in the form

$$\frac{\underline{i}_2}{\kappa} = -\nabla\Phi_2 + \frac{B}{\nu_i c_o \bar{V}_o F}\,\nabla\mu_e \tag{A-4}$$

where Φ_2 is the potential in the pore solution measured with a reference electrode of the same kind as the working electrode. The chemical potential of the electrolyte can be defined with

$$\nabla\mu_e = \frac{\nu RT}{c_o\bar{V}_o}\left(1 + \frac{d\ \ln\ \gamma}{d\ \ln\ m}\right)\nabla\ \ln\ c_i \tag{A-5}$$

where ν is the total number of cations and anions produced by dissociation of one molecule. Consequently, the parameter W in Eq. (3-7) is given by

$$W = \frac{\nu B}{\nu_i(c_o\bar{V}_o)^2}\left(1 + \frac{d\ \ln\ \gamma}{d\ \ln\ m}\right). \tag{A-6}$$

<u>Negative electrode of LiAl/FeS$_x$ Battery</u>

This high temperature system can use an electrolyte that comprises two binary molten salts with a common ion, such as the LiCl - KCl eutectic. In the derivation below, subscripts 1, 2, and 3 refer to Li^+, K^+, and Cl^- ions, respectively, and scripts A and B refer, in turn, to the LiCl and KCl salts. The superficial flux of lithium ions based on the molar average reference velocity is

$$\underline{N}_1 = -\frac{\varepsilon(c_A + c_B)^2 D\nu_1^A\nu^B}{c_T}\nabla x_A + \frac{t_1^{\star}\underline{i}_2}{z_1 F} + c_1\underline{v}^{\star}\ , \tag{A-7}$$

where $x_A = c_A/(c_A + c_B)$ is the mole fraction of LiCl in the electrolyte and c_T is the total concentration defined by $c_T = c_1 + c_2 + c_3$.

Combination of Eqs. (1) and (7) gives, on simplification, Eq. (3-4) with

$$B = \tilde{V}\left[\frac{c_A}{\nu_2^B}\left(\frac{s_2}{n} + \frac{t_2^{\star}}{z_2}\right) - \frac{c_B}{\nu_1^A}\left(\frac{s_1}{n} + \frac{t_1^{\star}}{z_1}\right)\right] , \tag{A-8}$$

provided that the molar volume of electrolyte $\tilde{V}$ is constant. Ohm's law for the pore electrolyte can be written in a form analogous to Eq. (4) as

$$\frac{i_2}{\kappa} = -\nabla\Phi_2 - \frac{G}{F}\nabla\mu_A , \tag{A-9}$$

where

$$G = \left(\frac{s_1}{n\nu_1^A} + \frac{t_1^c}{z_1\nu_1^A}\right)\left(1 + \frac{\nu_3^A c_A}{\nu_3^B c_B}\right) - \frac{s_3 c_A}{n c_B \nu_3^B} . \tag{A-10}$$

The activity coefficient of a salt in a binary molten salt electrolyte mixture is often defined without regard for dissociation and in terms of ion equivalent fractions or mole fractions.[16] (These composition variables are equivalent when $\nu_3^A = \nu_3^B$.) The gradient of chemical potential can be written as

$$\nabla\mu_A = RT\left(\nu_1^A + \frac{d \ln \gamma_A}{d \ln x_A}\right) \nabla \ln c_A , \tag{A-11}$$

and with this definition the parameter W in Eq. (3-7) becomes

$$W = -G \left(\nu_1^A + \frac{d \ln \gamma_A}{d \ln x_A} \right) . \qquad \text{(A-12)}$$

In the absence of experimental data for transference numbers it is assumed that transference numbers are directly proportional to the electrolyte mole fraction, viz: $\overset{*}{t}_1 = \nu_3^A x_A / \nu^A$, $\overset{*}{t}_2 = \nu_3^B x_B / \nu^B$, and $t_1^c = x_A$.

APPENDIX B

Physical Properties of the LiAl/LiCl,KCl/FeS System

Electrolyte conductivity

The dependence of bulk electrolyte conductivity on composition and temperature is described by

$$\kappa_\infty = (ax_A^2 + bx_A + c)e^{-E/T} , \tag{B-1}$$

where: $a = 18.9803$; $b = -5.0170$; $c = 9.0903$; $E = 1425.76$ K.[41,42] The effective conductivity in the porous medium is estimated from Eq. (3-6) and (3-8).

Transference number

Measurements of transference numbers in binary nitrate melts show that deviations from the relation $t_i^c = x_i$ are often relatively small.[43] Experiments in LiCl-KCl melts[44] also tend to substantiate the use of this assumption which, for the molar average velocity reference frame, gives: $t_1^\star = x_A/2$; $t_2^\star = (1-x_A)/2$.

Activity coefficient

If dissociation of electrolyte is disregarded,[16] the gradient of chemical potential of LiCl in the LiCl-KCl mixture can be written as

$$\nabla\mu_A = RT \left(1 + \frac{d \ln \gamma_A}{d \ln x_A}\right) \nabla \ln x_A . \tag{B-2}$$

Information from the LiCl-KCl phase diagram can be used to obtain the composition and temperature dependence of the activity coefficient.[45-47] A relationship of the form[48]

$$\ln \gamma_A = \frac{b}{T} \tanh \left(\frac{a(1-x_A)^n}{b x_A} \right) , \tag{B-3}$$

with a = -1023.84, b = -1555.11, and n = 3, has been chosen to represent the data.

Molar volume of electrolyte

The molar volume of electrolyte is defined as $\tilde{V} = \sum_k M_k x_k / \rho$ where the density ρ is given by $\rho = 1.735 - 0.15\, x_A$.

Diffusion coefficient

For the special case where the diffusion coefficients for binary interactions are all equal, it may be shown that

$$D_\infty = \frac{\kappa_\infty RT \tilde{V}}{2F^2} \left(1 + \frac{d \ln \gamma_A}{d \ln \gamma_A} \right) . \tag{B-4}$$

On this basis, it is assumed that

$$D_\infty = 2.442 \times 10^{-4} e^{-E/T} (x_A + 0.4) , \tag{B-5}$$

over the composition and temperature range of interest. The molecular diffusion coefficient in the porous media can be characterized by Eq. (3-5).

LiCl-KCl phase diagram

The equilibrium compositions that characterize the onset of precipitation of LiCl and KCl are approximated by[49]

$$\begin{aligned}(x_A)_{LiCl,sat} &= 0.34080 - 4.773 \times 10^{-4}\, T + 1.376 \times 10^{-6}\, T^2 \\ (x_A)_{KCl,sat} &= 0.14615 + 1.9117 \times 10^{-3}\, T - 1.948 \times 10^{-6}\, T^2 .\end{aligned} \qquad (B\text{-}6)$$

Matrix conductivity

In general, the matrix conductivity can be influenced by the volume fraction of the conducting phases, the inherent conductivity of each solid phase, and the manner in which the particles of conducting phases are interconnected. As a first approximation, it has been assumed that parallel conduction pathways exist in the positive electrode so that

$$\sigma = \sum_i \sigma_i \varepsilon_i^{\,q} , \qquad (B\text{-}7)$$

and q is taken to be 1.5. In the negative electrode, the conductivities of the active materials and the supporting grid are each very high ($\sigma_{Li} \cong 1.0 \times 10^5\ \Omega^{-1}cm^{-1}$; $\sigma_{Al} \cong 2.2 \times 10^5\ \Omega^{-1}cm^{-1}$; $\sigma_{Fe} \cong 2.3 \times 10^4\ \Omega^{-1}cm^{-1}$, at T = 450°C) and consequently the matrix conductivity is assumed to be infinite.

Current collector resistance

The combined resistance R_g of the grid and terminal is obtained from a preliminary estimate of the polarization conductance, as defined by Eq. (4-30). The resistance R_b of a bicell can be separated into electrochemical and current collector contributions, according to:

$$R_b = \frac{1}{2A} \frac{1}{Y} + R_g \quad . \tag{B-8}$$

In the calculations, it is assumed that $R_b = 4 m\Omega$, $Y = 1.013\ \Omega^{-1} cm^{-2}$,[5] and $A = 316\ cm^2$. This yields $R_g = 1.55\ \Omega\ cm^2$.

Table B-1. Physical parameters used in analysis

Parameter		Value
U_o	(V)	1.34
$\partial U_o/\partial T$	(V/K)	$-1.55\text{x}10^{-4}$
C_p	(kJ/kg.K)	1.03
h_o	$(W/m^2.K)$	$4.13\text{x}10^{-2}$
T_A	(K)	298.15
$\tilde{V}_{LiCl}$	(cm^3/mol)	20.50
$\tilde{V}_{KCl}$	(cm^3/mol)	37.58
$\tilde{V}_{FeS}$	(cm^3/mol)	18.55
$\tilde{V}_{Fe}$	(cm^3/mol)	7.11
$\tilde{V}_x$	(cm^3/mol)	46.23
σ_{Fe}	$(\Omega^{-1}cm^{-1})$	$8.23\text{x}10^4$
σ_{FeS}^{50}	$(\Omega^{-1}cm^{-1})$	$1.90\text{x}10^3$
σ_x	$(\Omega^{-1}cm^{-1})$	$5.00\text{x}10^2$
ρ_α	(g/cm^3)	2.70
ρ_β	(g/cm^3)	1.75
V_R^o/A	(cm)	0.03

APPENDIX C

Derivation of Polarization Equations for Negative Electrode

Discharge behavior

As discharge proceeds, a layer of α-Al develops at the solid-electrolyte interface (see Fig. 1). For a spherical particle, material balances for lithium and aluminum give, respectively,

$$r_i^3\ \bar{c}^{\beta}_{Li} + (r_o^3 - r_i^3)\ \bar{c}^{\alpha}_{Li} = (r^o_o)^3\ c^{\beta}_{Li} + \frac{3s_i}{4\pi NnF} \int_o^t \nabla\cdot\underline{i}_2\, dt \tag{C-1}$$

and

$$r_i^3\ \bar{c}^{\beta}_{Al} + (r_o^3 - r_i^3)\ \bar{c}^{\alpha}_{Al} = (r^o_o)^3\ \bar{c}^{\beta}_{Al}\ , \tag{C-2}$$

where $\bar{c}^{\alpha}_{Li}$ is the average concentration of lithium in the α-phase and N is the number of pellets per unit electrode volume. The average compositions $\bar{c}^{\alpha}_{Li}$ and $\bar{c}^{\alpha}_{Al}$ are related by

$$\bar{\bar{V}}^{\alpha}_{Al}\ \bar{c}^{\alpha}_{Al} + \bar{\bar{V}}^{\alpha}_{Li}\ \bar{c}^{\alpha}_{Li} = 1\ , \tag{C-3}$$

provided that $\bar{\bar{V}}^{\alpha}_{Al}$ and $\bar{\bar{V}}^{\alpha}_{Li}$ are assumed to be independent of position. Substitution of Eq. (1) and (3) into (2) gives, on differention:

$$\frac{4\pi N}{3} \left\{ (\bar{c}^{\beta}_{Al}\bar{\bar{V}}^{\alpha}_{Al} + \bar{c}^{\beta}_{Li}\bar{\bar{V}}^{\alpha}_{Li} - 1)\ \frac{dr_i^3}{dt} + \frac{dr_o^3}{dt} \right\} = -\ \bar{\bar{V}}^{\alpha}_{Li}\ \frac{\nabla\cdot\underline{i}_2}{F}\ , \tag{C-4}$$

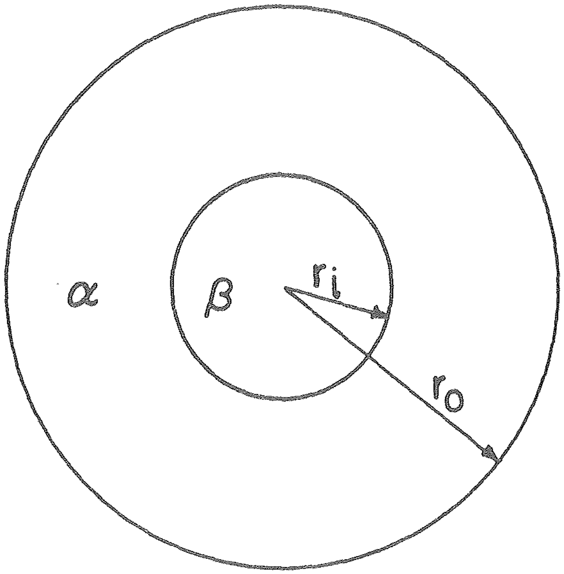

a) Discharge

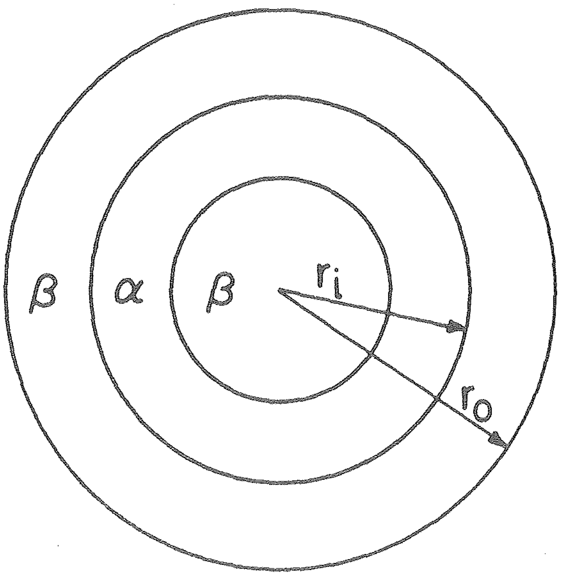

b) Charge

XBL 7912-14575

Fig. C-1. Schematic diagram of juxtaposition of phases in negative electrode matrix.

where it is assumed that $s_i/n = -1$. It should be noted that derivation of Eq. (4) does not necessitate an assumption of constant lithium concentration within the α-Al. This is not the case for Eq. (2) which, on differentiation, yields:

$$(\bar{c}^{\beta}_{Al} - \bar{c}^{\alpha}_{Al}) \frac{dr_i^3}{dt} + \bar{c}^{\alpha}_{Al} \frac{dr_o^3}{dt} = 0 \ . \tag{C-5}$$

An overall material balance for the solid phase can be written as

$$\frac{4\pi N}{3} \frac{dr_o^3}{dt} = A_o \nabla\cdot\underline{i}_2 \ . \tag{C-6}$$

Substitution of Eq. (4) and (5) into this expression gives

$$A_o = - \frac{(\bar{c}^{\beta}_{Al} - \bar{c}^{\alpha}_{Al})}{(\bar{c}^{\beta}_{Al}\bar{c}^{\alpha}_{Li} - \bar{c}^{\alpha}_{Al}\bar{c}^{\beta}_{Li})F} \ , \tag{C-7}$$

which is independent of the assumed morphology.

With these relationships, the characteristic radii, r_o and r_i, can be related to the state of charge by

$$r_o^3 = (r_o^o)^3 + \frac{3}{4\pi N} \int_o^t A_o \nabla\cdot\underline{i}_2 \, dt \ , \tag{C-8}$$

and

$$r_i^3 = (r_i^o)^3 + \frac{3}{4\pi N} \frac{1}{(1 - \bar{c}^{\beta}_{Al}/\bar{c}^{\alpha}_{Al})} \int_o^t A_o \nabla\cdot\underline{i}_2 \, dt \ . \tag{C-9}$$

At the α-β interface, a flux balance for each species may be written as

$$\underline{N}_k^\beta - \bar{c}_k^\beta \frac{dr_i}{dt} = N_k^\alpha - \bar{c}_k^\alpha \frac{dr_i}{dt} . \qquad \text{(C-10)}$$

The diffusion flux at r_i is given by

$$\underline{N}_{Li}^\alpha - \bar{c}_{Li}^\alpha \underline{v}_\alpha^\star = c_T^\beta (\bar{x}_{Li}^\alpha - \bar{x}_{Li}^\beta) \frac{dr_i}{dt} , \qquad \text{(C-11)}$$

because $\underline{N}_i^\beta = 0$. Differentiation of Eq. (9) and substitution into Eq. (11) gives

$$\underline{N}_{Li}^\alpha - \bar{c}_{Li}^\alpha \underline{v}^\star = \frac{(1-\bar{x}_{Li}^\alpha)}{4\pi NFr_i^2} \nabla \cdot \underline{i}_2 , \qquad \text{(C-12)}$$

at the inner boundary.

At the solid-electrolyte interface,

$$\underline{N}_{Li}^\alpha - \bar{c}_{Li}^\alpha \frac{dr_o}{dt} = \frac{\nabla \cdot \underline{i}_2}{4\pi NFr_o^2} , \qquad \text{(C-13)}$$

and

$$\underline{N}_{Al}^\alpha - \bar{c}_{Al}^\alpha \frac{dr_o}{dt} = 0 . \qquad \text{(C-14)}$$

Combination of Eq. (13) and (14) gives

$$\underline{N}^{\alpha}_{Li} - c^{\alpha}_{Li}\,\underline{v}^{\star}_{\alpha} = \frac{(1-x^{\alpha}_{Li})}{4\pi N F r_o^2}\,\nabla\cdot\underline{i}_2\ , \tag{C-15}$$

at the outer boundary.

The psuedo-state state approximation is based on the hypothesis that

$$D_{\alpha}\,\frac{dc^{\alpha}_{i}}{dr} \propto \frac{1}{r^2}\ , \tag{C-16}$$

where $\underline{N}^{\alpha}_{Li} - \bar{c}^{\alpha}_{Li}\,\underline{v}^{\star}_{\alpha} = D_{\alpha}\,dc^{\alpha}_{i}/dr$. Integration of Eq. (16) across the α-phase with $c^{\alpha}_{Li} = 0$ at the outer boundary defines the limiting transfer current as

$$(\nabla\cdot\underline{i}_2)_{lim} = \frac{4\pi N F D_{\alpha}(c^{\alpha}_{Li})_{sat}}{(1-\bar{x}^{\alpha}_{Li})(\frac{1}{r_i} - \frac{1}{r_o})}\ . \tag{C-17}$$

The surface concentration of lithium can be written in terms of $(\nabla\cdot\underline{i}_2)_{lim}$:

$$\frac{(c^{\alpha}_{Li})_{surface}}{(c^{\alpha}_{Li})_{sat}} = 1 - \frac{\nabla\cdot\underline{i}_2}{(\nabla\cdot i_2)_{lim}} \tag{C-18}$$

Equation (18) can be substituted into the Butler-Volmer Equation (4-15) to give a modified polarization relationship that includes the effects of solid state diffusion of lithium through the α-Al layer and electrochemical reaction at the solid-liquid interface:

$$\nabla \cdot \underline{i}_2 = \frac{e^{\alpha_a F\eta/RT} - e^{-\alpha_a F\eta/RT}}{\frac{1}{ai_o'} + \frac{e^{\alpha_a F\eta/RT}}{(\nabla \cdot \underline{i}_2)_{\lim}}} \quad . \tag{C-19}$$

In Eq. (19), the reference concentration for lithium atoms is taken as $(c^{\alpha}_{Li})_{sat}$ and the term ai_o' is given by

$$ai_o' = 4\pi N r_o^2 \, (i_o)_{ref} \sqrt{\frac{x_A}{x_{A,ref}}} \quad . \tag{C-20}$$

Changes in $(\nabla \cdot \underline{i}_2)_{\lim}$, r_i and r_o are predicted from Eq. (17), (8), and (9), respectively.

Charge Behavior

At any point in the electrode, it is assumed that an outer layer of β-LiAl forms immediately charging begins, and that the electrochemical reaction is restricted to the solid-electrolyte interface (see Fig. 1). The analysis of diffusion of lithium through the β-phase and the gradual reduction in thickness of the α-Al region parallels the model for discharge. Equation (7) and (8) apply directly, but Eq. (9) should be replaced with

$$r_i^3 = (r_i^o) + \frac{3}{4\pi N} \frac{1}{(1-\bar{c}^{\alpha}_{Al}/\bar{c}^{\beta}_{Al})} \int_o^t A_o \, \nabla \cdot \underline{i}_2 dt \quad , \tag{C-21}$$

and the limiting transfer current becomes

$$(\nabla\cdot\underline{i}_2)_{\lim} = \frac{4\pi NFD_\beta(c_{Li}^\beta)_{sat}}{(1-\bar{x}_{Li}^\beta)(\frac{1}{r_o}-\frac{1}{r_i})} \quad . \qquad \text{(C-22)}$$

Equations (19) and (20) can also be used, but the reference concentration in Eq. (18) should now be $(c_{Li}^\beta)_{sat}$.

APPENDIX D

Treatment of Governing Equations for LiAl/FeS Cell

The material balances are:

$$\frac{\partial(\epsilon x_A/\tilde{V})}{\partial t} + \nabla\cdot\left(x_A\underline{g} - \frac{\epsilon D}{\tilde{V}}\nabla x_A\right) = aj_{1n} \tag{D-1}$$

$$\frac{\partial(\epsilon x_B/\tilde{V})}{\partial t} + \nabla\cdot\left(x_B\underline{g} - \frac{\epsilon D}{\tilde{V}}\nabla x_B\right) = aj_{2n} \tag{D-2}$$

$$\frac{\partial(\epsilon+\epsilon_p)}{\partial t} = -\sum_j A_{oj}(ai_n)_j \quad , \tag{D-3}$$

where

$$A_{oj} = \sum_{\substack{\text{solid}\\ \text{phases},i}} s_{ij}\,\tilde{V}_i/n_jF \ . \tag{D-4}$$

Ohm's law can be written as:

$$\nabla\eta = \left(\frac{1}{\kappa}+\frac{1}{\sigma}\right)\underline{i}_2 - \frac{I}{\sigma} - \frac{RT}{Fx_A}\left(1+\frac{d\ \ln\ \gamma_A}{d\ \ln\ x_A}\right)\nabla x_A \ . \tag{D-5}$$

In the finite difference procedure, Eq. (1) to (3) are programmed at a mesh point, where as Eq. (5) is calculated midway between mesh points. The variables x_A, ϵ, η, and i_{nj} are defined at mesh points, but both $\underline{i}_2$ and $\underline{g}$ are specified between nodes, and placed in adjacent storage locations.

The numerical calculations can be simplified by eliminating the variables i_{nj} from the heart of the program. The difference equations can be represented as (6)

$$\sum_{k=1}^{\ell} A_{i,k}(n)C_k(n-1) + B_{i,k}(n)C_k(n) + D_{i,k}(n)C_k(n+1) = G_i(n) \ , \qquad \text{(D-6)}$$

and the central term can be subdivided into contributions from the variables C'_k, that only appear at mesh point n, and variables C''_k that appear at points n-1, n, and n+1:

$$B_{i,k}(n)C_k(n) = B'_{i,k}(n)C'_k(n) + B''_{i,k}(n)C''_k(n) \ . \qquad \text{(D-7)}$$

In this way the polarization equation can be written as:

$$B'_{\ell,k}(n)C'_k(n) = G_\ell(n) - B''_{\ell,k}(n)C''_k(n) \ . \qquad \text{(D-8)}$$

Inversion of Eq. (8) and substitution into Eq. (6) to eliminate $C'_k(n)$, gives modified expressions for $B_{i,k}(n)$ and $G_i(n)$:

$$B_{i,k}(n) = B''_{i,k}(n) - B'_{i,k}(n) \ [B'_{\ell,k}(n)^{-1} \ B''_{\ell,k}(n)] \qquad \text{(D-9)}$$

$$G_i(n) = G_i(n) - B'_{i,k}(n) \ [B'_{\ell,k}(n)^{-1} \ G_\ell(n)] \ . \qquad \text{(D-10)}$$

The boundary conditions for the electrolyte material balances (see Eq. (4-22) - (4-25)) can be included directly, in integrated forms of the differential equations. At the current collectors, one may use:

$$\frac{\Delta y/2}{\Delta t}\left[\left(\frac{\varepsilon x_i}{\tilde{V}}\right)_m - \left(\frac{\varepsilon x_i}{\tilde{V}}\right)_{m-1}\right]_p + (\underline{N}_i)_{m-\frac{1}{2},q} = \Delta y/2\ (aj_{in})_{m-\frac{1}{2},p}\ , \tag{D-11}$$

where q refers to a location halfway between the two end mesh points and p refers to a location halfway between q and the boundary. The subscript $m - \frac{1}{2}$ indicates a value averaged between the old time and the present one.

Similarly, a flux balance at the negative electrode/separator interface yields, for each species:

$$\frac{\partial}{\partial t}\left[\left(\frac{\varepsilon_s x_i}{\tilde{V}}\right)_p \frac{\Delta y_s}{2} + \left(\frac{\varepsilon x_i}{\tilde{V}}\right)_{-p} \frac{\Delta y_-}{2}\right] + [(\underline{N}_i)_q - (\underline{N}_i)_{-q}]_{m-\frac{1}{2}} = \frac{\Delta y_-}{2}\ (aj_{in})_{m-\frac{1}{2},-p}\ . \tag{D-12}$$

The subscripts -p and p in Eq. (12) correspond to the electrode and separator sides of the interface, respectively.

At the front of the positive it is necessary to include the change in volume of the electrolyte reservoir:

$$\frac{\partial}{\partial t}\left[\left(\frac{\varepsilon_s x_i}{\tilde{V}}\right)_{-p}\frac{\Delta y_s}{2}+\left(\frac{\varepsilon x_i}{\tilde{V}}\right)_p\frac{\Delta y_+}{z}+\frac{V_R}{A}\left(\frac{x_i}{\tilde{V}}\right)_{\text{interface}}\right]+\left[(\underline{N}_i)_q-(\underline{N}_i)_{-q}\right]_{m-\frac{1}{2}}$$

$$=\frac{\Delta y_+}{2}\,(aj_{in})_{m-\frac{1}{2},p}\ . \qquad \text{(D-13)}$$

Here, -p and p refer to the separator and electrode, respectively.

APPENDIX E

Computer Program

Program BATRY calculates the time-dependent and position-dependent behavior of the LiAl/LiCl,KCl/FeS cell for a given set of operating conditions. The program uses three subroutines: BAND and MATINV[6] solve the set of coupled, linear difference equations that represent the physical problem, and PROPS specifies the necessary physical property information. Input parameters and some key variables are listed below:

AA, AC	$(\alpha_{a,j})_+$, $(\alpha_{c,j})_+$
AIO1, AIO2	$(ai_o)_{IIA}$, $(ai_o)_{IIB}$
ALPHA, ALPHC	$(\alpha_a)_-$, $(\alpha_c)_-$
AON	$-A_o$
C	main variable array. IG, II, IJ, IN, IX, correspond to $\underline{g}$, $\underline{i}_2$, $\nabla\cdot\underline{i}_2$, $\eta = \Phi_1 - \Phi_2$, and x_A, respectively.
CHT	h_o
CON	κ_∞
CONV	convergence criterion
CPMA	mC_p/A
CR1	$(i_o)_-$
DA,DB	D_α,D_β
DELT	time step
DETA	$\eta - U_{IIA,o}$

DOCCPT	$(\partial U_o/\partial T)_p$
DSEPOT	$- U_{IIA,o}$
EFE	ε_{Fe}
EINIT, EINITB	ε_-^o, ε_+^o
EN	N
EONS, EONSB	n_-, $(n_j)_+$
EPK, EPL	$(\varepsilon_p)_{KCl}$, $(\varepsilon_p)_{LiCl}$
ESEP	ε_s
EX	ε_x
FACTOR	$q = 1.5$
GAM	γ_i
HFUSEK, HFUSEL	L_{KCl}, L_{LiCl}
H1, H2, H3	h_-, h_s, h_+
MAXITS	maximum number of iterations
NJ1, NJ2, NJ	number of mesh points from negative current collector to front of negative, front of positive, and positive current collector, respectively.
RBINIT	r_i^o
RGRID	R_g
RINKEP	$(r_i)_{m-1}$
ROA, ROB	ρ_α, ρ_β
ROINIT	r_o^o
ROUTA	r_o
S1, S1B	$(S_1)_-$, $(S_1)_+$
S3, S3B	$(S_3)_-$, $(S_3)_+$
SIGFE, SIGFES	σ_{Fe}, σ_{FeS}

SIGINV	$1/\sigma$
SIGX	σ_x
TAMB	T_A
TCD	I
TCV	V
TIME	t
TINIT	T_o
TSTOP	final time
UJO	U_o
VFE,VFES	$\tilde{V}_{Fe}$, $\tilde{V}_{FeS}$
VKCL, VLICL	$\tilde{V}_{KCl}$, $\tilde{V}_{LiCl}$
VOVERA	V_R/A
VSTAR	$\underline{v}^*$
WIDTH	w
XAINIT	x_A^o
XAR	$x_{A,ref}$
XASK, XASL	$(x_{A,KCl})_{sat}$, $(x_{A,LiCl})_{sat}$
XD	$x_A - x_A^o$

```
      PROGRAM BATRY(INPUT,OUTPUT,PUNCH)
C     PROGRAM TO FIND CURRENT,OVERPOTENTIAL AND REACTION RATE
C     DISTRIBUTION FOR LIAL,FES CELL
      DIMENSION A(6,6),B(6,6),C(6,401),D(6,13),G(6),X(6,6),Y(6,6),COLD(4
     1,401),DIST(401),V(401),DVX(401),EPKKEP(401),ESUM(401),DIFUSN(401),
     1DDX(401),        CON(401),DCONX(401),EFE(401),
     1DLNAC(401),D2LNAC(401),ZETA(401),DZETAX(401),EPLKEP(401),
     1ZETALD(401),CKEEP(6,401),RBETA(401),ROUTA(401),            EX(401)
     1,RIN(401),RINKEP(401),DPOL(3,401),EFES(401),Q(401)
     1,DVDT(401)           ,XD(401),XDKEEP(401),BIG(6),VSTAR(401),W(401)
     1,       GB(3,1),CJ1(401),CJ2(401),CJ1KEP(401),CJ2KEP(401),SS(4,2),
     1E1(6),E2(6),                        SIGINV(401),TALL(6)
     1,ELI2S(401),                        NONCF(401)
     1,R1(401),R2(401),RV1(401),RV2(401),EPL(401),EPK(401),DETA(401)
      EQUIVALENCE (EFES(1),W(1)),(EX(1),RBETA(1)),(ELI2S(1),RIN(1))
     1,(EFE(1),ROUTA(1)),(RINKEP(1),CJ2KEP(1))
      COMMON A,B,C,D,G,X,Y,N,NJ
      COMMON/1/V,DVX,DVDT          ,DIFUSN,DDX        ,SIGINV,CON,
     1DCONX,DLNAC,D2LNAC,ZETA,DZETAX          ,FACTOR,T,IX,NJ1,NJ2
     1,EX,EFES,EFE,SIGY,SIGFES,SIGFE,PIN43
      COMMON/2/R1,R2,RV1,RV2
      COMMON/3/S,AON,ACP1,ACP2,CJ1,CJ2,EXPAND
      DATA IX,IG,IE,IN,II,IJ/1,2,3,4,5,6/,R,F,TIME/8.3143,96487.0,0.0/
     1,JCOUNT      /0     /,COEFF/1.0E-11/,CUTOFF/1.0/
  100 FORMAT(1H1)
  101 FORMAT(3I5,5F10.0)
  102 FORMAT(* CUTOFF VOLTAGE REACHED*)
  103 FORMAT(*0MESH SIZES(H1,H2,H3)*5X*NUMBER OF MESH POINTS*5X*NUMBER O
     1F ITERATIONS*3X*CONVERGENCE CRITERION*4X*TIME(SECS)*)
  104 FORMAT(1H ,3F7.3,14X,I5,20X,I5,18X,E12.5,F16.6,/)
  105 FORMAT(7X*DIST*13X*XA*14X*E*15X*V*12X*I2*11X*J*13X*ETA*13X*J1*,/)
  106 FORMAT(4F15.0)
  107 FORMAT(7F10.0)
  108 FORMAT(I2,2F10.0)
  109 FORMAT(1H0,*VOL FRAC CURRENT COLLECTOR*,/,* IN NEG=*,E16.8,4X,
     1*IN POS=*,E16.8,/,* U20-U10=*,E16.8,*VOLTS*,/,* 1ST GUESS FOR ETA=
     1*,E16.8,/)
  110 FORMAT(6F10.0,F15.0)
  111 FORMAT(3E16.8,I5)
  112 FORMAT(1H1,*PARAMETERS FOR SIMULATION OF LI,AL/FES BATTERY*//* NJ1
     1=*,I3,4X,*NJ2=*,I4,4X ,*NJ=*,I4,/ ,* H1=*,E13.6,* H2=*,E13.6,* H3=*,
     1E13.6,/,* DELT(SECS)=*,E13.6,4X,*TSTOP=*,E13.6,/)
  113 FORMAT(1H0,*KINETIC PARAMETERS*/* GAM=*,E13.6,5X,*ALPHA=*,E13.6,5X
     1,*ALPHC=*,E13.6,/,* CR1=*,E14.7,/)
  114 FORMAT(1H0,*TCD=*,E12.5,4X,*V/A=*,E12.5,4X,*T(K)=*,E12.5,4X,
     1*FACTOR=*,E12.5,/)
  115 FORMAT(1H0,*S1=*,F6.3,4X,*S3=*,F6.3,4X,*EONS=*,F6.3,4X,/,* S1B=*,
     1F6.3,4X,*S3B=*,F6.3,4X,*EONSB=*,F6.3,/)
  116 FORMAT(7E16.8)
  117 FORMAT(1H0,6X,*TCD*,13X,*TCV*,11X,*DPHI2,SEP*,7X,*DPHI1,POS*,6X,
     1*C(IN,NJ1)*,7X,*C(IN,NJ2)*,8X,*VOVERA*)
  118 FORMAT(8E15.3)
  119 FORMAT(1H0,*OCCP(V)=*,E13.6,4X,*DOCCPT=*,E13.6,/,* RESERVOIR WIDTH
     1=*,E13.6,4X,*MEAN CELL HEAT CAPACITY(J/CM2.K)=*,E16.8,/,* TAMB=*,
     1E15.7,4X,*HTC(W/CM2.K)=*,E15.7,/)
  120 FORMAT(1H0,*NO. OF LI SPHERES/CM3=*,E13.5,4X,*DIF COEFF. IN ALPHA(
     1CM2/SEC)=*,E13.5,/,* AVG. CONC OF LI IN ALPHA/CLIASAT   =*,E13.5,4
     1X*XAR=*,E13.5,/)
  121 FORMAT(1H0,*EINIT=*,E16.8,4X,*EINITB=*,E16.8,4X,*ESEP=*,E16.8,/)
  122 FORMAT(1H0,*POSITIVE ELECTRODE PARAMETERS*,/,* AI01=*,E14.6,*AMP/C
     1M3*,4X,*AI02=*,E14.6,4X,/,* ALFA A=*,E14.6,4X,*ALFA C=*,E14.6,/,
```

```
    1* VFE,VFES,VX=*,3E16.6,*CM3/MOL*,/,* CONFE,CONFES,CCNX=*,3E16.6,
    1* /OHM/CM*,/,* VLI2S(CM3/MCL)=*,E16.8,/,* VLICL=*,E16.8,4X,*VKCL=*
    1,E16.8,/)
123  FORMAT(6F12.0)
124  FORMAT(6E16.8,I6)
125  FORMAT(1H0,*CELL TEMP.(DEG.K)=*,E15.8,X,* HEAT LOSS(W/CM2)=*,E16.8
    1,4X,*HEAT GAIN(W/CM2)=*,E16.8,/,* HEAT OF PPTE(W/CM2) KCL,LICL=*,
    12E16.8)
126  FORMAT(1H0,*JCOUNT=*,I2,*FRA( ERR MOLS LI=*,E16.8,4X,*F ERR MOLS K
    1=*,E16.8,/,* MCLS LI IN S,POS=*,E16.8,
    14X,*XASL=*,E16.8,4X,*XASK=*,E16.8,/,* MCLS LI IN S,NEG=*,E18.10,
    1/,* FRAC TOT LI SOL LCST=*,E16.8,4X,*CAP NEG=*,E16.8,4X,*CAP PCS=*
    1E16.8)
127  FORMAT(1H ,*NCT CONVERGEC AT J=*,I3,/,8E15.8,/)
128  FORMAT(1H0,*INTERRLPTER RESISTANCE(CHM.CM2)=*,E16.8,/)
129  FORMAT(* ACP1,AOP2=*,2E16.8)
132  FORMAT(1H0,6X*DIST*14X*G*14X*Q*9X*  ESUM *8X*RE/EP*12X*EFE*10X
    1*RO/EX*8X* CS /EFES*,/)
131  FCRMAT(1H0,*BARMA,BARMB,CALBET,CLIBET,CLIAS,CLIAM,CALAM,VALA,VLIA,
    1AON,QFMIN,DTCUT,TGAP=*,/,5E16.8,/,5E16.8,/,3E16.8,/)
133  FORMAT(1H0,*RGRIC=*,E16.8,4X,*EXTRA CCNDUCTIVITY(/CHM/CM)=*,E16.8)
134  FORMAT(1H ,*DELT HALVED*,4X,*KEY=*,I2)
135  FORMAT(1H0,*NCN-CONVERGEC SOLN AT*,E15.8,* SECS*,/)
136  FORMAT(* INITIAL VALUES. SLNC,SLPO,AMTLIC,AMTKO=*,/,4E18.9)
137  FORMAT(* PARAMETERS AT REACTION FRCNT*)
138  FORMAT(* RSUM=*,E16.8,4X,*VSUM=*,E16.8)
139  FORMAT(* PIN21,PIN22,DFC1,DFC2=*,4E16.8)
140  FORMAT(1H ,*QMAXB=*,E16.8,4X,*EFINAL=*,F16.8,4X,*GMAX=*,E15.8,/,
    1* E INTERMECIATE=*,E16.8)
     READ 101,NJ1,NJ2,NJ,TSTOP,H1,H2,H3,DELT
     READ 107,XAINIT,EINIT,EINITB,ESEP,TINIT,ECCN,ECCP
     READ 107,GAM,ALPHA,ALPHC,CR1,TGAP,ROA,ROE
     READ 108,MAXITS,CONV,ETAGES
     READ 107,TCD,UJO,DCCCPT,VCVERA,FACTOR,CCPADD,RGRIC
     READ 110,S1,S3,EONS,S1B,S3B,EONSB,CB
     READ 106,WIDTH,CPMA,TAMB,CHT
     READ 123,EN,CA,CMEAN,XAR,QFMIN,DTCUT
     READ 107,DSEPCT,AIO1,AIO2,AA,AC,VLICL,VKCL
     READ 107,VFE,VFES,VX,VLI2S,SIGFE,SIGFES,SIGX
     NJ1=81 $ NJ2=121 $ NJ=166 $ EINIT=0.39 $ EINITB=0.555$XAINIT=0.50
     HFUSEK=25500.0 $ KEY6=0 $ HFUSEL=13400.0
     MAXITS=16
     CHT=2.0*CHT $ EN=EN/2.0
     TINIT=743.15
     TSTOP=35000.0
     TGAP=TGAP*0.0416/TCD
     RES=0.0
     PRINT 112,NJ1,NJ2,NJ,H1,H2,H3,DELT,TSTOP
     PRINT 121,EINIT,EINITB,ESEP
     PRINT 113,GAM,ALPHA,ALPHC,CR1
     PRINT 120,EN,CA,CMEAN,XAR
     PRINT 122,AIO1,AIO2,AA,AC,VFE,VFES,VX,SIGFE,SIGFES,SIGX,VLI2S
    1,VLICL,VKCL
     PRINT 109,ECCN,ECCP,DSEPCT,ETAGES
     PRINT 114,TCD,VCVERA,TINIT,FACTOR
     PRINT 115,S1,S3,EONS,S1B,S3B,EONSB
     PRINT 119,UJO,COCCPT,WIDTH,CPMA,TAMB,CHT
C    EVALUATION OF SCME PARAMETERS USED THROUGHOUT PROGRAM
     BARMA=0.9*26.9815+0.1*6.939 $ BARMB=0.525*26.9815+0.475*6.939
     CALBET=0.525*ROB/BARMB $ CLIBET=0.475*ROB/BARMB
     CLIAS=0.1*ROA/BARMA $ CLIAM=CMEAN*CLIAS
     VLIA=(BARMB/ROB-0.525*BARMA/0.9/ROA)/(0.475-0.525*0.1/0.9)
```

```
      VALA=(1.0-CLIBET*VLIA)/CALBET $ CALAM=(1.0-VLIA*CLIAM)/VALA
      ACN=VLIA/F/(1.0-CALAM*(CALBET*VALA+CLIBET*VLIA-1.0)/(CALBET-
     1CALAM))
      PRINT 131,BARMA,BARMB,CALBET,CLIBET,CLIAS,CLIAM,CALAM,VALA,VLIA,
     1ACN,QFMIN,DTCUT,TGAP
      NJ1M1=NJ1-1 $ NJ2P1=NJ2+1  $ N=5 $ JP=N+1
      T1=0.02 $ T2=0.1 $ T3=0.4 $ T4=1.0 $ T5=4.0 $ T6=10.0 $ T7=30.0
      F1=0.02 $ F2=0.1 $ F3=0.2 $ F4=1.0 $ F5=2.0 $ F6=11.0 $ F7=30.0
      S=-0.15 $ F8=60.0 $ T8=60.0 $ PRINT 133,RGRID,CONACC
      T10=T1 $ T20=T2 $ T30=T3 $ T40=T4 $ T50=T5 $ T60=T6 $ T70=T7
      T80=T8 $                   TOTM=H1*FLOAT(NJ1-1)
      TOTS=H2*FLOAT(NJ2-NJ1) $ TOTL=TOTM+TOTS+H3*FLOAT(NJ-NJ2)
      TLAST=0.0                $ IPCLAP=1 $ TCADD=0.02
      RF=R/F                   $ VAL1=RF*S1/EONS  $ VAL2=RF*(1.0-S3/EONS)
      T=TINIT $ NJ1P1=NJ1+1 $ AOP2=0.0
      VAL1B=RF*S1B/EONSB  $ VAL2B=RF*(1.0-S3B/EONSB)
      ALRA=ALPHA/RF $ ALRC=ALPHC/RF $ ALR1=AA/RF $ ALR2=AC/RF
      NJ2M1=NJ2-1 $ ESEPPN=ESEP**FACTOR $ DELT2=DELT/2.0
      NJM1=NJ-1 $              AOP1=(VX+VFE-2.0*VFES)*0.5/F
      AOP2=AOP1
      PRINT 129,AOP1,AOP2
      PIN1=1.0/3.0  $ PIN4=12.56637*EN  $ PIN43=PIN4/3.0
      PIN21=PIN43*F*(CALBET*VALA+CLIBET*VLIA-CALBET/CALAM)/VLIA
      PIN5=-PIN43/ACN
      PIN51=PIN5 $ PIN52=PIN5
      DFC1=2.0*PIN4*F*DA*CLIAS/(1.0+(CLIBET/CLIAM)/((CLIBET/CLIAM)-(
     1CALBET/CALAM)))
      DFC2=PIN4*F*DB*CLIBET $ PIN22=PIN43*(1.0-CALAM/CALBET)/ACN
      DFC1=PIN4*F*DA*CLIAS/(1.0-0.1*CMEAN)
      DFC2=PIN4*F*DB*CLIBET/0.525
      PRINT 139,PIN21,PIN22,DFC1,DFC2
      ROINIT=((1.0-EINIT-ECON)/PIN43)**PIN1
      RBINIT=ROINIT
      U1=(CLIBET+(VALA*CALBET-1.0)/VLIA)*PIN43 $ U2=PIN43/VLIA
      U3=-ROINIT**3*VALA*CALBET/VLIA
      EXPAND=0.0
C     STOICHIOMETRIES FOR SOLID PHASES IN POSITIVE ELECTRODE REACTIONS
C     1=FE,2=FES,3=X,4=LI2S
      SS(1,1)=1.0 $ SS(2,1)=-2.0 $ SS(3,1)=1.0 $ SS(4,1)=0.0
      SS(1,2)=1.0 $ SS(2,2)=0.0 $ SS(3,2)=-1.0 $ SS(4,2)=2.0
      Y1=-SS(2,1)*VFES/EONSB/F $ Y21=-SS(3,1)*VX/EONSB/F
      Y22=-SS(3,2)*VX/EONSB/F $ Y31=-SS(1,1)*VFE/EONSB/F $ Y32=Y31*SS(1,
     12)/SS(1,1) $ EFESO=1.0-EINITB-ECOP
      Y42=-SS(4,2)*VLI2S/EONSB/F
C     CALCULATION OF ELECTRODE CAPACITIES
      QMAXB=-EFESO*F*EONSB/VFES $ QMNEG=(1.0-EINIT-ECON)*F*CLIBET
      EFINAL=EINITB+0.5*QMAXB*(AOP1+AOP2)$ EINT=0.5*(EFINAL+EINITB)
      PRINT 140,QMAXB,EFINAL,QMNEG,EINT
      PRINT 150
C     FIRST GUESS FOR UNKNOWN VARIABLES
      EBH2=EXP(-239.59*H3/2.0) $ ENH2=EXP(509.91*H1/2.0)
      DO 33 K=1,NJ  $ C(IX,K)=XAINIT $ DIST(K)=H1*FLOAT(K-1)/TOTL
      C(IG,K)=0.0 $ ROUTA(K)=0.0              $ W(K)=0.0 $ RBETA(K)=0.0
      CJ2(K)=0.0 $ CJ1(K)=0.0 $ Q(K)=0.0              $ ELI2S(K)=0.0
      EFE(K)=0.0 $  ESUM(K)=1.0 $ EPK(K)=0.0 $ EPL(K)=0.0
      XD(K)=0.0 $   ZETA(K)=0.0
      DETA(K)=0.0 $ C(IN,K)=0.0 $ IF(K.GT.NJ1) GO TO 31 $ C(IE,K)=EINIT
      C(IJ,K)=509.91*TCD*EXP(509.91*H1*FLOAT(K-NJ1))
      ROUTA(K)=ROINIT $ W(K)=1.0 $ RBETA(K)=RBINIT
      DETA(K)=C(IJ,K)/95669.2 $ C(II,K)=-C(IJ,K)/509.91*ENH2
      CPOL(2,K)=C(IJ,K)*0.02/TCD $ CPOL(1,K)=C(II,K)*0.02/TCD
      CPOL(3,K)=CPOL(2,K)/95669.2
```

```
      RIN(K)=RBETA(K)
      C(IN,K)=DETA(K) $ GO TO 33
   31 IF(K.GE.NJ2) GOTO 32  $ C(IE,K)=ESEP  $ C(II,K)=TCD
      CPOL(1,K)=0.02 $ CPOL(2,K)=0.0 $ CPOL(3,K)=0.0
      DIST(K)=(TOTM+H2*FLOAT(K-NJ1))/TOTL
      C(IJ,K)=0.0  $ C(IN,K)=0.0  $ GO TO 33
   32 C(IJ,K)=-236.59*TCD*EXP(236.59*H3*FLOAT(NJ2-K)) $ C(IE,K)=EINITB
      C(II,K)=-C(IJ,K)/236.59*EBH2 $ DETA(K)=C(IJ,K)/45903.0
      CPOL(2,K)=C(IJ,K)*0.02/TCD $ CPOL(1,K)=C(II,K)*0.02/TCD
      CPOL(3,K)=CPOL(2,K)/45903.0-CSEPCT
      DIST(K)=(TOTM+TOTS+H3*FLOAT(K-NJ2))/TOTL $ EFES(K)=EFESC
      C(IN,K)=DETA(K)-CSEPCT $ CJ1(K)=C(IJ,K)
  33  CONTINUE $ C(IG,NJ2)=VOVERA
1     CTEMP=0.0  $ DELT=0.0 $ JSPOT=0
2     DO 34 KV=1,NJ
      EPKKEP(KV)=EPK(KV) $ EPLKEP(KV)=EPL(KV) $ XDKEEP(KV)=XD(KV)
      ZETALD(KV)=ZETA(KV)  $ CJ1KEP(KV)= CJ1(KV) $ NONOF(KV)=0
      IF(KV.LE.NJ1) RINKEP(KV)=RIN(KV) $ IF(KV.GE.NJ2)CJ2KEP(KV)=CJ2(KV)
      DO 34 L=1,JP
   34 CKEEP(L,KV)=C(L,KV) $ IF(IPOLAR.EQ.0) GO TO 30 $ DELTMX=DELT
      JSET=0 $ DO 27 J=1,NJ1 $ IF(C(IJ,J).LE.0.0) GO TO 25
      DEL =RBETA (J)**3*PIN21/C(IJ,J)*2.0
      IF(DEL.GT.2.0*DELTMX) GO TO 27 $ IF(DEL.LE.DELTMX) NONOF(J)=1
      IF(DEL.GT.DELTMX.AND.DELT.GT.0.5*DELTMX) GO TO 26
      IF(DEL.GT.DELT) GO TO 27 $ DELT=DEL
      C(IJ,J)=0.0 $ JSET=J $ KSET=1 $ GO TO 27
   25 IF(C(IJ,J).EQ.0.0) GO TO 27 $ DEL=-Q(J)/C(IJ,J)*2.0
      IF(DEL.GT.2.0*DELTMX) GO TO 27 $ IF(DEL.LE.DELTMX) NONOF(J)=2
      IF(DEL.GT.DELTMX.AND.DELT.GT.0.5*DELTMX) GO TO 26
      IF(DEL.GT.DELT) GO TO 27 $ DELT=DEL
      C(IJ,J)=0.0 $ JSET=J $ KSET=2 $ GO TO 27
   26 DELT=0.5*DELT $ JSET=0
   27 IF(NONOF(J).NE.0) PRINT 124, DIST(J),DEL,Q(J),CKEEP(IJ,J),RBETA(J)
     1,RINKEP(J),NONOF(J)
      DO 275 J=NJ2,NJ $ EFESK=EFES(J)+Y1*DELTMX*CJ1(J)
      IF(EFESK.GE.0.0) GO TO 269
      NON=1 $ DEL=-EFES(J)/Y1/CJ1(J)*2.0 $ GO TO 278
  269 ELI2SK=ELI2S(J)+Y42*DELTMX*CJ2(J) $ IF(ELI2SK.GE.0.0) GO TO 271
      NON=2 $ DEL=-ELI2S(J)/Y42/CJ2(J)*2.0 $ GO TO 278
  271 EXK=EX(J)+DELTMX*(Y21*CJ1(J)+Y22*CJ2(J)) $ IF(EXK.GE.0.0) GO TO275
      IF(EFESK.GT.0.0) GO TO 273 $ DEL=-EX(J)/Y22/CJ2(J)*2.0 $ NON=3
      GO TO 278
  273 DEL=-EX(J)/Y21/CJ1(J)*2.0 $ NON=4
  278 IF(DEL.LE.DELTMX) NONOF(J)=NON
      IF(DEL.GT.DELTMX .AND. DELT.GT.0.5*DELTMX) GO TO 274
      IF(DEL.GT.DELT) GO TO 275 $ DELT=DEL $ JSET=J $ KSET=-NON
      IF(NON.EQ.1 .OR. NON.EQ.4) CJ1(J)=0.0
      IF(NON.EQ.2 .OR. NON.EQ.3) CJ2(J)=0.0 $ GO TO 275
  274 DELT=0.5*DELT $ JSET=0
  275 IF(NONOF(J).NE.0) PRINT 124, DIST(J),DEL,EFESK,CJ1(J),EXK,CJ2(J),
     1NONOF(J)
      DO 279 J=NJ2,NJ $ IF(J.EQ.JSET) GO TO 279
      IF(NONOF(J).EQ.1) CJ1(J)=CJ1KEP(J)*(1.0-DELT/(-EFES(J)/Y1/CJ1KEP
     1(J)*2.0))
      IF(NONOF(J).EQ.2) CJ2(J)=CJ2KEP(J)*(1.0-DELT/(-ELI2S(J)*2.0/Y42
     1/CJ2KEP(J)))
      IF(NONOF(J).EQ.3) CJ2(J)=CJ2KEP(J)*(1.0-DELT/(-EX(J)/Y22/CJ2KEP(J)
     1*2.0))
      IF(NONOF(J).EQ.4) CJ1(J)=CJ1KEP(J)*(1.0-DELT/(-EX(J)/Y21/CJ1KEP(J)
     1*2.0))
  279 CONTINUE
      DO 24 J=1,NJ1 $ IF(J.EQ.JSET) GO TO 24
```

```
      IF(NONOF(J).EQ.1) C(IJ,J)=CKEEP(IJ,J)*(1.0-DELT/(RBETA (J)**3
     1*PIN21/CKEEP(IJ,J)*2.0))
      IF(NONOF(J).EQ.2) C(IJ,J)=CKEEP(IJ,J)*(1.-DELT/(-Q(J)/CKEEP(IJ,J)
     1*2.0))
   24 CONTINUE
      KEY5=0 $ DTMIN=DELT/20.0 $ IF(DTMIN.LT.0.005) DTMIN=0.005
C     SET MAIN ITERATION LOOP COUNTER.INITIALISE ARRAY ELEMENTS
 3    JCOUNT=0 $ DENT2=0.5*DELT
      TIME=TIME+DELT $ T=T+DELT*DTEMP $ IF(DELT.NE.0.0) DTINV=1.0/DELT
      XASL=0.34080-0.0004773*T+0.000001376*T**2
      XASK=0.14615+0.0019117*T-0.000001948*T**2
      TCA=ALRA/T  $ TCC=ALRC/T       $TC1=ALR1/T  $ TC2=ALR2/T
 4    JCOUNT=JCOUNT+1  $ J=0  $ DO 35 I=1,JP $ DO 35 K=1,JP $ Y(I,K)=0.0
   35 V(I,K)=0.0 $ JPTERR=0 $ NTERR=0
C     CALCULATE PHYSICAL PROPERTIES
      DO 36 MI=1,NJ $ CALL PROPS(MI,C)
      IF(IPOLAR.NE.0 .OR. JCOUNT.NE.0) GO TO 36 $ IF(MI.GT.NJ1) GO TO 36
      IF(C(IN,MI).LT.0.0) W(MI)=1.1 $ IF(C(IN,MI).GE.0.0) W(MI)=0.9
   36 CONTINUE
      EFESP=0.0 $ EFEP=0.0 $ EXPP=0.0 $ ELI2SP=0.0
      DSIG1P=0.0 $ DSIG2P=0.0 $ SIGINV(1)=0.0
      F3N=0.0 $ DXOVN=0.0 $ BG=0.0 $ F3ND=0.0 $ FGP=0.0
      HP=H1 $ FLUXP=0.0 $ DXOVNP=(V(1)-C(IX,1)*DVX(1))/V(1)**2
      F3NP=C(IE,1)**FACTOR*DIFUSN(1)/V(1)
      F3NPD=C(IE,1)**FACTOR*(DDX(1)-DIFUSN(1)*DVX(1)/V(1))/V(1)
 5    J=J+1      $             DSIG1=DSIG1P $ DSIG2=DSIG2P
      EFESK=EFESP $ EXK=EXPP $ ELI2SK=ELI2SP
      DO 37 I=1,JP $ G(I)=0.0 $ B1(I)=0.0 $ B2(I)=0.0
      TALL(I)=0.0 $ IF(I.LE.4) CCLD(I,J)=C(I,J)
      DO 37 K=1,JP $ A(I,K)=0.0  $ B(I,K)=0.0
   37 D(I,K)=0.0
C     CALCULATE DERIVATIVES (BASED ON PREVIOUS GUESS)
      H=H2 $ IF(J.LE.NJ1) H=H1 $ IF(J.GE.NJ2) H=H3
      IF(J.GT.1) A(4,II)=1.0 $ IF(J.LT.NJ) B(4,II)=-1.0
      WE=H/4.0 $ IF(J.EQ.1.OR.J.EQ.NJ) WE=WE/2.0
      IF(J.EQ.NJ1) WE=H1/8.0 $ IF(J.EQ.NJ2) WE=H3/8.0
      B(4,IJ)=4.0*WE $ IF(J.EQ.NJ1.OR.J.EQ.NJ) B(5,II)=1.0
      IF(J.EQ.NJ) G(5)=-C(II,J) $ IF(J.EQ.NJ1) G(5)=TCD-C(II,J)
      IF(J.EQ.NJ1 .AND.ABS(G(5)).LE.COEFF*ABS(C(II,J))) G(5)=0.0
      TALL(4)=ABS(B(4,IJ)*C(IJ,J))
      IF(J.GT.1 .AND. ABS(C(II,J-1)).GT.TALL(4)) TALL(4)=ABS(C(II,J-1))
      IF(J.LT.NJ .AND. ABS(C(II,J)).GT.TALL(4)) TALL(4)=ABS(C(II,J))
      G(4)=-4.0*WE*C(IJ,J) $ IF(J.GT.1) G(4)=G(4)-C(II,J-1)
      IF(J.LT.NJ) G(4)=G(4)+C(II,J)
      WEP=H/4.0 $ IF(J+1.EQ.NJ1.OR.J+1.EQ.NJ) WEP=WEP/2.0
      IF(J+1.EQ.NJ2) WEP=H3/8.0
      DYINV=1.0/H $ IF(J.EQ.NJ1) DYINV=1.0/H2
      IF(J.NE.NJ) DXYFD=(XD(J+1)-XD(J))*DYINV
C     KINETIC EQUATION FOR NEGATIVE ELECTRODE. MODEL INCLUDES
C     REACTION AT S/L INTERFACE AND DIFFUSION OF LI IN ALPHA AL.
      ADDJ=DENT2*(C(IJ,J)+CKEEP(IJ,J)) $ IF(J.LT.NJ) SIGINV(J+1)=0.0
      IF(J.GT.NJ1) GO TO 45 $ KEY=-1
      B(6,IJ)=1.0 $ IF(NONOF(J).NE.0) GO TO 46
      IF(Q(J)+ADDJ.LT.0.0) GO TO 8
      IF(Q(J).LE.1.0E-05.AND.C(IN,J).LE.0.0) GO TO 44
      IF(RBETA(J).LE.1.0E-11.AND.C(IN,J).GE.0.0) GO TO 44
      RINK=RINKEP(J)
      IF(W(J).LE.1.0) GO TO  39 $ IF(C(IN,J).LT.0.0) GO TO 38
      W(J)=0.0 $ GO TO 40
   38 PIN5=PIN52 $ PIN2=PIN22 $ DFC=DFC2
      IF(W(J).GT.1.99) RINK=ROUTA(J)
      ROK=(ROUTA(J)**3+ADDJ/PIN52)**PIN1  $ KEY=-2
```

```
      RIN3=RINK   **3-ADDJ/PIN2 $ IF(RIN3.LT.0.0) GO TO 8
      RIN(J)=RIN3**PIN1
      TL=(1.0/RIN(J)  -1.0/ROK)/DFC $ GO TO 41
   39 IF(C(IN,J).GT.0.0) GO TO 40 $ W(J)=2.0 $ GO TO 38
   40 PIN5=PIN51 $ PIN2=PIN21 $ DFC=DFC1
      ROK=(ROUTA(J)**3+ADDJ/PIN51)**PIN1 $ KEY=-3
      RBETA3=RBETA (J)**3-ADDJ/PIN2 $ IF(RBETA3.LT.0.0) GO TO 8
      RBETAK  =RBETA3**PIN1 $ RIN(J)=RBETAK
      TL=           (1.0/PIN2+1.0/PIN5)*(C(J)+ADDJ)/(ROK**2+ROK
     1*RIN(J)+RIN(J)**2)/(DFC*ROK*RIN(J))
   41 SAREA=PIN4*ROK**2
      CR2=EXP(TCA*C(IN,J))   $ CR3=EXP(-TCC*C(IN,J))
      CR14=CR2-CR3 $ EXCHIA=SAFFA*CR1*(C(IX,J)/XAR)**GAM
      BIG(2)=CR2 $ IF(ABS(CR2).LT.ABS(CR3)) BIG(2)=CR3
      IF(ABS(C(IN,J)).GT.5.0E-04) GOTO 42
      CR14=C(IN,J)*    (TCA+TCC+(TCA**3+TCC**3)*C(IN,J)**2/6.0)
      BIG(2)=CR14
   42 CR15=TL*CR2+1.0/EXCHIA $ CR16=CR15**2
      B(6,IN)=(TCA*TL*CR14*CR2-CR15*(TCA*CR2+TCC*CR3))/CR16
      B(6,IX)=-CR14*GAM/CR16/EXCHIA/C(IX,J)
      B(6,IJ)=1.0+CR14/CR16*DELT/6.0*(CR2/DFC*(1.0/PIN2/RIN(J)**4  +1.0
     1/PIN5/ROK     **4)-2.0/EXCHIA/ROK      **3/PIN5)
      CR5=CR14/CR15 $ G(6)=-C(IJ,J)+CR5
      BIG(1)=C(IJ,J) $ BIG(2)=BIG(2)/CR15 $ TAIL=0.0 $ DO 43 K=1,2
      IF(TAIL.LT.ABS(BIG(K))) TAIL=ABS(BIG(K))
   43 CONTINUE $ IF(ABS(G(6)).LT.TAIL*COEFF) G(6)=0.0      $ GO TO 46
   44 B(6,IJ)=1.0  $ G(6)=-C(IJ,J)  $ GOTO 46
C     KINETIC EQUATIONS FOR POSITIVE ELECTRODE. 2 SIMULTANEOUS REACTIONS
C     ELECTROCHEMICAL RESISTANCE ONLY
   45 IF(J.LT.NJ2-1) GO TO 44 $ IF(J.EQ.NJ) GO TO 284
      EFESP=EFES  (J+1)+Y1*DENT2*(CJ1(J+1)+CJ1KEP(J+1))
      EFEP=EFE    (J+1)+DENT2*(Y31*(CJ1(J+1)+CJ1KEP(J+1))+Y32*(
     1CJ2(J+1)+CJ2KEP(J+1)))
      EXPP=EX    (J+1)+DENT2*(Y21*(CJ1(J+1)+CJ1KEP(J+1))+Y22*(
     1CJ2(J+1)+CJ2KEP(J+1)))
      ELI2SP=ELI2S (J+1)+DENT2*Y42*(CJ2(J+1)+CJ2KEP(J+1))
C     CALCULATION OF MATRIX CONDUCTIVITY
      SUM1=CONADD $ SUM2=0.0 $ SUM3=0.0
      IF(EFEP.LE.0.0) GO TO 281 $ SUM1=SIGFE*EFEP**FACTOR
      SUM2=SUM1/EFEP*FACTOR*VFE $ SUM3=SUM2
  281 IF(EFESP.LE.0.0) GO TO 282
      ADD=SIGFES*EFESP**FACTOR $ SUM1=SUM1+ADD
      SUM2=SUM2-2.0*ADD/EFESP*FACTOR*VFES
  282 IF(EXPP.LE.0.0) GO TO 283
      ADD=SIGX*EXPP**FACTOR $ SUM1=SUM1+ADD
      SUM2=SUM2+ADD/EXPP*FACTOR*VX $ SUM3=SUM3-ADD/EXPP*FACTOR*VX
  283 SIGINV(J+1)=1.0/SUM1 $ DSIG1=-SUM2*DENT2/SUM1**2/EONSB/F
      DSIG2=-SUM3*DENT2/SUM1**2/EONSB/F
      IF(J.LT.NJ2) GO TO 44
  284 GB(2,1)=0.0 $ GB(3,1)=0.0
C     FIRST EQUATION
      B(6,IJ)=1.0 $ G(6)= CJ1(J)+CJ2(J)-C(IJ,J)
      TAIL=0.0 $ BIG(1)=CJ1(J) $ BIG(2)=CJ2(J) $ BIG(3)=C(IJ,J)
      DO 285 K=1,3 $ IF(TAIL.LT.ABS(BIG(K))) TAIL=ABS(BIG(K))
  285 CONTINUE $ IF(ABS(G(6)).LT.TAIL*COEFF) G(6)=0.0
C     SECOND EQUATION
      IF(DELT.EQ.0.0) GO TO 287 $ IF(J.EQ.JSET) GO TO 297
      IF(NONCF(J).NE.0) GO TO 297
      IF(EFES(J).EQ.0.0 .AND. EFESK.LT.0.0) EFESK=0.0
      IF(ELI2S(J).EQ.0.0 .AND. ELI2SK.LT.0.0) ELI2SK=0.0
      IF(EX(J).EQ.0.0 .AND. EXK.LT.0.0) EXK=0.0
      IF(ELI2SK.LT.0.0) GO TO 286
```

```
      IF(EXK  .GE.0.0.AND.EFESK  .GE.0.0) GC TC 287
  286 KEY=1 $ PRINT 118,DIST(J),EFESK,EXK,ELI2SK,CJ1(J),CJ2(J),
     1CJ1KEP(J),CJ2KEP(J)
      IF(DELT.GE.10.0.OR.C(IJ,J)*CKEEP(IJ,J).GE.0.0) GO TC 8
      NONOF(J)=5 $ IF(CJ1(J).LT.0.0) CJ1(J)=-EFES(J)/DENT2/Y1-CJ1KEP(J)
      IF(CJ1(J).GT.C.0) CJ1(J)=-EX(J)/CENT2/Y21-CJ1KEP(J)
      IF(CJ2(J).LT.C.0) CJ2(J)=-EY(J)/CENT2/Y22-CJ2KEP(J)
      IF(CJ2(J).GT.C.0) CJ2(J)=-ELI2S(J)/CENT2/Y42-CJ2KEP(J)
      C(IJ,J)=CJ1(J)+CJ2(J)
      G(4)=-4.0*WE*C(IJ,J) $ IF(J.GT.1) G(4)=G(4)-C(II,J-1)
      IF(J.LT.NJ) G(4)=G(4)+C(II,J)
      GC TO 297
  287 ETAS=DETA(J) $ IF(EXK.LE.0.0.AND.ETAS.GT.0.0) GO TO 291
      IF(EFESK  .LE.0.0 .ANC. ETAS.LT.C.C) GO TO 291
      CI1=EXP(TC1*ETAS) $ CI2=EXP(-TC2*ETAS)
      EXPDIF=CI1-CI2 $ AIOXA=AIC1*C(IX,J)
      IF(ABS(ETAS*TC1).GT.4.0E-03) GOTC 289
      EXPDIF=ETAS*((TC1+TC2)*(1.0+0.5*(TC1-TC2)*ETAS)+(TC1**3+TC2**3)*
     1ETAS**2/6.0)
  289 B1(IX)=-AIO1*EXPCIF $ B1(IN)=-AICXA*(TC1*CI1+TC2*CI2)
      GB(2,1)=-(CJ1(J)+C(IX,J)*B1(IX))
      TAIL=0.0 $ BIG(1)=CJ1(J) $ BIG(2)=AICXA*CI1
      BIG(3)=AIOXA*CI2        $ CC 290 K=1,3
      IF(TAIL.LT.ABS(BIG(K))) TAIL=ABS(BIG(K))
  290 CONTINUE $ IF(ABS(GB(2,1)).LT.TAIL*COEFF) GB(2,1)=0.0
      GO TO 292
  291 GB(2,1)=-CJ1(J)
C     THIRD EQUATION
  292 IF(ELI2SK  .LE.0.0 .ANC. C(IN,J).GT.0.0) GO TO 296
      IF(EXK  .LE.0.0 .AND. C(IN,J).LT.0.0) GC TC 296
      CI1=EXP(TC1*C(IN,J)) $ CI2=EXP(-TC2*C(IN,J))
      EXPDIF=CI1-CI2 $ IF(ABS(TC1*C(IN,J)).GT.4.0E-03) GCTC 294
      EXPDIF=C(IN,J)*((TC1+TC2)*(1.0+0.5*(TC1-TC2)*C(IN,J))+(TC1**3+
     1TC2**3)*C(IN,J)**2/6.0)
  294 AICXB=AIO2*C(IX,J) $ B2(IX)=-AIO2*EXPCIF
      B2(IN)=-AIOXB*(TC1*CI1+TC2*CI2)
      GB(3,1)=-(CJ2(J)+B2(IX)*C(IX,J))
      TAIL=0.0 $ BIG(1)=CJ2(J) $ BIG(2)=AIOXB*CI1
      BIG(3)=AIOXB      *CI2 $ DO 295 K=1,3
      IF(TAIL .LT. ABS(BIG(K))) TAIL=ABS(BIG(K))
  295 CONTINUE $ IF(ABS(GB(3,1)).LT.TAIL*COEFF) GB(3,1)=0.0  $ GOTO 297
  296 GB(3,1)=-CJ2(J)
  297 G(6)=G(6)+GB(2,1)+GB(3,1) $ B(6,IN)=B1(IN)+B2(IN)
      B(6,IX)=B1(IX)+B2(IX)
C     OHMS LAW EQUATION
   46 IF(J.EQ.NJ1.OR.J.EQ.NJ) GC TC 311
      IF(J.GT.NJ1.AND.J.LT.NJ2) GO TO 52
      CONJ=CON(J)*C(IE,J)**FACTOR $ CONJP1=CON(J+1)*C(IE,J+1)**FACTOR
      TDLNA2=T*DLNAC(J+1)   $ XB2=1.0-C(IX,J+1)
      TDLNA1=T*DLNAC(J)   $ XB1=1.0-C(IX,J)       $ IF(J.GT.NJ2) GO TO 51
      TER1=(VAL1+VAL2*C(IX,J))/XB1/C(IX,J)   $ F120=TER1*TCLNA1
      DF12XO=T*D2LNAC(J)*TER1+TDLNA1*(VAL2*C(IX,J)**2-VAL1*(1.0-2.0*
     1C(IX,J)))/((XB1*C(IX,J))**2)
      TER2=(VAL1+VAL2*C(IX,J+1))/XB2/C(IX,J+1)   $ F12S=TER2*TDLNA2
      DF12XS=T*D2LNAC(J+1)*TER2+TDLNA2*(VAL2*C(IX,J+1)**2-VAL1*(1.0-2.0*
     1C(IX,J+1)))/((XB2*C(IX,J+1))**2)
   47 CG3=C(II,J)*0.5 $ CG4=(F12O+F12S)*DYINV*0.5
      B(5,IX)=-CG3*DCONX(J)/CONJ/CON(J)             -CG4+DF12XO*0.5*DXYFD
      C(5,IX)=0.5*DF12XS*DXYFD-CG3*DCONX(J+1)/CONJP1/CON(J+1)+CG4
      DSIG=0.0 $ DSIGP=0.0 $ IF(CJ1(J).EQ.0.0) GO TO 48
      DSIG=DSIG1 $ DSIGP=DSIG1P
   48 IF(CJ2(J).EQ.0.0) GO TO 49 $ DSIGP=DSIG2P $ DSIG=DSIG2
```

```
   49 B(5,IE)=-CG3*FACTOR/CONJ/C(IE,J)
      C(5,IE)=-CG3*FACTOR/CONJP1/C(IE,J+1)
      B(5,IJ)=0.5*(C(II,J)-TCD)*CSIG
      C(5,II)=0.5*(C(II,J)-TCD)*CSIGP*WEP
      B(5,II)=0.5*(1.0/CONJ+1.0/CONJP1+SIGINV(J)+SIGINV(J+1))
      B(5,IN)=DYINV  $ D(5,IN)=-DYINV
      BIG(1)=SIGINV(J)*0.5*TCD $ BIG(2)=DYINV*DETA(J+1)
      BIG(3)=0.5*C(II,J)/CONJ $ BIG(4)=0.5*F12S*XD(J)*DYINV
      IF(CONJP1.LT.CONJ) BIG(3)=BIG(3)*CONJ/CONJP1
      G(5)=0.5*TCD*(SIGINV(J)+SIGINV(J+1))      -B(5,II)*C(II,J)
     1+DYINV*(DETA(J+1)-DETA(J))+CG8*(XD(J)-XD(J+1))
      B(5,II)=B(5,II)-C(5,II)
      DO  50 K=1,4 $ IF(TALL(5).LT.ABS(BIG(K))) TALL(5)=ABS(BIG(K))
   50 CONTINUE  $  GO TO 311
C     OHMS LAW EQUATION,POSITIVE ELECTRODE.
   51 TER1 =(VAL1B+VAL2B*C(IX,J))/XB1/C(IX,J) $ F12O=TER1*TDLNA1
      CF12XO=T*D2LNAC(J)*TER1+TDLNA1*(VAL2B*C(IX,J)**2-VAL1B*(1.0-2.0*
     1C(IX,J)))/((XB1*C(IX,J))**2)
      TER2B=(VAL1B+VAL2B*C(IX,J+1))/XB2/C(IX,J+1)
      F12S=TER2B*TDLNA2
      CF12XS=T*D2LNAC(J+1)*TER2B+TDLNA2*(VAL2B*C(IX,J+1)**2-VAL1B*(1.0-
     12.0*C(IX,J+1)))/((XB2*C(IX,J+1))**2) $ GO TO 47
   52 B(5,IN)=1.0 $ G(5)=-C(IN,J)
C     EQUATION 1. MATERIAL BALANCE.
  311 IF(DELT.EQ.0.0) GO TO 329
      F3NM=F3N $       FLUXM=FLUXP $ F3N=F3NP
      F3NMD=F3ND $ F3ND=F3NPD  $ FGM=FGP
      HM=HP $ WM=WP $ DXOVNM=DXOVN $ DXOVN=DXOVNP $ BGM=BG
      JE=J                $ IF(J.NE.NJ) GO TO 312
      WM=0.375*H3 $ FLUXP=0.0 $   FGP=0.0 $ JE=J-1 $ GO TO 315
  312 DXOVNP =(V(J+1)-C(IX,J+1)*DVX(J+1))/V(J+1)**2
      F3NP=C(IE,J+1)**FACTOR*DIFUSN(J+1)/V(J+1)
      F3NPD=C(IE,J+1)**FACTOR*(DDX(J+1)-DIFUSN(J+1)*DVX(J+1)/V(J+1))/V(
     1J+1)
      JGP=J $ IF(J.GE.NJ2) JGP=J+1 $ IF(J.EQ.1) JE=J+1 $ JGM=JGP-1
      IF(J.EQ.1) WM=0.375*H1
      IF(J.EQ.NJ2-1) F3NP=F3NP*(ESEP   /C(IE,J+1))**FACTOR
      IF(J.EQ.NJ2-1) F3NPD=F3NPD*(ESEP/C(IE,J+1))**FACTOR
      IF(J.NE.NJ1) GO TO 313 $ JE=J-1            $ HP=H2
      WM=0.375*H1 $ RAT=(ESEP/C(IE,J))**FACTOR $ F3N=F3N*RAT
      F3ND=F3ND*RAT $ GO TO 314
  313 IF(J.NE.NJ2) GO TO 314 $ F3N=C(IE,J)**FACTOR*DIFUSN(J)/V(J)
      F3ND =C(IE,J)**FACTOR*(DDX(J)-DIFUSN(J)*DVX(J)/V(J))/V(J)
      JE=JE+1             $ HP=H3 $         WM=0.375*H3 $ JGM=J-1
  314 BG=0.25*(C(IX,J+1)+C(IX,J)) $ FGP=C(IG,JGP)
      FLUXP=2.0*BG*C(IG,JGP)-0.5*(F3NP+F3N)*(XD(J+1)-XD(J))/HP
  315 R1K  =FLUXM-FLUXP+WE/F* C(IJ,J)*4.0
      R2K  =WE*C(IE,J)*(3.0*C(IX,J)/V(J)+C(IX,JE)/V(JE))
     1+WE/VLICL*4.0*EPL(J)
      RV1K=FGM-FGP+WE*C(IJ,J)/F*4.0
      RV2K  =WE*C(IE,J)*(3.0/V(J)+1.0/V(JE))
     1+WE*4.0*(EPL(J)/VLICL+EPK(J)/VKCL)
      IF(J.EQ.NJ1) RV2K=RV2K+ESEP*H2/8.*(3./V(J)+1./V(J+1))
      IF(J.EQ.NJ2) RV2K=RV2K+ESEP*H2/8.*(3./V(J)+1./V(J-1))+C(IG,J)/V(J)
      IF(J.EQ.NJ1) R2K=R2K+ESEP*H2/8.*(3.*C(IX,J)/V(J)+C(IX,J+1)/V(J+1))
      IF(J.EQ.NJ2) R2K  =R2K  +ESEP*H2/8.*(3.*C(IX,J)/V(J)+C(IX,J-1)/V(J
     1-1))+C(IG,J)*C(IX,J)/V(J)
      RV3=DTINV*(RV2K-RV2(J)) $ VDIF=RV3-0.5*(RV1K+RV1(J))
      R3=DTINV*(R2K-R2(J)) $ RDIF=R3-0.5*(R1K+R1(J))
      IF(J.GE.NJ2) GO TO 316 $ B(1,IG)=BG $ B(2,IG)=0.5 $ GO TO 317
  316 IF(J.EQ.NJ) GO TO 315 $ D(1,IG)=BG $ D(2,IG)=0.5
  317 C(1,IX)=      0.25*C(IG,JGP)-(F3NP+F3N+F3NPD*(XD(J+1)-XD(J)))/HP/4.
```

```
      B(1,IX)=     0.25*C(IG,JGP)+(F3NP+F3N-F3ND*(XD(J+1)-XD(J)))/HP/4.
      IF(J.GE.NJ1.AND.J.LT.NJ2) GO TO 318
      B(1,IE)=B(1,IE)-FACTOR/4.*F3N/HP*(XD(J+1)-XD(J))/C(IE,J)
      C(1,IE)=-0.25*FACTOR /HP    *F3NP*(XD(J+1)-XD(J))/C(IE,J+1)
  318 IF(J.EQ.NJ2) F3N=F3N*(ESEP/C(IE,J))**FACTOR
      IF(J.EQ.NJ2) F3ND=F3ND*(ESEP      /C(IE,J))**FACTOR
      IF(J.EQ.NJ1) F3ND=F3ND*(C(IE,J)/ESEP)**FACTOR
      IF(J.EQ.NJ1) F3N=F3N*(C(IE,J)/ESEP)**FACTOR
      IF(J.LE.NJ2) GO TO 319 $ B(1,IG)=-BGM $ B(2,IG)=-0.5 $ GO TO 320
  319 IF(J.EQ.1) GO TO 321 $ A(1,IG)=-BGM    $ A(2,IG)=-0.5
  320 B(1,IX)=B(1,IX)-     0.25*C(IG,JGM)+(F3NM+F3N+F3ND*(XD(J)-XD(J-1)))
     1/HM/4.
      A(1,IX)=(F3NMD*(XD(J)-XD(J-1))-F3NM-F3N)/HM/4.-0.25*C(IG,JGM)
      IF(J.GT.NJ1.AND.J.LE.NJ2) GO TO 321
      A(1,IE)=0.25*FACTOR/HM     *F3NM*(XD(J)-XD(J-1))/C(IE,J-1)
      B(1,IE)=B(1,IE)+FACTOR/4.*F3N/HM*(XD(J)-XD(J-1))/C(IE,J)
  321 B(1,IX)=B(1,IX)+WM*C(IE,J)*DTINV*DXOVN$ B(1,IJ)=-2.0*WE/F
      B(1,IE)=B(1,IE)+WE*(3.0*C(IX,J)/V(J)+C(IX,JE)/V(JE))*DTINV
      B(2,IE)=WE*(3.0/V(J)+1.0/V(JE))*DTINV $ B(2,IJ)=-2.0*WE/F
      B(2,IX)=-WM*DTINV*C(IE,J)*DVX(J)/V(J)**2
      IF(J.NE.1) GO TO 322 $ D(1,IX)=D(1,IX)+H1/8.*C(IE,1)*DTINV*DXOVNP
      C(2,IX)=-H1/8.*DTINV*C(IE,J   )*DVX(J+1)/V(J+1)**2  $ GO TO 325
  322 IF(J.NE.NJ) GO TO 323
      A(1,IX)=A(1,IX)+H3/8.*C(IE,NJ   )*DTINV*DXOVNM
      A(2,IX)=-H3/8.*DTINV*C(IE,J   )*DVX(J-1)/V(J-1)**2 $ GO TO 325
  323 IF(J.NE.NJ1) GO TO 324 $ RAT=(ESEP/C(IE,J))**FACTOR
      F3N=F3N*RAT $ F3ND=F3ND*RAT
      A(1,IX)=A(1,IX)+H1/8.*C(IE,J   )*DTINV*DXOVNM
      B(2,IX)=-DTINV*0.375*H2*ESEP*DVX(J)/V(J)**2   +B(2,IX)
      C(2,IX)=-DTINV*H2/8.*ESEP*DVX(J+1)/V(J+1)**2
      A(2,IX)=-H1/8.*DTINV*C(IE,J   )*DVX(J-1)/V(J-1)**2
      C(1,IX)=D(1,IX)+H2/8.*ESEP*DTINV*DXOVNP
      B(1,IX)=B(1,IX)+0.375*H2*ESEP*DTINV*DXOVN $ GO TO 325
  324 IF(J.NE.NJ2) GO TO 325 $ RAT=(C(IE,J)/ESEP)**FACTOR
      F3N=F3N*RAT $ F3ND=F3ND*RAT
      B(1,IG)= DTINV*C(IX,J)/V(J) $ B(2,IG)= DTINV/V(J)
      C(2,IX)=-H3/8.*DTINV*C(IE,J   )*DVX(J+1)/V(J+1)**2
      A(1,IX)=A(1,IX)+H2/8.*ESEP*DTINV*DXOVNM
      B(1,IX)=B(1,IX)+DTINV*DXOVN*(0.375*H2*ESEP+ C(IG,J))
      C(1,IX)=D(1,IX)+H3/8.*C(IE,J   )*DTINV*DXOVNP
      A(2,IX)=-DTINV*H2/8.*ESEP*DVX(J-1)/V(J-1)**2
      B(2,IX)=-DTINV*DVX(J) /V(J)**2*(C(IG,J)+H2*0.375*ESEP)+B(2,IX)
  325 G(1)=-RDIF $ G(2)=-VDIF
      IF(EPL(J).GT.0.0.OR.EPK(J).GT.0.0) GO TO 326
C     D(VOID FRACTION)/D(TIME)=AJ.
      B(3,IX)=-C(IJ,J)*DZETAX(J)/2.0   $ B(3,IE)=DTINV
      B(3,IJ)=-ZETA(J)/2.0 $ BIG(1)=DTINV*CKEEP(IE,J)
      BIG(2)=0.5*ZETALC(J)*CKEEP(IJ,J) $ BIG(3)=B(3,IJ)*C(IJ,J)
      BIG(4)=DTINV*EPLKEP(J) $ BIG(5)=DTINV*EPKKEP(J)
      DO 53 K=1,5 $ IF(TALL(3).LT.ABS(BIG(K))) TALL(3)=ABS(BIG(K))
   53 CONTINUE
      G(3)=DTINV*(CKEEP(IE,J)+EPLKEP(J)+EPKKEP(J)-C(IE,J))+BIG(2)-BIG(3)
      GO TO 328
  326 B(3,IX)=1.0 $ XANS=XASK $ IF(EPL(J).GT.0.0) XANS=XASL
      G(3)=XANS-C(IX,J) $ IF(EPL(J).EQ.0.0) GO TO 327
      B(1,IE)=B(1,IE)-WE/VL ICL*4.0*DTINV
      B(2,IE)=B(2,IE)-WE/VL ICL*4.0*DTINV
      B(1,IJ)=B(1,IJ)+WE/VL ICL*4.0*ZETA(J)/2.0
      B(2,IJ)=B(2,IJ)+WE/VL ICL*4.0*ZETA(J)/2.0
      B(2,IX)=B(2,IX)+WE/VL ICL*4.0*DZETAX(J)*C(IJ,J)/2.0
      B(1,IX)=B(1,IX)+WE/VL ICL*4.0*DZETAX(J)*C(IJ,J)/2.0 $ GO TO 328
  327 B(2,IE)=B(2,IE)-WE/VKCL *4.0*DTINV
```

```
      B(2,IJ)=B(2,IJ)+WE/VKCL *4.0*ZETA(J)/2.0
      B(2,IX)=B(2,IX)+WE/VKCL *4.0*DZETAX(J)*C(IJ,J)/2.0
  328 CONTINUE
      BIG(1)=DTINV*C(IE,J)*C(IX,J)/V(J)*WE*3.0
      BIG(2)=0.25*DYINV *XD(J)*F3N   $ BIG(3)=2.0*C(IJ,J)/F*WE
      BIG(5)=4.0*WE*DTINV*EPL(J)/VLICL
      BIG(4)=0.25       *C(IG,J)*C(IX,J)       $ DO 54 K=1,5
   54 IF(TALL(1).LT.ABS(BIG(K))) TALL(1)=ABS(BIG(K))
      BIG(1)=DTINV*WE*C(IE,J)*3.0/V(J)  $ BIG(2)=0.5*C(IG,J)
      BIG(3)=2.0*WE       *C(IJ,J)/F
      BIG(4)=4.0*WE*EPK(J)*DTINV/VKCL
      BIG(5)=4.0*WE*DTINV*EPL(J)/VLICL $ DO 55 K=1,5
      IF(TALL(2).LT.ABS(BIG(K))) TALL(2)=ABS(BIG(K))
   55 CONTINUE $ GO TO 60
  329 B(1,IX)=1.0 $ B(2,IG)=1.0 $ B(3,IE)=1.0 $ IF(IPOLAR.EQ.0) GO TO 60
      VABAR=V(J)+(1.0-C(IX,J))*CVX(J) $ IF(J-NJ2) 306, 60,308
  306 B(2,IG)=-0.5*(V(J)+V(J+1)) $ IF(J.EQ.1) GO TO 309
      A(2,IG)=0.5*(V(J)+V(J-1)) $ G(2)=-A(2,IG)*C(IG,J-1) $ GO TO 309
  308 B(2,IG)=0.5*(V(J)+V(J-1)) $ IF(J.EQ.NJ) GO TO 309
      D(2,IG)=-0.5*(V(J)+V(J+1)) $ G(2)=-D(2,IG)*C(IG,J+1)
  309 B(2,IJ)=(VABAR/F-ZETA(J))*WE*4.0
      B(2,IE)=CVDT(J)*CTEMP/V(J)*WE*4.0
      G(2)=G(2)-B(2,IJ)*C(IJ,J)-B(2,IE)*C(IE,J)-B(2,IG)*C(IG,J)
      IF(J.EQ.NJ1) G(2)=G(2)-      CTEMP/V(J)*H2/2.0*ESEP*CVDT(J)
      TALL(2)=ABS(B(2,IG)*C(IG,J))
      IF(TALL(2).LT.ABS(B(2,IJ)*C(IJ,J))) TALL(2)=ABS(B(2,IJ)*C(IJ,J))
   60 IF((J.GT.NJ1).AND.(J.LT.NJ2)) GO TO 6
C     REMOVAL OF TRANSFER CURRENT
      BINV=1.0/B(6,IJ) $ G(6)     =BINV*G(6) $ DO 61 MN=1,N
   61 IF(J.LT.NJ2) B(6,MN)=BINV*B(6,MN) $ DO 62 L=1,N
      G(L)=G(L)-G(6)     *B(L,IJ)
      IF(TALL(L).LT.ABS(G(6)     *B(L,IJ))) TALL(L)=ABS(G(6)     *B(L,IJ))
      DO 62 MN=1,N
   62 B(L,MN)=B(L,MN)-B(6,MN)*B(L,IJ) $ NERR=0
      DO  63 JW=1,N  $ IF(ABS(G(JW)).LT.TALL(JW)*COEFF) G(JW)=0.0
      IF(G(JW).NE.0.0) NERR=NERR+1
      IF(JW.NE.5.OR.J.NE.NJ1) GO TO 63
      IF(TCD.EQ.0.0. AND .G(JW).NE.0.0) NERR=NERR-1
   63 CONTINUE $ NTERR=NTERR+NERR
      IF(IPOLAR.EQ.0 .AND. JCOUNT.LT.9) GO TO 6
      IF(JCOUNT.GE.7 .AND. NERR.NE.0) PRINT 118, DIST(J),(G(K),K=1,N)
     1,C(IN,J)
 6    IF(IPOLAR.NE.0) GO TO 64 $ B(1,1)=B(4,II) $ B(1,2)=B(4,IN)
      A(1,1)=A(4,II) $ A(1,2)=A(4,IN) $ A(2,1)=A(5,II) $ A(2,2)=A(5,IN)
      D(1,1)=D(4,II) $ D(1,2)=D(4,IN) $ D(2,1)=D(5,II) $ D(2,2)=D(5,IN)
      B(2,1)=B(5,II) $ B(2,2)=B(5,IN) $ G(1)=G(4) $ G(2)=G(5) $ N=2
   64 CALL BAND(J) $ N=5 $ IF(J.LT.NJ) GO TO 5
      DO 65 J=1,NJ $ IF(IPOLAR.NE.0) GO TO 65 $ C(II,J)=C(1,J)
      C(IN,J)=C(2,J) $ C(1,J)=0.0 $ C(2,J)=0.0 $ C(3,J)=0.0
  65  CONTINUE
C     REEVALUATION OF MAIN VARIABLES.
      DO 67 J=1,NJ  $ XD(J)=XD(J)+C(IX,J) $ C(II,J)=TCD
      DETA(J)=DETA(J)+      C(IN,J) $ DO 67 K=1,4
   67 C(K,J)=      C(K,J)+COLD(K,J) $ C(II,1)=0.0
      AVILIM=0.0 $ DO 443 J=1,NJ1
      H=H1 $ IF(J.EQ.1 .OR. J.EQ.NJ1) H=H/2.0
      IF(J.GT.1) C(II,J)=C(II,J-1)
      IF(NONCF(J).NE.0) GO TO 445
      IF(Q(J).LE.1.0E-05.AND.C(IN,J).LE.0.0) GO TO 444
      IF(RBETA(J).LE.1.0E-11.AND.C(IN,J).GE.0.0) GO TO 444
      DO 442 K5=1,4 $ ADDJ=DENT2*(C(IJ,J)+CKEEF(IJ,J))
      RINK=RINKEP(J)
```

```
      IF(W(J).LE.1.0) GO TO 439 $ IF(C(IN,J).LT.0.0) GO TO438
      W(J)=0.0 $ GO TC 440
  438 FIN5=PIN52 $ PIN2=PIN22 $ DFC=DFC2
      IF(W(J).GT.1.99) RINK=ROUTA(J)
      ROK=(ROUTA(J)**3+ADDJ/PIN52)**PIN1
      RIN3=RINK  **3-ADDJ/PIN2 $ IF(RIN3.LT.0.0) GO TO 444
      RIN(J)=RIN3**PIN1
      TL=(1.0/RIN(J)  -1.0/ROK)/DFC $ GC TO 441
  439 IF(C(IN,J).GT.0.0) GO TO 440 $ W(J)=2.0 $ GO TO 438
  440 FIN5=PIN51 $ PIN2=PIN21 $ DFC=DFC1
      ROK=(ROUTA(J)**3+ADDJ/PIN51)**PIN1
      RBETA3=RBETA (J)**3-ADDJ/PIN2 $ IF(RBETA3.LT.0.0) GC TO 444
      RBETAK  =RBETA3**PIN1 $ RIN(J)=RBETAK
      TL=           (1.0/PIN2+1.(/PIN5)*(Q(J)+ADDJ)/(ROK**2+ROK
     1*RIN(J)+RIN(J)**2)/(DFC*ROK*RIN(J))
  441 SAREA=PIN4*ROK**2
      CR2=EXP(TCA* C(IN,J)) $ CR3=EXP(-TCC*C(IN,J))
      CR14=CR2-CR3 $ IF(ABS(C(IN,J)).GT.C.0005) GO TO 437
      CR14=C(IN,J)*(TCA+TCC+(TCA**3+TCC**3)*C(IN,J)**2/6.0)
 437  EXCHIA=SAREA*CR1*(C(IX,J)/XAR)**GAM
      CR15=TL*CR2+1.0/EXCHIA        $ CR16=CR15**2
      B(6,IJ)=1.0+CR14/CR16*DELT/6.0*(CR2/DFC*(1.0/PIN2/RIN(J)**4  +1.0
     1/PIN5/ROUTA(J)**4)-2.0/EXCHIA/ROUTA(J)**3/PIN5)
      C(IJ,J)=C(IJ,J)-(C(IJ,J)-CR14/CR15)/B(6,IJ)
  442 IF(ABS(C(IJ,J)-CR14/CR15).LE.COEFF*ABS(CR14/CR15)*.01) GC TO 445
      GC TO 445
 444  C(IJ,J)=0.0
 445  IF(TL.LT.1.0E-19) AVILIM=2.0*TCD $ IF(TL.LT.1.0E-19) GC TO 443
      AVILIM=AVILIM+H/TL
  443 C(II,J)=C(II,J)+H*C(IJ,J)
      IF(AVILIM.LT.TCD.AND.IPOLAR.EQ.0) GO TO 98
      C(II,NJ)=0.0 $ DO 295 JB=NJ2,NJ $ J=NJ-JB+NJ2 $ H=H3
      IF(J.EQ.NJ2 .OR. J.EQ.NJ) H=H/2.0  $ IF(NONOF(J).NE.0) GC TO 293
      ETAS=DETA(J) $ CJ1(J)=0.0 $ CJ2(J)=0.0
      IF(EFES(J).EQ.0.0 .AND. ETAS.LT.0.0) GO TO 280
      IF(EX(J).EQ.0.0 .AND. ETAS.GT.0.0) GC TO 280
      EXPDIF=ETAS*((TC1+TC2)*(1.0+0.5*(TC1-TC2)*ETAS)+(TC1**3+TC2**3)*
     1ETAS**2/6.0)
      IF(ABS(TC1*ETAS).GT.0.004) EXPDIF=EXP(TC1*ETAS)-EXP(-TC2*ETAS)
      CJ1(J)=EXPDIF*AIC1*C(IX,J)
  280 ETAS=C(IN,J) $ IF(EX(J).EQ.0.0 .AND. ETAS.LT.0.0) GC TO 293
      IF(ELI2S(J).EQ.0.0 .AND. ETAS.GT.0.0) GC TO 293
      EXPDIF=ETAS*((TC1+TC2)*(1.0+0.5*(TC1-TC2)*ETAS)+(TC1**3+TC2**3)*
     1ETAS**2/6.0)
      IF(ABS(TC1*ETAS).GT.0.004) EXPDIF=EXP(TC1*ETAS)-EXP(-TC2*ETAS)
      CJ2(J)=EXPDIF*AIC2*C(IX,J)
  293 C(IJ,J)=CJ1(J)+CJ2(J)
  298 C(II,J-1)=C(II,J)-H*C(IJ,J)
C     CALCULATE TOTAL CELL VOLTAGE
      PHI1=0.0 $ DO 68 J=1,NJ1M1
   68 PHI1=PHI1+0.5*(SIGINV(J)+SIGINV(J+1))*(C(II,J)-TCD)*H1
      RG=0.0  $ DO 69JB=NJ1P1,NJ2M1
      RG=RG+C(II,JB)/CON(JB)/ESEPPN+(VAL1+VAL2*C(IX,JB))*T*CLNAC(JB)*
     1(C(IX,JB+1)-C(IX,JB-1))*0.5/H2/(1.0-C(IX,JB))/C(IX,JB)
   69 CONTINUE
      PHI2=-H2*(RG+.5*(C(II,NJ1)/CON(NJ1)/ESEPPN+(VAL1+VAL2*C(IX,NJ1))*
     1T*CLNAC(NJ1)*(4.0*C(IX,NJ1+1)-3.0*C(IX,NJ1)-C(IX,NJ1+2))*0.5/H2/
     1(1.0-C(IX,NJ1))/
     1C(IX,NJ1)+C(II,NJ2)/CON(NJ2)/ESEPPN+(VAL1+VAL2*C(IX,NJ2))*T*
     1CLNAC(NJ2)*(-4.0*C(IX,NJ2-1)+3.0*C(IX,NJ2)+C(IX,NJ2-2))*0.5/H2/
     1(1.0-C(IX,NJ2))/C(IX,NJ2))) $ PHI3=0.0 $ DO 70 J=NJ2,NJM1
   70 PHI3=PHI3+0.5*(SIGINV(J)+SIGINV(J+1))*(C(II,J)-TCD)*H3
```

```
      PHI4=-TCD*WICTH/CON(NJ2)
      TCV=PHI1+PHI2+PHI3+PHI4       +UJO+C(IN,NJ2 )-C(IN,NJ1)-RGRID*TCD
      IF(IPOLAR.EQ.0) GO TO  7  $ IF(DELT.EQ.0.0)
     1DTEMP=(TCD*(UJO-TINIT*DOCCPT-TCV)-CHT*(T-TAMB))/CPPA
      CO  74 M=1,NJ $ IF(M-NJ2) 71,72,73
   71 VSTAR(M)=0.5*(V(M)+V(M+1))*(C(IG,M)-0.5/F*C(II,M)) $ GCTC 74
   72 VSTAR(M)=C(IG,M) $ GO TO 74
   73 VSTAR(M)=0.5*(V(M)+V(M-1))*(C(IG,M)-0.5/F*C(II,M-1))
   74 CONTINUE
C      CALCULATE NEW RESERVOIR VOLUME (CM3/CM2 SEPARATOR)
      VOVERA=C(IG,NJ2)
C      CONSIDER PRECIPITATION OF LICL OR KCL
      CO 333 J=1,NJ
      DEPS=EPKKEP(J)+EPLKEP(J)+CKEEP(IE,J)-C(IE,J)+0.5*DELT *(ZETA(J)
     1*C(IJ,J)+ZETALD(J)*CKEEP(IJ,J)) $ IF(EPL(J).LE.0.0) GO T( 330
      EPL(J)=DEPS $ IF(EPL(J).GT.0.0) GC TO 333
      PRINT 307,J,EPL(J),C(IX,J)
      C(IX,J)=(C(IE,J)*C(IX,J)+EPL(J))/(C(IE,J)+EPL(J))
      XD(J)=C(IX,J)-XAINIT
      C(IE,J)=C(IE,J)+EPL(J) $ EPL(J)=0.0 $ GO TO 333
  307 FORMAT (I5,2F12.6)
  330 IF(EPK(J).LE.0.0) GO TO 331 $ EPK(J)=CEPS
      IF(EPK(J).GT.0.0) GO TO 333 $ PRINT 307,J,EPK(J),C(IX,J)
      C(IX,J)=C(IE,J)*C(IX,J)/(C(IE,J)+EPK(J))
      XD(J)=C(IX,J)-XAINIT
      C(IE,J)=C(IE,J)+EPK(J) $ EPK(J)=0.0 $ GC TO 333
  331 IF(C(IX,J).LT.XASL) GC TO 332 $ IF(JCCUNT.NE.3) GC TC 333
      PRINT 307, J,EPL(J),C(IX,J) $ JPTERR=1
      EPL(J)=C(IE,J)*(XASL-C(IX,J))/(XASL-1.0) $ XD(J)=XASL-XAINIT
      C(IE,J)=C(IE,J)-EPL(J) $ C(IX,J)=XASL $ GO TO 333
  332 IF(C(IX,J).GT.XASK) GO TC 333 $ IF(JCCUNT.NE.3) GO TO 333
      PRINT 307, J,EPK(J),C(IX,J)     $ JPTERR=1
      EPK(J)=C(IE,J)*(XASK-C(IX,J))/XASK $ XD(J)=XASK-XAINIT
      C(IE,J)=C(IE,J)-EPK(J) $ C(IX,J)=XASK
  333 CONTINUE $ KEY=4
      CO  75 M4=1,NJ $ IF(C(IE,M4).GT.0.0) GOTC 75
      PRINT 111,DIST(M4),C(IE,M4),C(IJ,M4),JCOUNT $ GO TC 8
   75 CONTINUE
C      CONVERGENCE TEST.
 7    CO 76 K=1,NJ
      IF(ABS(C(IN,K)-CCLD(IN,K)).LT.1.0E-29.ANC.TCD.EQ.0.0) GC TO 76
      IF(ABS(C(IN,K)-CCLD(IN,K)).GT.CONV*ABS(DETA(K))) GC TO 77
      IF(ABS(C(IN,K)-CCLD(IN,K)).GT.CONV*ABS(C(IN,K))) GOTO 77
   76 CONTINUE  $ GCTO 10
   77 IF(JCOUNT.GE.7)PRINT 127, K,CIST(K),C(IX,K),C(IE,K),VSTAR(K),
     1C(II,K),C(IJ,K),C(IN,K),CJ1(K)
      IF(JCOUNT.LT.MAXITS) GCTC 4
      IF(IPOLAR.NE.0) GO TO 59 $ IF(TCD.EQ.0.0.AND.JCOUNT.LT.23)GOTO 4
  59  PRINT 135,TIME $ PRINT 105
      PRINT 118,(CIST(J),C(IX,J),C(IE,J),VSTAR(J),C(II,J),C(IJ,J),
     1C(IN,J),CJ1(J),J=     1,NJ )
      KEY=6
C      HALVE TIME STEP
 8    PRINT 134,KEY  $ JSET=0        $ TIME=TIME-DELT
      T=T-DELT*DTEMP $ DELT=0.5*DELT $ IF(KEY.EQ.1.AND.CELT.GE.0.005)
     1GO TO 9
      JSPOT=JSPOT+1
 9    CO  78 M2=1,NJ $ XD(M2)=XDKEEP(M2) $ DETA(M2)=CKEEP(IN,M2)
      NONOF(M2)=0       $ EPL(M2)=EPLKEP(M2) $ EPK(M2)=EPKKEP(M2)
      IF(M2.GE.NJ2)CETA(M2)=CKEEP(IN,M2)+DSEPOT $ CJ1(M2)=CJ1KEP(M2)
      IF(M2.LE.NJ1) RIN(M2)=RINKEP(M2) $ IF(M2.GE.NJ2)CJ2(M2)=CJ2KEP(M2)
      CO 78 M1=1,JP
```

```
   78 C(M1,M2)=CKEEP(M1,M2) $ IF(IPOLAR.EQ.0) GO TO 3
      IF(DELT.LT.DTMIN) GO TO 14
      IF(KEY.EQ.6) KEY6=KEY6+1 $ IF(KEY6.EQ.9) GO TO 14
      JCOUNT=0 $ GO TO 2
C     CONVERGED SOLUTION - PRINT RESULTS
 10   IF(JPTERR.NE.0) GO TO 4 $ IF(IPOLAR.EQ.0) GO TO 12
      PRINT 103  $ PRINT 104,H1,H2,H3,NJ,JCOUNT,CONV,TIME $ PRINT 105
      JPRINT=1 $ DO  80 J=1,NJ
      Q(J)=Q     (J)+DENT2*(C(IJ,J)+CKEEP(IJ,J))
      IF(J.EQ.JPRINT.OR.J.EQ.NJ) GO TO 79
      IF(J.EQ.NJ1.OR.J.EQ.NJ2) GO TO 79
      IF(EPL(J).EQ.0.0.AND.EPK(J).EQ.0.0) GO TO 80
   79 PRINT 118,DIST(J),C(IX,J),C(IE,J),VSTAR(J),C(II,J),C(IJ,J),C(IN,J)
     1,CJ1(J) $ JPRINT=J+4
   80 CONTINUE $ IF(TCC.LE.0.0) GO TO 83
C     CHECK RESULTS
      DO 82 K=NJ2,NJ
      IF(C(IJ,K).LE.0.0) GO TO 82 $ KEY=5
      KEY5=KEY5+1 $ IF(KEY5.GE.2.OR.DELT.LE.120.0) GO TO 82
      PRINT 118,(DIST(M),C(IX,M),C(IE,M),C(IG,M),C(II,M),C(IJ,M),
     1C(IN,M),CJ1(M),M=K-1,K+1) $ GO TO 8
   82 CONTINUE
C     CALCULATE PARAMETERS NEEDED AT NEXT TIME STEP
   83 IF(DELT.EQ.0) GO TO 11
      IF(KSET.LT.0) KSET=-KSET
      DO 84 J=1,NJ1 $ ADDJ=(C(IJ,J)+CKEEP(IJ,J))*DENT2 $ PIN5=PIN51
      DFC=DFC1               $ IF(C(IJ,J).GT.0.0) GO TO 81
      DFC=DFC2 $ PIN5=PIN52
   81 ROUTA(J)=(ROUTA(J)**3+ADDJ/PIN5)**PIN1
      IF(C(IJ,J).GE.0.0) RBETA(J)=PIN(J)
      ESUM(J)=C(IE,J)+PIN43*ROUTA(J)**3+EPK(J)+EPL(J)+ECCN
      W(J)=1.0-C(IJ,J)*(1.0/RIN(J)   -1.0/ROUTA(J))/DFC
      IF(W(J).LT.0.0) W(J)= 0.0
      IF(J.NE.JSET) GO TO 84 $ IF(KSET.EQ.2) Q(J)=0.0
      IF(KSET.EQ.1) RBETA(J)=0.0
   84 CONTINUE $ DO 299 J=NJ2 ,NJ
      CADD1=CJ1(J)+CJ1KEP(J) $ CADD2=CJ2(J)+CJ2KEP(J)
      EFES(J)=EFES  (J)+Y1  *CADD1*DENT2
      EFE(J)=EFE    (J)+(Y31*CADD1+Y32*CADD2)*DENT2
      ELI2S(J)=ELI2S (J)+Y42*DENT2*CADD2
      EX(J)=EX    (J)+(Y21*CADD1+Y22*CADD2)*DENT2
      IF(J.NE.JSET) GO TO 299
      IF(KSET.EQ.1) EFES(J)=0.0 $ IF(KSET.EQ.2) ELI2S(J)=0.0
      IF(KSET.EQ.3 .OR. KSET.EQ.4) EX(J)=0.0
      IF(KSET.EQ.4) EFE(J)= 0.0
  299 ESUM(J)=C(IE,J)+EPL(J)+EPK(J)+ELI2S(J)+EFES(J)+EX(J)+EFE(J)+ECCF
C     PRINT MORE RESULTS
 11   DO 87 J=NJ2,NJM1 $ IF(CJ1(J).NE.0.0.OR.CJ1(J+1).EQ.0.0) GO TO 86
   85 PRINT 137 $ PRINT 118,(DIST(K),C(IX,K),C(IE,K),VSTAR(K),C(II,K),C(
     1IJ,K),C(IN,K),CJ1(K),K=J,J+1) $ GO TO 87
   86 IF(CJ2(J).NE.0.0.OR.CJ2(J+1).EQ.0.0) GO TO 87 $ GO TO 85
   87 CONTINUE
      PRINT 132 $ JPRINT =1 $ DO  91 J=1,NJ
      IF(J.EQ.JPRINT.OR.J.EQ.NJ) GO TO 88
      IF(J.EQ.NJ1.OR.J.EQ.NJ2) GO TO 88
      IF(EPL(J).EQ.0.0.AND.EPK(J).EQ.0.0) GO TO 91
   88 IF(J.GT.(NJ1+NJ2)/2)  GO TO 89
      PRINT 118,DIST(J),C(IG,J),Q(J),ESUM(J),RIN(J)   ,EPL(J),ROUTA(J),
     1W(J) $ GO TO 90
   89 PRINT 118,DIST(J),C(IG,J),Q(J),ESUM(J),EPK(J),EFE(J),EX(J),EFES(J)
   90 JPRINT=J+4
   91 CONTINUE
```

```
      CO 94 J=NJ2,NJM1 $ IF(CJ1(J).NE.0.0.CR.CJ1(J+1).EQ.C.0) GO TC 93
   92 FRINT 137 $ PRINT 118, (CIST(K),C(IG,K),C(K),ESUM(K),EFK(K),EFE(K)
     1,EX(K),EFES(K),K=J,J+1) $ GO TO 94
   93 IF(CJ2(J).NE.C.0.OR.CJ2(J+1).EQ.0.0) GO TO 94 $ GC TC 92
   94 CONTINUE
C     RESET PARAMETERS AT OLC TIME
C     TEST OF ELECTRCLYTE MATEFIAL BALANCE
      H=H1 $ FLUXP=C.0  $ FGP=0.0 $ RSUM=0.G $ VSUM=0.0
      F3NP=C(IE,1)**FACTOR*CIFUSN(1)/V(1) $ DIFKCL=0.0
      CIFLCL=0.0
      CO 300 J=1,NJ $ FLUXM=FLUXP $ F3N=F3NP $ FGM=FGP
      IF(DELT.EQ.0.0) GO TO 301
      R1KEP   =R1(J) $ R2KEF   =R2(J)$ RV1KEP=RV1(J)$ RV2KEF=RV2(J)
  301 JE=J $ WE=H/4.0          $ IF(J.NE.NJ) GC TC 302
      WE=WE/2.0 $ FGP=C.0 $ FLUXP=C.C $ JE=J-1 $ GO TO 305
  302 F3NP=C(IE,J+1)**FACTOR*DIFUSN(J+1)/V(J+1)
      JGP=J $ IF(J.CE.NJ2) JCP=J+1 $ IF(J.EG.1) JE=J+1
      IF(J.EG.1) WE=WE/2.C
      IF(J.EQ.NJ2-1) F3NP=F3NP*(C(IE,J)/C(IE,J+1))**FACTOR
      IF(J.NE.NJ1) GO TO 303 $ JE=J-1 $ WE=H1/8.0 $ H=H2
       F3N=F3N*(C(IE,J+1)/C(IE,J))**FACTCR $ GC TO 304
  303 IF(J.NE.NJ2) GO TO 304 $ JE=JE+1 $ WE=H3/8.0 $ H=H3
      F3N=F3N*(C(IE,J)/C(IE,J-1))**FACTOR
  304 FLUXP=0.5*(C(IX,J+1)+C(IX,J))*C(IG,JGF)-0.5*(F3NP+F3N)
     1*(XD(J+1)-XC(J))/H     $ FGP=C(IG,JGP)
  305 R1(J)=FLUXM-FLUXF+WE/F*4.0*C(IJ,J)
      R2(J)=WE*C(IE,J)*(3.0*C(IX,J)/V(J)+C(IX,JE)/V(JE))
     1+WE/VLICL*4.0*EPL(J)
      RV1(J)=FGM-FGF+WE/F*4.0*C(IJ,J)
      RV2(J)=WE*C(IE,J)*(3.0/V(J)+1.0/V(JE))
     1+WE*4.0*(EPL(J)/VLICL+EPK(J)/VKCL)
      IF(J.EQ.NJ1) RV2(J)=RV2(J)+ESEP*H2/8.*(3./V(J)+1./V(J+1))
      IF(J.EQ.NJ2) RV2(J)=RV2(J)+ESEP*H2/8.*(3./V(J)+1./V(J-1))+C(IG,J)/
     1V(J)
      IF(J.EQ.NJ1) R2(J)=R2(J)+ESEF*H2/8.*(3.0*C(IX,J)/V(J)+C(IX,J+1)/V(
     1J+1))
      IF(J.EG.NJ2) R2(J)=R2(J)+ESEP*H2/8.*(3.*C(IX,J)/V(J)+C(IX,J-1)/V(J
     1-1))+C(IG,J)*C(IX,J)/V(J)
      IF(DELT.EQ.0.C  ) GO TC 300 $ R3=(R2(J)-R2KEP)/DELT
      RCIF=R3-0.5*(R1(J)+R1KEP   )
      RV3=(RV2(J)-RV2KEP)/DELT $ VCIF=RV3-0.5*(RV1(J)+PV1KEP)
      IF(ABS(RCIF).GT.1.0E-11.CR.ABS(VCIF).GT.1.0E-11) PRINT 118,DIST(J)
     1,RCIF,VCIF
      RSUM=RSUM+RCIF
      VSUM=VSUM+VCIF $ IF(J.EQ.NJ) PRINT 138,RSUM,VSUM
      IF(DELT.EQ.C.0) GO TO 300
      IF(J.GT.NJ1) GC TO 310
      IF(ABS(EPL(J)-EPLKEP(J)).LT.1.0E-14) GC TC 300
      RU=1.0 $ IF(J.EG.1.OR.J.EG.NJ1) RU=0.5
      CIFLCL=RU*(EPL(J)-EPLKEP(J))+DIFLCL
 310  IF(J.LT.NJ2) GO TO 300
      IF(ABS(EPK(J)-EPKKEP(J)).LT.1.0E-14) GO TO 300 $ RN=1.0
      IF(J.EG.NJ2.OR.J.EG.NJ) RN=0.5 $ CIFKCL=RN*(EPK(J)-EPKKEP(J))+
     1CIFKCL
  300 CONTINUE $   SLN=0.0 $ CAPN=C.C $ CAPP=0.0
      IF(DELT.NE.0.C) CIFKCL=DIFKCL*H3*HFUSEK/VKCL/DELT
      IF(DELT.NE.0.0) CIFLCL=DIFLCL*H1*HFUSEL/VLICL/DELT
      HTLOSS=CHT*(T-TAMB) $ HTGAIN=(UJC-TCV-TINIT*DOCCPT)*TCC
      CTEMP=(HTGAIN+CIFKCL+CIFLCL-HTLOSS)/CFMA
      FRINT 125,T,HTLCSS,HTGAIN,CIFKCL,CIFLCL
C     CHECK TOTAL NC. CF MOLS LI AND K, ELECTRCLYTE AND SCLIC FHASES.
      AMTLI=0.0    $ AMTK=0.0   $ SOLIDL=0.0 $ DO  95 M=1,NJ
```

```
      H=H2 $ IF(M.LE.NJ1) H=H1 $ IF(M.GE.NJ2) H=H3
      WM=H*C(IE,M) $ IF(M.EQ.1 .OR. M.EQ.NJ) WM=0.375*WM
      IF(M.EQ.NJ1-1 .OR. M.EQ.NJ-1) WM=WM+0.125*H*C(IE,M+1)
      IF(M.EQ.NJ2-1 .OR. M.EQ.NJ1+1) WM=1.125*WM
      IF(M.EQ.2 .OR. M.EQ.NJ2+1) WM=WM+0.125*H*C(IE,M-1)
      IF(M.EQ.NJ1) WM=0.375*(H1*C(IE,M)+H2*ESEF)
      IF(M.EQ.NJ2) WM=0.375*(H3*C(IE,M)+H2*ESEF)+C(IG,M)
      IF(M.EQ.NJ1 .OR. M.EQ.NJ2) H=H/2.0
      IF(M.EQ.1 .OR. M.EQ.NJ) H=H/2.0
      IF(M.GE.NJ2) CAPP=CAPP+H*C(M)
      IF(M.GE.NJ2) SOLIDL=SOLIDL+2.*H*(ELI2S(M)/VLI2S+EX(M)/VX)
      AMTLI=AMTLI+WM*C(IX,M)/V(M)+EPL(M)*H/VLICL
      IF(M.GT.NJ1) GO TO 95 $ CAPN=CAPN+H*Q(M)
      SLN=SLN+H *(U1*REETA(M)**3+U2*ROUTA(M)**3+U3)
   95 AMTK=AMTK+WM*(1.0-C(IX,M))/V(M)+EPK(M)*H/VKCL
      IF(TIME.GT.0.0) GO TO 96
      SLNO=SLN $ SLPO=SOLIDL $ AMTLIO=AMTLI $ AMTKO=AMTK
      PRINT 136 , SLNO,SLPO,AMTLIO,AMTKO
   96 FAMTLI=AMTLI/AMTLIO-1.0 $ FAMTK=AMTK/AMTKO-1.0
      FSL=(SLN+SOLIDL)/(SLNO+SLPO)-1.0
      PRINT 126,JCOUNT,FAMTLI,FAMTK,SOLIDL,      XASL,XASK,SLN,FSL,
     1CAPN,CAPP
      PRINT 117
      PRINT 116,TCD,TCV,PHI2,PHI3,C(IN,NJ1),C(IN,NJ2),VOVERA
      IF(TCV.LT.CUTOFF.OR.TCV.GT.1.65) GO TO 15
      IF(TIME.LT.TGAP+TLAST) GO TO 13
      IF(TCV.LT.1.20.OR.TCV.GT.1.48) TGAP=300.0*0.0416/TCD
C     CALCULATION OF POLARISATION CURVE
      IPOLAR=0 $ TCD1=TCD $ TCD=-TCADD $ TLAST=TLAST+TGAP $ DELTSV=DELT
      DELT=0.0 $ IF(ABS(TCD1-0.02).GT.1.E-7) GO TO 2
   29 DO 97 J=1,NJ $ CPOL(1,J)=C(II,J) $ CPOL(2,J)=C(IJ,J)
   97 CPOL(3,J)=C(IN,J) $ IF(TCD.GE.0.0) GO TO 30 $ GO TO 2
 12   PRINT 124,TCD,TCV,PHI2,PHI3,C(IN,NJ1),C(IN,NJ2),JCOUNT
      IF(ABS(TCD-0.02).LT.1.E-7) GO TO 29 $ IF(TCD.EQ.0.0) GO TO 436
   30 TCD=TCD+TCADD $ IF(ABS(TCD-TCD1).LT.1.0E-7) TCD=TCD+TCADD
      IF(TCD.GE.0.12) GO TO 98 $ IF(ABS(TCD-TCD1).LE.0.02) GO TO 9
      IF(TCD.GT.0.041) GO TO 3  $ DO 28 J=1,NJ $ C(II,J)=CPOL(1,J)
      C(IN,J)=CPOL(3,J) $ DETA(J)=CPOL(3,J) $ NONOF(J)=0
      IF(J.GE.NJ2) DETA(J)=DETA(J)+DSEPOT
   28 C(IJ,J)=CPOL(2,J) $ GO TO 3
   98 TCD=TCD1 $ DELT=DELTSV  $ PRINT 128,RES
      IPOLAR=1
      DO  99 K=1,NJ $ DETA(K)=CKEEP(IN,K) $ CJ1(K)=CJ1KEP(K)
      IF(K.LE.NJ1 .AND. DETA(K).GE.0.0) W(K)=0.9
      IF(K.LE.NJ1 .AND. DETA(K).LT.0.0) W(K)=1.1
      IF(K.LE.NJ1) RIN(K)=RINKEP(K) $ IF(K.GE.NJ2) CJ2(K)=CJ2KEP(K)
      IF(K.GE.NJ2) DETA(K)=DETA(K)+DSEPOT   $ DO 99 I=4,6
   99 C(I,K)=CKEEP(I,K)
 13   IF(TIME.GE.TSTOP) GO TO 14
C     RESET TIME STEP.
      IF(DELT.EQ.0.0) DELT=2.0*DELT2
      IF(TIME.GE.T1) DELT=F1
      IF(TIME.GE.T2) DELT=F2
      IF(TIME.GE.T3) DELT=F3
      IF(TIME.GE.T4) DELT=F4
      IF(TIME.GE.T5) DELT=F5
      IF(TIME.GE.T6) DELT=F6
      IF(TIME.GE.T7) DELT=F7
      IF(TIME.GE.T8) DELT=F8
      IF(TIME.GE.120.0) DELT=120.0
      IF(JSPOT.EQ.0) GOTO 2    $ DELT=DELT/2.0**JSPOT $ JSPOT=JSPOT-1
      IF(DELT.GT.DTMIN) GO TO 2
```

```
C      CURRENT INTERRUPTION AND CHARGING
 14    CONTINUE
       STOP
       GO TO 143
       IF(TCD.LE.0.0) GO TO 143
       DO 142 J=1,NJ $ PUNCH 141,(C(K,J),K=1,6)
       PUNCH 141,EPK(J),EPL(J),RBETA(J),RCUTA(J),RIN(J),Q(J)
       PUNCH 141,EFES(J),EX(J),EFE(J),ELI2S(J),CJ1(J),CJ2(J)
       PUNCH 141,W(J),DETA(J),ZETA(J),(CPOL(K,J),K=1,3)
 142   CONTINUE
 141   FORMAT(6E13.7)
       PUNCH 141,TCV,T,VOVERA,XAINIT,DTEMP,TIME
 143   CONTINUE
       KEY6=0  $ IF(TCD.LT.0.0) STOP $ IF(TCC.EQ.0.0) TCD=-0.020
       IF(TCD.GT.0.0) TSTOP=0.25*TIME  $ IF(TCD.GT.0.0) TCC=0.0
       IF(TCD.LT.0.0) GO TO 449
C      CALCULATION OF INTERRUPTER RESISTANCE
 436   RES=0.0 $ DO 446 J=2,NJ1M1
 446   RES=RES+H1*SIGINV(J)/(1.0+CON(J)*C(IE,J)**FACTOR*SIGINV(J))
       DO 447 J=NJ1P1,NJ2M1
 447   RES=RES+H2/CON(J)/C(IE,J)**FACTOR $ DO 448 J=NJ2P1,NJM1
 448   RES=RES+H3*SIGINV(J)/(1.0+CON(J)*C(IE,J)**FACTOR*SIGINV(J))
       RES=RES+0.5*(H1*(SIGINV(1)/(1.0+CON(1)*C(IE,1)**FACTOR*SIGINV(1))
      1+SIGINV(NJ1)/(1.0+CON(NJ1)*C(IE,NJ1)**FACTOR*SIGINV(NJ1)))+H2*(1.0
      1/CON(NJ1)/C(IE,NJ1)** FACTOR+1.0/CON(NJ2)/C(IE,NJ2)**FACTOR)+
      1H3*(SIGINV(NJ2)/(1.0+CON(NJ2)*C(IE,NJ2)**FACTOR*SIGINV(NJ2))+
      1SIGINV(NJ)/(1.0+CON(NJ)*C(IE,NJ)**FACTOR*SIGINV(NJ))))
        IF(IPOLAR.EQ.0) GO TO 30
       PRINT 128,RES
 449   TSTOP=TSTOP+TIME $ T1=T10+TIME  $ TGAP=600.0
       IF(TCD.LT.0.0) TSTOP=TSTOP+TIME
       T2=T20+TIME $ T3=T30+TIME $ T4=T40+TIME $ T5=T50+TIME
       T6=T60+TIME $ T7=T70+TIME $ T8=T80+TIME $ GO TO 1
 15    PRINT 102   $ GO TO 14 $ END
       SUBROUTINE PROPS(J,C)
C      PROGRAM TO CALCULATE PHYSICAL PROPERTIES FOR MATRIX
C      COEFFICIENTS IN MAIN PROGRAM *BATRY*
       DIMENSION V(401),DVX(401),             DVDT(401), DIFUSN(401),
      1DDX(401),CJ1(401),  SIGINV(401),CJ2(401)  ,CON(401),DCONX(401),
      1DLNAC(401),D2LNAC(401),ZETA(401),DZETAX(401)          ,C(6,401)
      1,EX(401),EFES(401),EFE(401),FBFIN(401)
        COMMON/1/V,DVX,DVDT       ,DIFUSN,DDX      ,SIGINV,CON,
      1DCONX,DLNAC,D2LNAC,ZETA,DZETAX       ,FACTOR,T,IX,NJ1,NJ2
      1,EX,EFES,EFE,SIGD,SIGFES,SIGFE,PIN43
        COMMON/3/S,AON,ACP1,ACP2,CJ1,CJ2,EXPAND
        XSQD=C(IX,J)**2
C      MOLAR VOLUME OF ELECTROLYTE AND DERIVATIVES WRT XA. RO IN G/CM3
       RODASH=2.1623194-0.00073684*T $ XADASH=0.00147368*T-0.36253409
       RO=RODASH+S*(C(IX,J)-XADASH)
       DVDT(J)=0.0
       V(J)=(74.555-32.161*C(IX,J))/RO
       DVX(J)=-(32.161+S*V(J))/RO
C      DIFFUSION COEFFICIENT OF ELECTROLYTE AND DERIVATIVES WRT XA.
C      D IN CM2/SEC
       ACT=EXP(-1425.76/T)
       DDX(J)=0.0002442*ACT $ DIFUSN(J)=DDX(J)*(C(IX,J)+0.4)
C      ELECTRICAL CONDUCTIVITY IN MHO/CM
       CON(J)=ACT*(18.9903*XSQD-5.017*C(IX,J)+9.0903)
       DCONX(J)=ACT*(37.9806*C(IX,J)-5.017)
C      ACTIVITY COEFFICIENT FOR ELECTROLYTE
       XB=1.0-C(IX,J)  $ GAM=1.0+2.0*C(IX,J)  $ XB3=XB**3
       THAN=TANH(0.65837*XB3/C(IX,J))
```

```
      BIN=1023.84*(THAN**2-1.0)/T/C(IX,J)
      CLNAC(J)=1.0-BIN*GAB*XB**2
      C2LNAC(J)=BIN*XB*(4.0*XSOC+C(IX,J)+1.0-1.31674*THAN*GAB**2*XB3/
     1C(IX,J))/C(IX,J)   $ IF(J.GE.NJ2) GOTO 1
C     NEGATIVE ELECTRODE
C     SOLID MOLAR VOLUMES IN G MOLE/CM3
      ZETA(J)=AON+EXPAND $ DZETAX(J)=0.0
      IF(J.GT.NJ1) ZETA(J)=0.0 $ GOTO 2
C     POSITIVE ELECTRODE
    1 CONTINUE
C     SOLID MOLAR VOLUMES IN G MOLE/CM3
      DZETAX(J)=0.0
      AOP=AOP1 $ IF(ABS(CJ2(J)).GT.ABS(CJ1(J))) AOP=AOP2
      ZETA(J)=AOP
  2   RETURN $ END
      SUBROUTINE MATINV(N,M,DETERM)
      COMMON A(6,6),B(6,6),C(6,401),D(6,13)
      DIMENSION ID(5)
      DETERM=1.0 $ DO 1 I=1,N
   1  ID(I)=0 $ DO 18 NN=1,N $ BMAX=1.0 $ DO 6 I=1,N
      IF(ID(I).NE.0) GOTO 6 $ BNEXT=0.0 $ BTRY=0.0 $ DO 5 J=1,N
      IF(ID(J).NE.0) GOTO 5 $ IF(ABS(B(I,J)).LE.BNEXT) GOTO 5
      BNEXT=ABS(B(I,J)) $ IF(BNEXT.LE.BTRY) GOTO 5 $ BNEXT=BTRY
      BTRY=ABS(B(I,J)) $ JC=J
   5  CONTINUE $ IF(BNEXT.GE.BMAX*BTRY ) GOTO 6
      BMAX=BNEXT/BTRY $ IROW=I $ JCOL=JC
   6  CONTINUE $ IF(ID(JC).EQ.0) GOTO 8 $ DETERM=0.0 $ RETURN
   8  ID(JCOL)=1 $ IF(JCOL.EQ.IROW) GOTO 12 $ DO 10 J=1,N
      SAVE=B(IROW,J) $ B(IROW,J)=B(JCOL,J)
  10  B(JCOL,J)=SAVE $ DO 11 K=1,M $ SAVE=D(IROW,K)
      D(IROW,K)=D(JCOL,K)
  11  D(JCOL,K)=SAVE
  12  F=1.0/B(JCOL,JCOL) $ DO 13 J=1,N
  13  B(JCOL,J)=B(JCOL,J)*F $ DO 14 K=1,M
  14  D(JCOL,K)=D(JCOL,K)*F $ DO 18 I=1,N $ IF(I.EQ.JCOL) GO TO 18
      F=B(I,JCOL) $ DO 16 J=1,N
  16  B(I,J)=B(I,J)-F*B(JCOL,J) $ DO 17 K=1,M
  17  D(I,K)=D(I,K)-F*D(JCOL,K)
  18  CONTINUE $ RETURN $ END
      SUBROUTINE BAND(J)
      DIMENSION A(6,6),B(6,6),C(6,401),D(6,13),G(6),X(6,6),Y(6,6),E(5,6,
     1401)
      COMMON A,B,C,D,G,X,Y,N,NJ
  101 FORMAT (15H0DETERM=0 AT J=,I4)
      IF (J-2)  1,6,8
    1 NP1= N + 1
      DO 2 I=1,N
      D(I,2*N+1)= G(I)
      DO 2 L=1,N
      LPN= L + N
    2 D(I,LPN)= X(I,L)
      CALL MATINV (N,2*N+1,DETERM)
      IF (DETERM)  4,3,4
    3 PRINT 101,J
    4 DO 5 K=1,N
      E(K,NP1,1)= D(K,2*N+1)
      DO 5 L=1,N
      E(K,L,1)= - D(K,L)
      LPN= L + N
    5 X(K,L)= - D(K,LPN)
      RETURN
    6 DO 7 I=1,N
```

```
      DO 7 K=1,N
      DO 7 L=1,N
    7 D(I,K)= D(I,K) + A(I,L)*X(L,K)
    8 IF (J-NJ)  11,9,9
    9 DO 10 I=1,N
      DO 10 L=1,N
      G(I)= G(I) - Y(I,L)*E(L,NP1,J-2)
      DO 10 M=1,N
   10 A(I,L)= A(I,L) + Y(I,M)*E(M,L,J-2)
   11 DO 12 I=1,N
      D(I,NP1)= - G(I)
      DO 12 L=1,N
      D(I,NP1)= D(I,NP1) + A(I,L)*E(L,NP1,J-1)
      DO 12 K=1,N
   12 B(I,K)= B(I,K) + A(I,L)*E(L,K,J-1)
      CALL MATINV (A,NP1  ,DETERM)
      IF (DETERM)  14,13,14
   13 PRINT 101,J
   14 DO 15 K=1,N
      DO 15 M=1,NP1
   15 E(K,M,J)= - D(K,M)
      IF (J-NJ)  20,16,16
   16 DO 17 K=1,N
   17 C(K,J)= E(K,NP1,J)
      DO 18 JJ=2,NJ
      M= NJ - JJ + 1
      DO 18 K=1,N
      C(K,M)= E(K,NP1,M)
      DO 18 L=1,N
   18 C(K,M)= C(K,M) + E(K,L,M)*C(L,M+1)
      DO 19 L=1,N
      DO 19 K=1,N
   19 C(K,1)= C(K,1) + X(K,L)*C(L,3)
   20 RETURN
      END
   66  106  146 14400.0   0.004      0.004      0.004      0.01
0.6670     0.249      0.5        0.75       723.15     0.0        0.0
 0.5       0.5        0.5        2.80       600.0      2.7        1.75
10 0.000001   0.001
0.0416     1.3074     -0.000155 0.03        1.5        0.0        1.55
 -1.0      0.0        1.0        -2.0       0.0        2.0        0.00000004
0.0             1.89             298.15          0.000004125
110524260.  .0000000004 0.50          0.58          0.450         60.0
-0.0326   2000.0     2000.0     1.0        1.0        20.5       37.58
7.1056     18.55      46.227     27.677     82300.0    1900.0     500.0
```